

Dissertation zur Erlangung des Doktorgrades
der Fakultät für Chemie und Pharmazie
der Ludwig-Maximilians-Universität München

**Dissection of the Topology, Structure and Function of the INO80 Chromatin
Remodeler**



Alessandro Tosi

aus

München, Deutschland

2013

Erklärung

Diese Dissertation wurde im Sinne von §7 der Promotionsordnung vom 28. November 2011 von Herrn Prof. Dr. Karl-Peter Hopfner betreut.

Eidesstattliche Versicherung

Diese Dissertation wurde eigenständig und ohne unerlaubte Hilfe erarbeitet.

München, am 07.10.2013

Alessandro Tosi

Dissertation eingereicht am 07.10.2013

1. Gutachter: Herr Prof. Dr. Karl-Peter Hopfner

2. Gutachter: Herr Prof. Dr. Roland Beckmann

Mündliche Prüfung am 22.11.2013

My PhD thesis has been prepared from March 2010 to Oktober 2013 in the laboratory of Prof. Dr. Karl-Peter Hopfner at the Gene Center of the Ludwig-Maximilians-University of Munich (LMU).

Parts of this thesis have been published in scientific journals:

Alessandro Tosi*, Caroline Haas*, Franz Herzog*, Andrea Gilmozzi, Otto Berninghausen, Charlotte Ungewickell, Christian B. Gerhold, Kristina Lakomek, Ruedi Aebersold, Roland Beckmann and Karl-Peter Hopfner: Structure and subunit topology of the INO80 chromatin remodeler and its nucleosome complex. **Cell**, Volume 154, Issue 6, 1207-1219, 12 September 2013.

*These authors contributed equally

Parts of this thesis have been presented at international conferences:

Poster presentation at the EMBO practical course “Protein-protein and protein-nucleic acid cross-linking and mass spectrometry”, Göttingen, Germany, 23-29. October 2011.

Poster presentation at the “Epigenetics & Chromatin: Interactions and processes” conference, Boston, USA, 11-13. March 2013.

Oral and poster presentation at the “Helicases and nucleic acid translocases” EMBO, Harden conference, Cambridge, UK, 04-08. August 2013.

1 Table of Contents

<u>1</u>	<u>TABLE OF CONTENTS</u>	<u>4</u>
<u>2</u>	<u>SUMMARY</u>	<u>7</u>
<u>3</u>	<u>INTRODUCTION</u>	<u>9</u>
3.1	DYNAMIC CHROMATIN ENVIRONMENT	9
3.2	SWI2/SNF2 REMODELERS	11
3.3	CHROMATIN REMODELERS	13
3.4	THE INO80/SWR1 FAMILY	14
3.5	INO80 COMPLEX	16
3.5.1	THE COMPONENTS OF THE INO80 COMPLEX	16
3.5.2	THE CHROMATIN REMODELING COMPLEX INO80 IS INVOLVED IN DNA PROCESSING AND METABOLISM	20
3.5.3	INO80 MEDIATES CHECKPOINT PATHWAYS	21
3.6	HYBRID APPROACHES HELP TO DISSECT THE MOLECULAR ARCHITECTURE OF LARGE COMPLEXES	22
<u>4</u>	<u>RESULTS</u>	<u>25</u>
4.1	RECONSTITUTION OF A NUCLEOSOME	25
4.2	A NOVEL PURIFICATION PROCEDURE OF INO80 IMPROVES COMPLEX HOMOGENEITY	27
4.3	NANOBODIES AGAINST THE INO80 COMPLEX	31
4.4	ASSESSMENT OF THE ACTIVITY OF THE PURIFIED INO80	33
4.5	CHEMICAL CROSS-LINKING AND MASS SPECTROMETRY ANALYSIS OF THE INO80 COMPLEX	35
4.5.1	MAPPING OF SUBUNIT INTERACTIONS BY CROSS-LINKING AND MASS SPECTROMETRY	35
4.5.2	SUBUNIT TOPOLOGY AND STRUCTURAL MODULES OF INO80	38
4.6	VALIDATION OF INO80'S MODULES <i>IN VIVO</i>	40
4.7	STRUCTURE OF THE INO80 COMPLEX	41
4.7.1	ELECTRON MICROSCOPY OF INO80	41
4.7.2	TOWARDS A CRYSTAL STRUCTURE OF INO80	43
4.8	RVB1/2 FORM A HETERO-DODECAMER	43
4.8.1	RVB1/2 IS COMPOSED OF TWO HEXAMERIC RINGS IN INO80	43
4.8.2	RVB1/2 ASSEMBLE AS HETERO-HEXAMERS INTERACTING VIA THE DOMAIN 2 WITHIN INO80	44

4.9 THE CATALYTIC CORE OF INO80	47
4.9.1 THE SWI2/SNF2 DOMAIN OF INO80	47
4.9.2 EXPRESSION AND PURIFICATION STUDIES OF THE ATPASE DOMAIN OF INO80 WITH IES2 AND RVB1	48
4.10 LOCALIZATION OF THE ARP8-, ARP5- AND NHP10-MODULE	48
4.11 THE NHP10-MODULE	50
4.11.1 RECONSTITUTION OF THE NHP10 MODULE: NHP10-Ies1-Ies3-Ies5-INO80 (N-TERMINUS)	50
4.11.2 THE NHP10 SUB-COMPLEX FORMS A STABLE DNA COMPLEX	53
4.12 DISSECTING THE FUNCTION AND ACTIVITY OF INO80-MODULES	55
4.12.1 FUNCTIONAL CHARACTERIZATION OF INO80-MODULES	55
4.12.2 INTERACTION AND VISUALIZATION OF AN INO80-NUCLEOSOME COMPLEX	57
4.13 INO80 FORMS A STABLE COMPLEX WITH THE MEC1 COMPLEX	61
<u>5 DISCUSSION</u>	<u>63</u>
5.1 HYBRID VIEW ON INO80	63
5.2 THE CHROMATIN REMODELER INO80	64
5.3 STRUCTURE OF RVB1/2 IN THE INO80 COMPLEX	65
5.4 THE NHP10-MODULE	68
5.5 THE ARP8-MODULE	69
5.6 THE NUCLEOSOME REMODELER INO80	70
5.7 CHROMATIN REGULATORS FACILITATE TRANSCRIPTION	75
<u>6 MATERIAL AND METHODS</u>	<u>77</u>
6.1 MATERIALS	77
6.2 YEAST STRAINS	78
6.3 PLASMID LISTS	78
6.4 OLIGONUCLEOTIDE LIST	79
6.5 BUFFER LIST	81
6.6 MOLECULAR BIOLOGY METHODS	82
6.6.1 CLONING IN BACTERIA	82
6.6.2 CLONING IN YEAST	83
6.7 PROTEIN EXPRESSION AND PURIFICATION	83
6.7.1 PROTEIN EXPRESSION IN E. COLI	83

6.7.2	PROTEIN EXPRESSION IN INSECT CELLS	84
6.7.3	CULTURING OF YEAST	84
6.7.4	SDS-PAGE AND WESTERN BLOT ANALYSIS	85
6.7.5	SILVER STAINING	86
6.7.6	PURIFICATION OF HISTONES AND RECONSTITUTION OF NUCLEOSOMES	87
6.7.7	ESTABLISHMENT OF AN INO80 PURIFICATION PROTOCOL	89
6.7.8	PURIFICATION OF THE SWI2/SNF2 SUB-COMPLEX	92
6.7.9	PURIFICATION OF THE NHP10 SUBCOMPLEX	92
6.8	GENERATION OF INO80 BINDING NANOBODIES	93
6.9	CROSS-LINKING AND MASS SPECTROMETRY	94
6.9.1	TITRATION OF CROSS-LINKER	94
6.9.2	SAMPLE PREPARATION FOR MASS SPECTROMETRY ANALYSIS	94
6.9.3	SAMPLE ANALYSIS	95
6.10	ANALYSIS OF SUBUNIT COMPOSITION OF INO80'S KNOCK-OUT MUTANTS	96
6.11	ANALYSIS OF DISTANT RESTRAINTS	96
6.12	FUNCTIONAL ASSAYS	97
6.12.1	ELECTROPHORETIC MOBILITY SHIFT ASSAYS	97
6.12.2	REMODELING ASSAY	97
6.12.3	ATP HYDROLYSIS ASSAYS	98
<u>7</u>	<u>REFERENCES</u>	<u>99</u>
<u>8</u>	<u>CURRICULUM VITAE</u>	<u>111</u>
<u>9</u>	<u>ACKNOWLEDGMENTS</u>	<u>113</u>

2 Summary

Eukaryotic genomes are organized into highly condensed chromatin. This packaging obviously impedes essential DNA mediated processes. ATP-dependent chromatin remodelers are therefore required to establish a dynamic chromatin environment. The chromatin remodeler INO80 is involved in various fundamental nuclear processes such as DNA repair, DNA replication and transcription. INO80 is thought to contribute to these processes by controlling genome wide levels of the histone variant H2A.Z. The INO80 chromatin remodeler is a macro-molecular complex composed of >15 subunits and a molecular mass of ~1.3 MDa. INO80 is found in human, fly and yeast. INO80 contains core subunits, which are conserved across species, as well as species-specific proteins. Not much was known about the organization of the INO80 subunits and their contribution to chromatin remodeling. Therefore, a hybrid approach was applied on yeast INO80 combining chemical cross-linking and mass spectrometry (XL-MS) (in collaboration with Franz Herzog, Ruedi Aebersold's group, ETH, Zurich), electron microscopy (EM) (in collaboration with Caroline Haas, Roland Beckmann's group, Gene Center, Munich) and biochemical analysis. For this, firstly the purification of INO80 was established. In order to yield sufficient amounts of highly purified and monodisperse complex, INO80 was purified endogenously from yeast by a combination of affinity and chromatography methods. In addition, nanobodies targeting the INO80 complex were generated that could yield even larger amounts of INO80 in the future. EM analysis revealed that INO80 is an embryo-shaped particle with a dynamic head-neck-body-foot architecture that can undergo large conformational changes. XL-MS unraveled the interaction map of the INO80 complex. The analysis of INO80 deletion mutants verified the observed interactions *in vivo* and proved the modular architecture of INO80. Additionally, the gained knowledge allowed the design and purification of stable and novel sub-complexes that could improve crystallization behavior. An integration of the results from different techniques deepened our understanding of the molecular architecture of INO80. The enigmatic subunits Rvb1 and 2 assemble as a dodecamer composed of two hetero-hexameric rings within the head of the INO80 complex. Rvb1/2 is flanked by the Swi2/Snf2 ATPase of Ino80 and the actin

related protein (Arp) 5 in the neck. The Nhp10-module localizes to the body and the Arp8-module to the foot. Biochemical analysis showed that the Nhp10-module is a high affinity DNA/nucleosome binder. The Nhp10-module might together with the Arp8-module target INO80 to chromatin. The Arp5-module is catalytically crucial for nucleosome remodeling and senses the histone entity in chromatin. In order to map interaction sites to the substrate, INO80-nucleosome complexes were analyzed by XL-MS and were visualized by EM. Two-dimensional class averages showed that the nucleosome bound to the central groove of INO80 and was flanked by the head and foot module. The nucleosome was oriented in respect to INO80 as the H2A/H2B dimer- the moiety to be exchanged- was in contact with subunits situated in the neck. All INO80 modules contribute to nucleosome binding and the observed flexibility proposes a mechanism of how INO80 may remodel its substrate. This study established a structural and functional framework of these large remodelers. The investigation of the interaction with the checkpoint kinase Mec1 will contribute to the understanding of the obscure signaling of INO80.

3 Introduction

3.1 Dynamic chromatin environment

Eukaryotic genomes are organized into chromatin to compact DNA. The basic unit of chromatin is the nucleosome that consists of 147 base pairs of DNA wrapped in approximately two superhelical turns around a histone octamer composed of two heterodimers of histone H2A-H2B and a histone hetero-tetramer (H3-H4)₂ (Luger et al., 1997). Histones in principal consist of two functional and structural distinct folds, the flexible N-terminal tail and the histone fold. The histone fold is composed of three α -helices, which are connected by two loops (α 1-L1- α 2-L2- α 3) (Luger et al., 1997). The nucleosome core particle is based on protein-protein and protein-DNA interactions. The histones form dimer pairs that assemble via an interaction of the histone folds in a head-to-tail-arrangement in the characteristic handshake manner (Arents et al., 1991). The assembled octamer contacts the nucleosomal DNA at its entire length. The histone folds interact with the DNA minor groove at the inner site of the supercoil (Luger et al., 1997). The DNA entry and exit sites are exclusively organized by the N-terminus of H3.

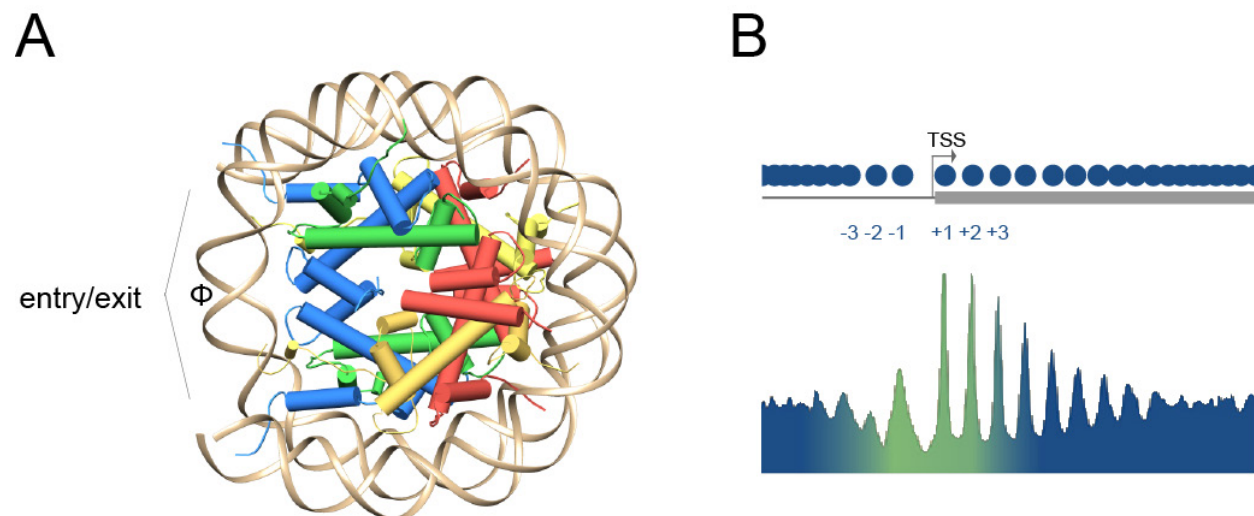


Figure 1. The basic unit of chromatin, the nucleosome. A) Structure of the fly nucleosome core particle (PDB:2pyo, (Clapier et al., 2008)). Histones are colored: H2A, yellow; H2B, red; H3, blue and H4, green and depicted as pipes. The dyad axis (ϕ) and DNA entry/exit sites are indicated. B) The nucleosomal (blue circles) distribution at yeast promoters and genes. Peaks represent consensus distribution of nucleosomes relative to transcription start site (TSS). Green indicates high degree of H2A.Z, acetylation, H3K4 methylation and phasing. Figure adapted from (Pugh, 2013).

The nucleosome core particle is the repetitive unit of nucleosomal arrays defining the 11 nm structure (“bead on a string”). The linker histone H1 further compacts the arrays in the condensed 30 nm chromatin fiber (Robinson et al., 2006), which is then further compacted in the highest order chromosome (Felsenfeld and Groudine, 2003). The packaging into chromatin obviously impedes fundamental DNA-dependent nuclear processes that require free access to genomic information as DNA replication, repair and transcription. A dynamic chromatin environment is generated by (i) remodeling of nucleosomes, (ii) chemical modification of histones or incorporation of variants, (iii) non-histone DNA binding proteins and (iv) non-coding RNAs.

Chromatin remodelers are versatile tools that catalyze a broad range of chromatin changing reactions including sliding of an octamer across the DNA (nucleosome sliding), changing the conformation of nucleosomal DNA and changing the composition of the octamers (histone variant exchange). Histone variants differ from the canonical histones in their primary sequence. They show different physiochemical properties compared to canonical histones and can alter protein-protein and protein-DNA interactions thereby changing the chromatin structure (Billon and Cote, 2012). Two major variants of histone H3 have been studied extensively, the centromer specific CenH3 and H3.3. Variants of H2A are much more abundant in number, including H2A.X and H2A.Z (Zlatanova and Thakar, 2008), which are required for cell stability and viability (Redon et al., 2002). H2A.X is phosphorylated upon DNA damage by DNA-activated protein kinases from the phosphatidylinositol 3-kinase-related kinases (PIKKs) family that mediate DNA damage response. H2A.Z associates with actively transcribed chromatin (Stargell et al., 1993). H2A.Z shares only 60% sequence identity with the canonical H2A, but is conserved within higher eukaryotes (Jackson et al., 1996). Major differences within H2A.Z are in the C-terminal docking domain that organizes the penultimate 10 bp of the DNA (Shukla et al., 2011) and in the acidic patch that is involved in the interaction with interacting proteins as for instance the viral latency-associated nuclear antigen (LANA) peptide (Barbera et al., 2006; Luger et al., 2012). The overall crystal structure of a H2A.Z containing nucleosome is similar to the crystal structure of a nucleosome containing canonical histones, but the interaction between the histone pairs is subtly destabilized (Suto et al., 2000). However, further studies could not

unambiguously clarify, if H2A.Z promotes destabilization or stabilization of chromatin (Abbott et al., 2001; Fan et al., 2002; Placek et al., 2005; Thambirajah et al., 2006; Zhang et al., 2005). The interaction between the acidic patch of H2A.Z and the N-terminus of H4 increases intramolecular folding of nucleosomal arrays (Fan et al., 2002). Nucleosome arrays are interrupted by nucleosome free regions (NFR), which normally contain the promoter sequences. The nucleosomes flanking the array are referred as -1 and +1 nucleosomes (Bernstein et al., 2004; Jiang and Pugh, 2009; Yuan et al., 2005). The -1 nucleosome is followed by a NFR, the 5' NFR and then the transcriptions start site (TSS). Among all genome wide distributed nucleosomes, the +1 is the tightest positioned or phased nucleosome (Mavrich et al., 2008). The combination of histone variants H2A.Z and H3.3 in one nucleosome lead to the most unstable state of chromatin (Jin and Felsenfeld, 2007) and H2A.Z incorporated in the +1 nucleosome was suggested to destabilize this region to accelerate gene activation (Guillemette et al., 2005; Jin and Felsenfeld, 2007; Li et al., 2005; Meneghini et al., 2003; Zhang et al., 2005). The stabilization could also be influenced by post-translational modifications on H2A.Z (Billon and Cote, 2012) and by the number of H2A.Z incorporated per nucleosome. A nucleosome that contains two copies of H2A.Z-H2B dimers was more unstable than one with only one copy (Luk et al., 2010; Weber et al., 2010).

To establish a dynamic chromatin environment specific variants are incorporated into the nucleosome by specialized ATP-dependent remodeling complexes.

3.2 Swi2/Snf2 remodelers

In general, chromatin remodelers are versatile molecular machines that use the energy of ATP hydrolysis in order to disrupt protein-protein or protein-nucleic acid contacts. The motor domain that creates this chemo-mechanical force is a Swi2/Snf2 ATPase. The Snf2 protein was originally discovered to regulate mating type switching (SWI) and sucrose fermentation (Sucrose Non Fermenting) (SNF) by a genetic screen and was subsequently identified as the catalytic subunit of the SWI/SNF complex (Sudarsanam and Winston, 2000). Members of the

Snf2 family are characterized by seven helicase-related sequence motifs, which were found in DExx box helicases (Eisen et al., 1995) (Figure 2).

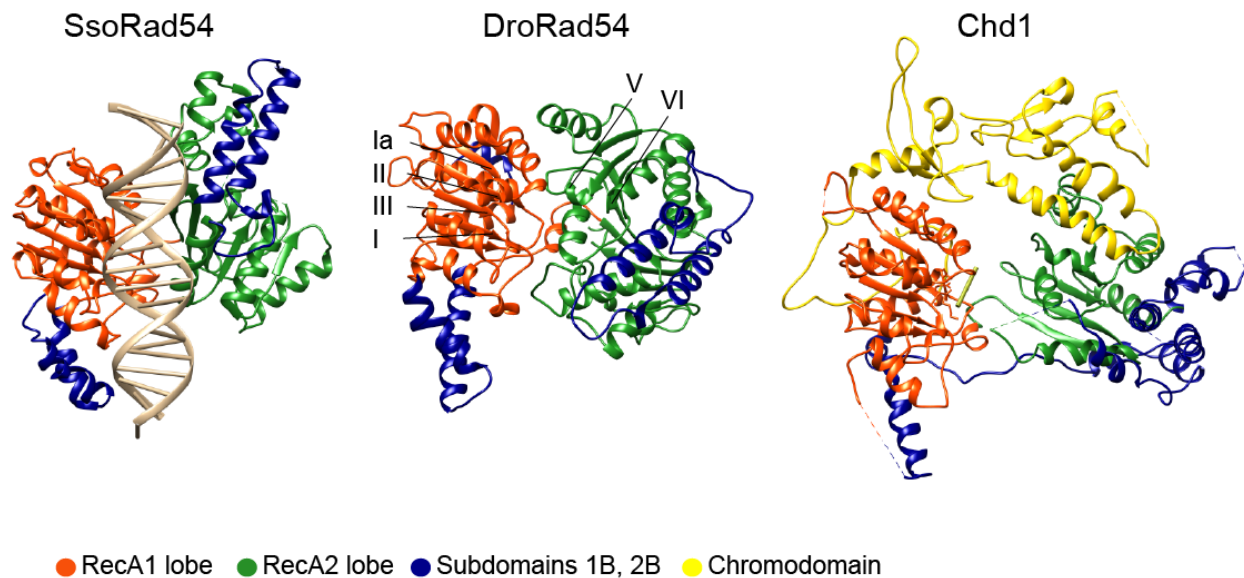


Figure 2. Swi2/Snf2 ATPases. Structures of the Swi2/Snf2 ATPase domain of Rad54 in complex with DNA (beige) from *Solifolubus solfataricus* (SsoRad54; PDB: 1Z63 (Durr et al., 2005)), *Danio rerio* (DroRad54; PDB: 1Z3I (Thoma et al., 2005)) and of Chd1 (PDB: 3MWY (Hauk et al., 2010)) from *Saccharomyces cerevisiae* were depicted. In droRad54 the canonical helicase motifs I, II, III, IV, V and VI are indicated. The chromodomain of Chd1 contacts both ATPase lobes and occupies the DNA binding cleft.

The Snf2 ATPases are assigned to the superfamily 2 (SF2) of helicase-related proteins that also includes DEAD box RNA and DNA helicases or innate immune sensors (Fairman-Williams et al., 2010). In general, SF2 enzymes show a similar two lobed structure consisting of two RecA-like domains, termed RecA1 and RecA2 (DExx and HELICc). Enzymes of the SF2 share canonical helicase specific sequence motifs, which mediate closure of the central cleft, ATP binding and hydrolysis (Figure 2) (Gorbalenya and Koonin, 1993; Hauk et al., 2010). Upon closing and aligning, these motifs are poised for productive DNA or RNA binding along the central cleft (Jankowsky et al., 2011). Substrate binding might also activate the enzyme. The Chd1 remodeler was crystallized in an inactive open state (Hauk et al., 2010), where an acidic helix of the chromodomains blocked the DNA binding site (Figure 2). Duplex DNA and ATP were shown to bind in this cleft of the Snf2 protein Rad54 from *Sulfolobus solfataricus* (Sso) (Durr et al., 2005). A structural switch in the SsoRad54 could lead to translocation along the DNA. This screwing motion could disrupt or remodel protein-DNA interfaces.

The Snf2 ATPase folds have been shown to mediate the remodeling reaction of multi-subunit chromatin remodelers. The ATPase binds to nucleosomal DNA and provides the major ATP hydrolysis activity (Cote et al., 1994; Shen et al., 2000) and thus delivers energy to the core remodeling reaction.

3.3 Chromatin remodelers

Chromatin remodelers are classically divided into 4 families: SWI/SNF, ISWI (imitation switch), Mi-2/CHD (chromodomain-helicase-DNA-binding) and INO80 (inositol auxotroph mutant 80).

The SWI/SNF family is the best structural characterized family of large remodelers. They catalyze several remodeling events depending of the chromatin context including sliding and eviction of the octamers (Clapier and Cairns, 2009, 2012; Gangaraju and Bartholomew, 2007). Electron microscopy (EM) studies on members of the SWI/SNF as RSC (remodel the structure of chromatin), the human homolog PBAF and the SWI/SNF complex itself are available (Asturias et al., 2002; Chaban et al., 2008; Dechassa et al., 2008; Leschziner, 2011; Leschziner et al., 2005; Leschziner et al., 2007; Skiniotis et al., 2007; Smith et al., 2003). The RSC and PBAF complex are globular complexes with a C-shaped architecture and an obvious binding pocket that could accommodate a nucleosome (Chaban et al., 2008; Leschziner, 2011; Leschziner et al., 2005). In the structure of a RSC-nucleosome complex the density could not account for the complete nucleosome and the authors suggested that the remodeling activity of the complex could have partially disrupted the nucleosome particle (Chaban et al., 2008). Despite the presence of several conserved subunits including actin related proteins 7 and 9 (Arp) the structure of the RSC-related SWI/SNF remodeler is somewhat different and has no obvious nucleosome binding groove, but it was proposed that it could occur at a large depression (Dechassa et al., 2008; Smith et al., 2003).

The ISWI/ACF (ATP dependent chromatin-assembly factor) remodelers contain two to four subunits and are thus smaller than the SWI/SNF family complexes (Clapier and Cairns, 2009; Gangaraju and Bartholomew, 2007). In contrast to the SWI/SNF family that randomizes

arrays, ISWI remodelers evenly space nucleosomes and are implicated in gene silencing and condensation. In addition to their catalytic Swi2/Snf2 ATPase, ISWI remodelers also contain auxiliary domains and subunits. The HAND-SANT-SLIDE domain is located C-terminally of the ATPase in flies ISWI (Grune et al., 2003). SANT-SLIDE domains recognize linker DNA and nucleosomes and target the complex to the substrate. How ISWI remodelers space nucleosomes is still under debate. One model suggests that the ISWI is bound to two nucleosomes simultaneously and pulls them together until its helical linker-DNA-binding domain-SLIDE-SANT prevents further movement and thus works as a molecular ruler (Yamada et al., 2011). In the other scenario each of the two ISWI protomers take turns in moving the nucleosome on either side with the protomer at the longer linker DNA translocating more efficiently and frequently (Blosser et al., 2009; Racki et al., 2009).

CHD and Mi-2 remodelers have characteristic N-terminal tandem chromodomains reviewed in Seeber et al., 2012. Interestingly, in Chd1 the chromodomains contact the Swi2/Snf2 ATPase lobes and thereby disrupt the DNA engagement (Hauk et al., 2010). This keeps Chd1 in an auto-inhibited state that could be released by nucleosomal DNA binding. The chromodomains target Chd1 to lysine 4-methylated H3 tails, which is a hallmark of actively transcribed chromatin (Flanagan et al., 2005). In contrast, Chd3 or Chd4 are members of the Mi-2/NURD complex (nucleosome remodeling deacetylase) that deacetylates chromatin and thus represses transcription (Seeber et al., 2013b). CHD1 complex has various functions and was shown to assemble, slide and space nucleosomes (Lusser et al., 2005; Stockdale et al., 2006). It can even incorporate the histone variant H3.3 *in vivo* (Konev et al., 2007).

3.4 The INO80/SWR1 family

The INO80 family includes following complexes: INO80 and SWR1 (sick with rat8 or SWI/SNF related) in *Saccharomyces cerevisiae* (*S. c.*); INO80, SRCAP (Snf2-related CBP activator protein) and p400 in mammals and INO80 and p400 in *Drosophila melanogaster* (*D. melanogaster*) (Table 1) (reviewed in (Bao and Shen, 2011; Billon and Cote, 2012; Morrison and Shen, 2009)). INO80/SWR1 are involved in various chromatin related processes (see 3.5) and contribute to the genome wide distribution of the histone variant H2A.Z (Kobor et al., 2004; Mizuguchi et al.,

2004; Papamichos-Chronakis et al., 2011). According to the dogma, SWR1 incorporates H2A.Z while INO80 evicts H2A.Z in a unidirectional and stepwise manner. Both complexes show a strong preference for the -1 and +1 nucleosome flanking the NFR (Yen et al., 2012; Yen et al., 2013). The NFR is sufficient to target SWR1 and histone acetylation has a positive effect on this recruitment. The cooperative relationship was shown to be a hierarchical one (Ranjan et al., 2013). Higher eukaryotic SRCAP and p400 have been shown to harbor H2A exchange functions, too (Kusch et al., 2004; Ruhl et al., 2006). The p400 subunit is associated with the Tip60 complex, which is an acetyltransferase. This relationship physically merges the yeast SWR1 with the NuA4 (nucleosomal acetyltransferase of H4) histone acetyltransferase complex (Auger et al., 2008; Billon and Cote, 2012; Doyon et al., 2004).

Table 1 Homologous INO80, SWR1 and SRCAP complexes. Subunits of the INO80 and SWR1 complex were assigned in homologous features from *S. cerevisiae* and *Homo sapiens*. Conserved domains were identified by pFAM search. Used abbreviations: BAF53A, BRG1-associated factor 53A; CCDC95, coiled-coil domain-containing 95; DMAP1, DNA methyltransferase 1-associated protein 1; GAS41, glioma amplified sequence 41; MCRS1, microspherule protein 1; NFRKB, nuclear factor related to kB-binding protein; SRCAP, SNF2-related CBP activator protein; Swc, SWR1 complex; UCH37, ubiquitin C-terminal hydrolase 37; XPG, xeroderma pigmentosa group G; Yaf9, yeast AF9; YEATS, Yaf9, ENL, AF9, Taf14, Sas5; YY1, yin yang 1; Znf-HIT1, zinc finger-His triad protein 1. The table was adapted from (Morrison and Shen, 2009).

Subunit type	INO80 complex		SWR1 complex	
	<i>S. cerevisiae</i>	<i>Human</i>	<i>S. cerevisiae</i>	<i>Human</i>
Swi2/Snf2 ATPase	Ino80	INO80	Swr1	SRCAP
RuvB-like	Rvb1 and Rvb2	RUVBL1 and RUVBL2	Rvb1 and Rvb2	RUVBL1 and RUVBL2
Actin	Act	β-Actin	Act	β-Actin
Actin related proteins	Arp4, Arp5 and Arp8	BAF53, Arp5 and Arp8	Arp4 and Arp6	BAF53 and Arp6
YEATS	Taf14	-	Yaf9	GAS41
YL-1	Ies6	IES6	Swc2	YL1
PAPA-1	Ies2	IES2	-	-
DNA binding subunit (domain)	Nhp10 (HMG-box)	YY1 (Zn-finger C ₂ H ₂)	Swc3 (SANT/myb)	XPG (H3TH)
Non conserved	Ies1, Ies3, Ies4, Ies5	Amida, CCDC95, FLJ20309, MCRS1, NFRKB, UCH37	Bdf1, Swc3 - 7	DMAP1, GAS41, tubulin, Znf-HIT1

The INO80 family is evolutionary conserved owing to the high degree of homology in the Swi2/Snf2 ATPase containing subunits, which share the unique insertion loop between the

RecA1 and RecA2 domains. The INO80 and SWR1 remodelers are both large multi-subunit complexes with at least 14 components. This class of chromatin remodelers has been the structurally most obscure.

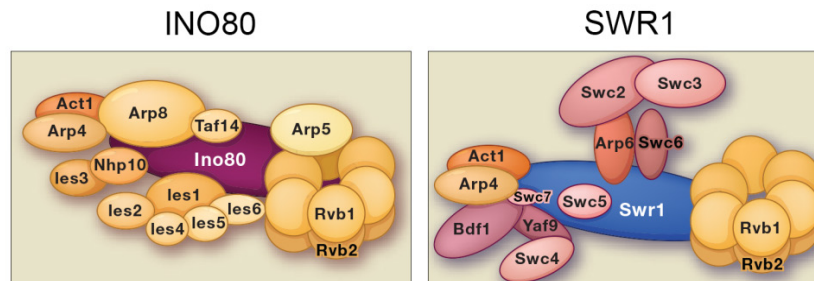


Figure 3. Composition of INO80 and SWR1. Subunit organization of the budding yeast INO80 and SWR1 is depicted with the state of knowledge before this study. The Ino80 and Swr1 subunits are the assembly platforms for the specific sub-complexes. The figure was adapted from (Bao and Shen, 2011).

The N- and C-terminal regions of yeast Swr1 recruit the Bdf1-Arp4-Act-Swc4-Yaf9-Swc7 module (N-module) and Swc3-Swc2-Arp6-Swc6-Rvb1/2 (C-module), respectively (Wu et al., 2005; Wu et al., 2009) (Figure 3). The composition of INO80 is described in detail below. Deletion of the insertion of the split ATPase of Swr1 lead to a loss of Rvb1/2 (RuvB-like) (Wu et al., 2005). In addition to the Rvb1/2, the SWR1 and INO80 complexes share Arp4, Act (Actin1) and some domains (Table 1).

3.5 INO80 complex

3.5.1 The components of the INO80 complex

The INO80 complex is involved in various DNA mediated processes and has been identified in yeast, flies, plants and mammals (Ebbert et al., 1999; Fritsch et al., 2004; Jin et al., 2005; Klymenko et al., 2006; Shen et al., 2000). INO80 was initially identified as the transcriptional regulator of inositol-responsive gene expression (Ebbert et al., 1999). Further characterizations revealed that INO80 also plays central roles apart from transcription specifically in DNA repair, DNA damage checkpoint response and chromosomal DNA replication (Bao and Shen, 2007).

The budding yeast *S. c.*, INO80 complex has a molecular mass of 1.3 MDa and consists of 15 subunits: the Swi2/Snf2 subunit Ino80, Rvb1 and Rvb2, Act, Arp4, Arp5 and Arp8 (actin related protein), Taf14 (TBP associated factor 14), Nhp10 (non-histone protein 10), Ies1-Ies6 (Ino eighty subunits) (Shen et al., 2000; Shen et al., 2003).

The Ino80 subunit not only harbors the DNA translocase activity, but also provides a recruiting platform for its additional subunits. The HSA (helicase SANT associated) domain in the N-terminus of Ino80 is essential for forming a complex with Arp4, Arp8 and Act (Shen et al., 2003; Szerlong et al., 2008). In general, remodelers that contain Act and/or Arps include a HSA domain in the core ATPase subunit. The HSA domain selectively binds to the specific Arps that are part of the respective complex (Szerlong et al., 2008). Arp4 and Arp8 are involved in histone interactions and Act has been associated with binding to extranucleosomal linker DNA (Gerhold et al., 2012; Harata et al., 1999; Kapoor et al., 2013; Saravanan et al., 2012). The HSA^{Ino80}-Arp4-Arp8-Act subcomplex and its components, Arp4 and Arp8 prefer binding to the (H3-H4)₂ tetramer over the H2A-H2B dimer (Gerhold et al., 2012). Apart from the function as chromatin binding modules, Arp4 and Arp8 have been shown to impair Actin filament growth and to depolymerize F-Actin sequestering monomeric Actin for incorporation into INO80 (Fenn et al., 2011). Once incorporated in INO80, HSA^{Ino80}-Arp4-Arp8-Act can nucleate Actin filaments. Thus, Arps regulate Actin dynamics in the context of chromatin remodeling.

Taf14 was identified to negatively influence Actin organization, thus it was previously named actin non-complementing 1 (ANC1) (Welch and Drubin, 1994). Taf14 is a member of various multi-subunit complexes, as TFIID, TFIIF, Mediator, NuA3, SWI/SNF, RSC and INO80 (Schulze et al., 2010). It comprises a YEATS domain at the N-terminus and a C-terminal domain, which is responsible for binding to transcription and remodeler complexes (Schulze et al., 2010). Although the precise role in those complexes is unknown, the YEATS domain of Yaf9, a subunit of the SWR1 complex is similar to that of the histone chaperone Asf1 (Wang et al., 2009). In addition, Yaf9 interacts with histones H3 and H4 that is in agreement with a histone chaperone function.

Nhp10 is a member of the HMG (High Mobility Group) family (Ray and Grove, 2009, 2012). Nhp10 consists of two HMG-boxes, which is followed by an acidic patch. In general, HMG-boxes are composed of three α -helices that form an L-shaped fold and bind primarily in the minor groove of DNA bending it towards the major groove (Allain et al., 1999; Klass et al., 2003; Love et al., 1995; Masse et al., 2002; Stott et al., 2006; Stros, 2010). HMG-box proteins are DNA binders that show a strong affinity for non-canonical DNA substrates (Stros, 2010). The *in vivo* DNA binding sites are still mostly unknown and are likely to represent DNA structures. Nhp10 has been recently observed to bind to distorted DNA and DNA ends *in vitro* (Ray and Grove, 2009, 2012) and it binds to a cognate motif (RCCGGGGA) situated in the NFR (Badis et al., 2008). Reb1 that is found at promoters and mediates gene activation or repression through transcription factors mirrors the genome wide distribution of Nhp10 and Ies5 (Badis et al., 2008; Yen et al., 2013).

The Ies1, 3, 4 and 5 subunits are yeast specific subunits and are not sequence conserved in other eukaryotes. Instead, metazoan INO80 contains specific subunits as the deubiquitinating enzyme Uch37 or the less characterized Amida (Chen et al., 2011; Yao et al., 2008) (Table 1). Human, fly and fission yeast (*Saccharomyces pombe*) INO80 share a GLI-Kruppel zing finger containing subunit, named YY1 (Ying-Yang 1), Pleiohomeotic and Iec1 (Ino eighty complex), respectively (Cai et al., 2007; Hogan et al., 2010; Klymenko et al., 2006; Wu et al., 2007). Ies2 and Ies6 are conserved in eukaryotes. Ies6 contains an YL-1 domain that is also found in Swc2 of SWR1. Swc2 is enriched in charged amino acids. A feature that is typically found in histone chaperones and indeed Swc2 preferentially binds to the histone variant H2A.Z over H2A (Wu et al., 2005). Furthermore, loss of Ies6 resulted in increased ploidy and chromosome missegregation (Chambers et al., 2012). Ies2 contains a less well characterized PAPA-1 domain (Pim-1-associated protein-1 (PAP-1)-associated protein-1) that seems to be important for protein interactions (Kuroda et al., 2004).

Rvb1 and 2 are AAA+ ATPases (ATPase associated with diverse cellular activities) and are eukaryotic homologues of the bacterial DNA dependent helicase RuvB (Putnam et al., 2001; Yamada et al., 2001). AAA+ ATPases form oligomeric complexes, often hexamers, therefore the

complex will be referred as Rvb1/2 (reviewed in (Jha and Dutta, 2009)). Rvb1 and 2 are highly conserved across species and have a unique molecular architecture among AAA+ ATPases: domains 1 and 3 fold back to form the ATPase core and domain 2 is attached via a long flexible hairpin-shaped linker composed of two β -sheets (Matias et al., 2006). Parts of domain 2 resemble the single strand binding protein RPA (replication protein A), which is thus referred as oligonucleotide binding domains (OB) (Matias et al., 2006). Rvb1/2 is involved in various processes and a component of several large nucleic acid metabolic complexes including INO80, SWR1 and TIP60/NuA4 (Jha and Dutta, 2009). Furthermore, Rvb1/2 represses transcription via cMyc/Miz-1 (Wanzel et al., 2005) and Polycomb, β -catenin, and nuclear factor (NF)- κ B (Bauer et al., 2000; Diop et al., 2008; Kim et al., 2005). In addition, Rvb1/2 is involved in small nucleolar ribonucleolar protein (snoRNPs) assembly (Jha and Dutta, 2009). Rvb1/2 is associated with a multiplicity of processes and complexes and structure function analysis could not clarify their molecular role in these so far. They have been extensively studied in an isolated state, though the organization of the protomers is controversially discussed. It is not clear, if Rvb1/2 form hetero- or homo-hexamers and if they are associated in hexameric or dodecameric complexes within the respective protein assemblies (Cheung et al., 2010; Gorynia et al., 2011; Gribun et al., 2008; Lopez-Perrote et al., 2012; Matias et al., 2006; Niewiarowski et al., 2010; Puri et al., 2007; Torreira et al., 2008).

Deletion of Rvb1 and Rvb2 from INO80 resulted in the loss of Arp5 and indicating that Arp5 forms a complex with Rvb1/2 (Jonsson et al., 2004). The deletion of Arp5 prevented H2A.Z exchange and resulted in increased levels of this histone variant (Yen et al., 2013). The conserved subunits, Ies2, Ies6, Arp5 and Rvb1/2 bind to the C-terminus of human Ino80 including the Swi2/Snf2 ATPase and metazoan specific components were associated with the N-terminal part (Chen et al., 2011). A detailed topology of the subunits was however missing.

3.5.2 The chromatin remodeling complex INO80 is involved in DNA processing and metabolism

Faithfull repair of DNA lesions is essential for genome integrity and the survival of a cell. Therefore, DNA repair pathways and cell cycle checkpoints are crucial. In eukaryotes, double strand breaks (DSBs) are repaired mainly by two pathways: Non-homologous end-joining (NHEJ) and homologous recombination (HR) (Harper and Elledge, 2007). In NHEJ the DNA strands are tethered and directly religated after processing of DNA ends resulting in potentially mutagenic changes. In contrast, HR is error-free as the sister chromatids are used as templates. Both pathways are dependent on the central repair machinery, the Mre11:Rad50:Nbs1 (MRN) complex. MRN together with other factors creates resection to single-stranded DNA (Mimitou and Symington, 2008) and activates ATM (ataxia telangiectasia mutated) kinase. Rad50 can bridge other MR complexes via dimerization and thereby promote homology search and strand invasion (de Jager et al., 2001; Hopfner et al., 2002).

In response to DNA damage the histone variant H2A.X is rapidly phosphorylated on its C-terminus (referred as γ -H2A.X) at places surrounding the damage by the PIKK family kinases ATM and ATR (ATM- and Rad3-related) (Burma et al., 2001; Ward and Chen, 2001). Yeast has no identical histone variant but show analogous modification of histone H2A. γ -H2A.X serves as docking sites for several DNA damage response proteins including INO80 and SWR1 complexes (Downs et al., 2004; Fernandez-Capetillo et al., 2004; Morrison et al., 2004).

The yeast INO80 complex has already been implicated early in DNA repair (Shen et al., 2000). Indeed, the INO80 complex is recruited to HO endonuclease-induced DSB at the mating type locus in yeast (Morrison et al., 2004; van Attikum et al., 2007; van Attikum et al., 2004). The specific interaction between Ino80 and γ -H2AX in turn is dependent on Nhp10 as the recruitment of the INO80 complex to DSB site was compromised in a *nhp10* deletion strain (Morrison et al., 2004). A sub-complex comprising Nhp10 and Ies3 was indicated as the INO80 complex from strains lacking Nhp10 showed not only reduced γ -H2AX but also decreased Ies3 binding (Morrison et al., 2004). Arp4 has been shown to physically interact with γ -H2AX (Downs et al., 2004). At the DSB INO80 is involved in the nucleosome eviction and thereby supports

association of DNA repair factors and downstream events (Tsukuda et al., 2005; van Attikum et al., 2007). SWR1 conversely is not evicting nucleosomes surrounding the DSB (van Attikum et al., 2007). A likely model is that the DSB and its DNA overhang mimic a NFR and thus INO80 is recruited through this common structural motif.

The DNA repair pathways function cooperatively with the S-phase DNA damage response checkpoint that orchestrates DNA replication and allow re-entry into the cell cycle when lesions are repaired. DNA replication machinery is stalled when encountering a DNA lesion. A stalled replication fork can collapse and cause DNA damage (Branzei and Foiani, 2008). The INO80 complex associates with stalled replication forks induced by DNA damaging agents and regulates its efficient progression (Papamichos-Chronakis and Peterson, 2008; Vincent et al., 2008). The SWR1 complex is not enriched at replication origins and complex mutations have no influence on viability (Mizuguchi et al., 2004). The exact role of INO80 at replication forks is not understood so far. It seems, however that INO80 together with the ISW2 remodelers and γ H2A.X cooperatively mediate replisome integrity (Vincent et al., 2008).

3.5.3 INO80 mediates checkpoint pathways

Cell cycle checkpoints coordinate stalling and progression of DNA mediated processes and are predominately controlled by three PIKK family kinases: ATM, ATR and DNA-PK (DNA-dependent protein kinase). ATM and DNA-PK respond primarily to DNA double strand breaks, whereas ATR reacts to replisome stability and origin firing (Cimprich and Cortez, 2008). In the canonical signaling ATR is recruited to RPA covered ssDNA via ATRIP (ATR-interacting protein) or LCD1 in yeast. ATR and ATRIP form a stoichiometric complex also without a DNA damage signal (Ball et al., 2005; Unsal-Kacmaz and Sancar, 2004). The recruitment of ATR-ATRIP to stalled replication forks or DNA lesions alone is not sufficient for activation but requires TOPBP1 (topoisomerase-binding protein 1) (Kumagai et al., 2006). TOPBP1 is recruited via modified 9-1-1 (Rad9-Hus1-Rad1) complex (Delacroix et al., 2007). Once activated, ATR phosphorylates serine and threonine residues followed by a glutamine residue (S/TQ) of hundreds of proteins, but one of

the key players is Chk1 (checkpoint kinase 1), which modulates entry into mitosis (Liu et al., 2000).

The Ies4 subunit of the INO80 complex is also a target of ATR and its phosphorylation modulates DNA replication checkpoint response (Morrison et al., 2007). INO80 is therefore acting downstream of checkpoint activation and is needed for increased global chromatin mobility, which can be advantageous for the cell in promoting homology search in HR (Neumann et al., 2012; Seeber et al., 2013a). Mutations of Ies4 residues mimicking constitutive phosphorylation showed elevated S phase checkpoint activation resulting in decreased viability when treated with DNA damaging agents. The viability of yeast H2A.Z mutants was decreased when nucleotide levels were diminished indicating a role of H2A.Z in DNA damage response (Mizuguchi et al., 2004). As a direct target of ATM and ATR, γ -H2A.X is enriched at DNA lesions. Arp5 promotes the accumulation of γ -H2AX in human cells and in addition *Arabidopsis* Arp5 is required to acquire resistance to DNA damaging agents (Kandasamy et al., 2009; Kitayama et al., 2009). Nhp10 and Arp4 also contribute to recruitment of INO80 to γ -H2A.X (Downs et al., 2004; Morrison et al., 2004). Histone variants including γ -H2A.X and H2A.Z could thereby form a platform for INO80 recruitment, which then could directly function at the hazardous DNA site.

Various aspects of INO80's function have been elucidated; however the structural framework remains mainly unclear. Large and low abundant complexes are difficult to crystallize, thus an integrative structural approach contributes to the understanding of their structure and function relationship.

3.6 Hybrid approaches help to dissect the molecular architecture of large complexes

Hybrid methods refer to a combination of structural techniques to determine the molecular structure of complexes. Low resolution data is thereby typically complemented with additional low or high resolution information of larger assemblies. NMR (nuclear magnetic resonance) and X-ray crystallography are used to produce high resolution data. In traditional NMR, the size is

limited to approximately 40 kDa covering either only domains or small protein complexes. The major obstacle for X-ray crystallography is that diffracting protein crystals are required. If atomic structures are available, they can be docked into low resolution SAXS (small angle X-ray scattering) or EM (electron microscopy) shapes allowing a pseudo-atomic interpretation. SAXS allows to study the molecule in solution in a native environment (Petoukhov and Svergun, 2013). Cryo EM structures are also derived from molecules in a quasi native vitreous ice environment. EM is not limited by size, but rather the bigger the complex the better it is suitable for EM (Lander et al., 2012). The newest add-on into the hybrid toolbox is the combined approach of chemical cross-linking and mass spectrometry (XL-MS) analysis.

XL-MS was already developed more than 10 years ago (Young et al., 2000). Further advances in high end mass spectrometers and modified cross-linkers improved this technique and enabled the assessment of macro molecular complexes (Leitner et al., 2012b). The aim of this technique is to identify two sites that are in spatial proximity and thereby infer structural information from the molecule. For this, a covalent bond is formed by a chemical reactive compound that connects either two proximate residues from a single or between two polypeptide chains. The cross-linked peptides are then analyzed and identified by a mass spectrometer. The covalent bond between two polypeptide chains, termed inter-link or between one chain, termed intra-link is not the only reaction product. The bi-functional cross-linker (two reactive groups) can be bound to only one site in the protein and the second group is hydrolyzed. Such a link is referred as mono-link. Typically cross-linkers with two reactive sites and good leaving groups connected via a linker are used. Commonly cross-linkers react with the primary amino group of lysines. This amino acid is a good target due to its high prevalence in proteins. Active esters as N-hydroxysuccinimidyl or sulfosuccinimidyl are good reagents with high reaction rates for coupling. To facilitate the analysis, the cross-linker includes features as stable isotope labels, affinity tags or distinct fragmentation patterns (Leitner et al., 2012b). The isotopic feature facilitates identification of cross-linked peptides among the large majority of unmodified fragments and thereby reduces the search space and helps with the interpretation of the data (Rinner et al., 2008). Identification of cross-linked sites by MS allows the identification of novel binding partners, of protein-protein interaction sites or even enables to

build complete interaction maps. Beyond, XL-MS reveals the position of spatial proximity between polypeptide chains. Therefore, this technique provides intermediate resolution structural data, which is perfectly suited to build larger macro molecular assemblies, which are not amenable for crystallization from single protein atomic coordinates. For instance, the initiation factor, TFIIF could be oriented on the RNA polymerase II core complex (Chen et al., 2010) and the register of the coiled-coils and the organization of the tetramerization domain of Ndc80 could be determined (Ciferri et al., 2007; Ciferri et al., 2008). The structural restraints can also be used to complement moderate resolved EM shapes (Rossmann et al., 2005) and thus further restrain the fitting of X-ray structures. For example, building of a complete model of the molecular architecture of the chromatin modifier, PRC2 (polycomb repressive complex 2) was assisted by protein-protein cross-links that refined the fitting of available high resolution crystal structures into a low resolution EM structure (Ciferri et al., 2012).

Cross-linking data thus provides a bridge in space between high resolution and low resolution coordinates. In addition, the cross-linker catches conformational heterogeneity in a native environment and therefore expands the snapshots gained by X-ray structures. The structural constraints also help to design optimized constructs for improved crystallization of proteins and protein sub-complexes. Furthermore, the cross-linking data can be integrated in molecular modeling approaches to further constrain the conformational space of atomic models (Alber et al., 2008).

Single structural techniques are strong by themselves; however the complete big picture can only be tackled by a combination of them. In this study, a hybrid approach was used to elucidate the molecular architecture of INO80 (Tosi et al., 2013). EM and XL-MS were combined to zoom in for a close-up picture gaining molecular contact points.

4 Results

4.1 Reconstitution of a nucleosome

Nucleosomes consist of nucleosomal DNA wrapped around a histone octamer core particle containing histones H2A, H2B, H3 and H4 (Luger et al., 1997). The histone variant H2A.Z is highly conserved. In *D. melanogaster* the homologue of H2A.Z is H2A.v (van Daal and Elgin, 1992), which is a hybrid combining features of H2A.X and H2A.Z. H2A.v was cloned for reconstitution of an H2A.v containing nucleosome. Genes of canonical histones were codon-optimized. Canonical histones and H2A.v from *D. melanogaster* were expressed in *E. coli* BL21 Star (DE3) cells and purified under denaturing conditions. Histones were enriched by SP cation exchange and DNA was removed by Q anion exchange chromatography (Figure 4A). All four canonical histones were purified successfully; however, the H2A.v variant could not be sufficiently enriched (Figure 4B). In order to improve expression level and ultimately the purity of H2A.v a codon-optimized gene will be used in future studies. Octamers composed of canonical histones (Figure 4C) as well as of the histone variant H2A.v (Figure 4D) were reconstituted and octamers were separated from smaller molecular weight species by size exclusion chromatography. The canonical octamer showed stoichiometric presence of all histones (Figure 4E), but the H2A.v containing octamer failed to reconstitute properly (Figure 4F).

Nucleosomes were reconstituted with diverse DNAs using salt-gradient dialysis (Figure 4G). A DNA sequence covering the TSS to 359 bp downstream of the *INO1* gene was used to reconstitute *INO1* nucleosomes. These nucleosomes were shown to have alternative positioning sites and *INO80* locally re-mobilize nucleosomes along this DNA (Ford et al., 2007). In addition, core nucleosome as well as off-centered and centered nucleosomes were reconstituted with DNA overhangs of 40 and 20 bp or none (Figure 4G). To correctly position the octamer the 601 positioning sequence was included (Huynh et al., 2005; Lowary and Widom, 1998).

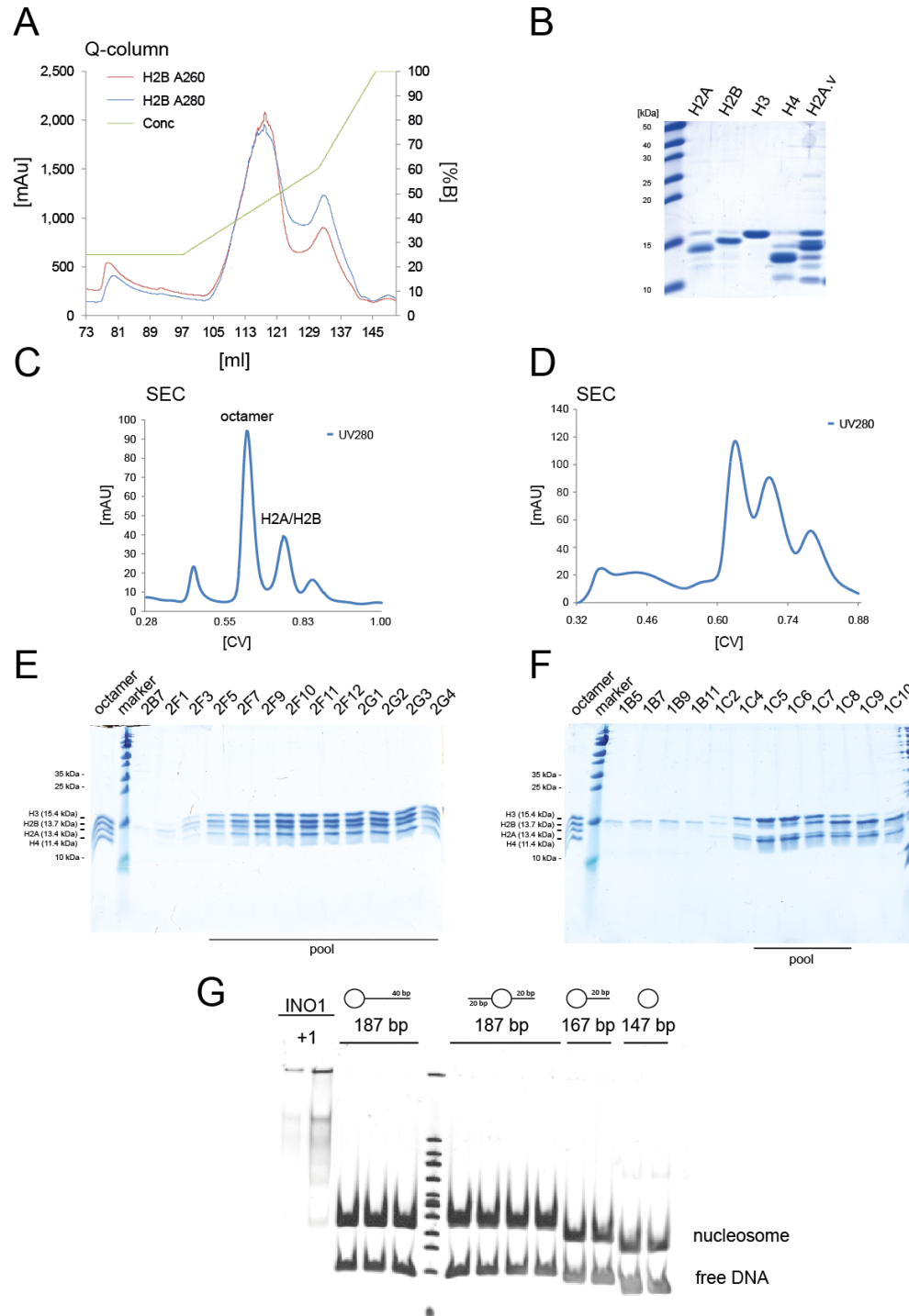


Figure 4 Reconstitution of nucleosomes. A) Histones were purified by cation- and anion-exchange chromatography. Depicted is chromatogram of the cation-exchange chromatography of H2AB. B) All canonical histones were sufficiently enriched despite the variant H2A.v showed a high degree of impurities. C and D) Size exclusion chromatography of the canonical octamer (C) and the octamer composed of the histone variant H2A.v. E and F) SDS-PAGE showing the size exclusion chromatography of the canonical octamer (E) and the H2A.v containing octamer (F). G) Reconstituted nucleosomes were analyzed by native gel electrophoresis.

4.2 A novel purification procedure of INO80 improves complex homogeneity

The previously described purification of the INO80 complex (Shen, 2004; Shen et al., 2000) yielded not sufficiently enriched and homogenous INO80 for structural analysis. This protocol only included one immunopurification step via a FLAG tag. In our hands INO80 purified according to this protocol was contaminated with over 300 proteins. The most identified proteins were heat shock proteins and DNA associated factors as the RSC remodeler. Indeed, the preparation was contaminated with DNA and DNA could be a scaffold for contaminations. To reduce the DNA associated with INO80, we included polytron shearing and sonication to fragment the DNA. During optimization of buffer conditions and other modifications in the purification protocol, a planetary ball mill was used to crack the yeast cells under freezing conditions. To up-scale and increase the yield of INO80, bead-beaters were used allowing cell lysis of up to 500 g yeast cells simultaneously. For both cell lysis methods the chromatin fragmentation was assessed and DNA was fragmented to a length of 500 – 2,000 bp. (Figure 5A).

Subsequently, the cell lysate was cleared by centrifugation and sticky proteins were removed by pre-clearing the lysate with unspecific protein G beads. The INO80 complex was immunopurified with M2 FLAG-beads (Sigma-Aldrich) and eluted from beads by FLAG-peptide (Figure 5B). As INO80 was not quantitatively pulled-out of the lysate, the beads were re-incubated with the lysate over night. This step increased the yield of up to 100% (Figure 5B).

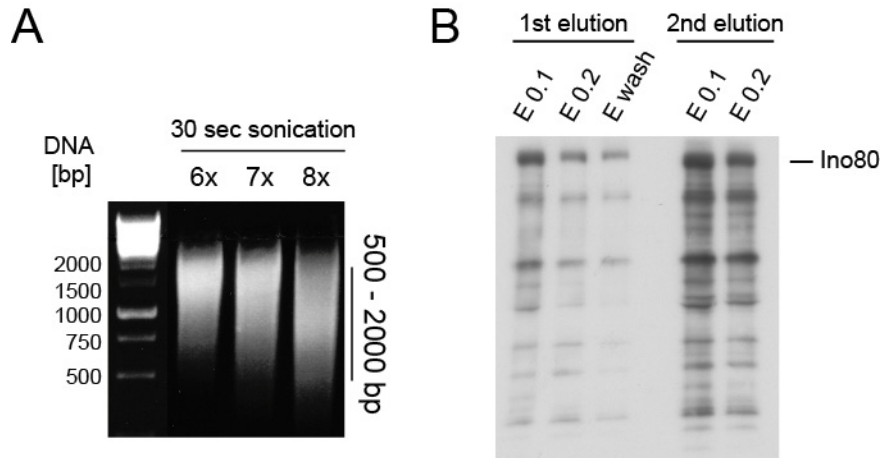


Figure 5 Chromatin assessment and optimization of elution of INO80-FLAG. A) Chromatin was fragmented using shearing by polytron and sonication for up to 8 rounds of sonifying for 30 s. Total DNA was isolated and the degree of fragmentation was analyzed on a native PAGE. B) INO80 was pulled-out of the lysate using the FLAG-tag and eluted by FLAG-peptide. Re-incubation of affinity beads after elution increased the yield of purified INO80.

To remove DNA and contaminations from the crude INO80 purification, it was required to further purify INO80. It was not possible to concentrate INO80 using conventional Amicon centrifugal filters, since INO80 aggregated on the membrane. In order to concentrate INO80, stringent elution from different chromatography materials (Heparin, cation- (S) and anion- (Q) exchange chromatography) was assessed. INO80 bound to the Heparin material quantitatively eluted at 360 mM KCl (Figure 6A and B). However, the elution peak was broad and stringent washing with salt was not possible due to early elution of the complex. INO80 did not quantitatively bind to cation exchange chromatography material, but was detected in the flow through (Figure 6 C and D). In contrast, INO80 was binding quantitatively to anion exchange chromatography material. The appropriate salt concentrations were tested by the stepwise increase of the KCl concentration in 10% steps (80 mM). INO80 eluted at 520 mM (40% of high-salt buffer) from the Q-material in sharp peaks and thus high protein concentration (Figure 6E - G). In addition, the elution at high salt concentrations allowed stringent washing conditions with lower salt concentrations.

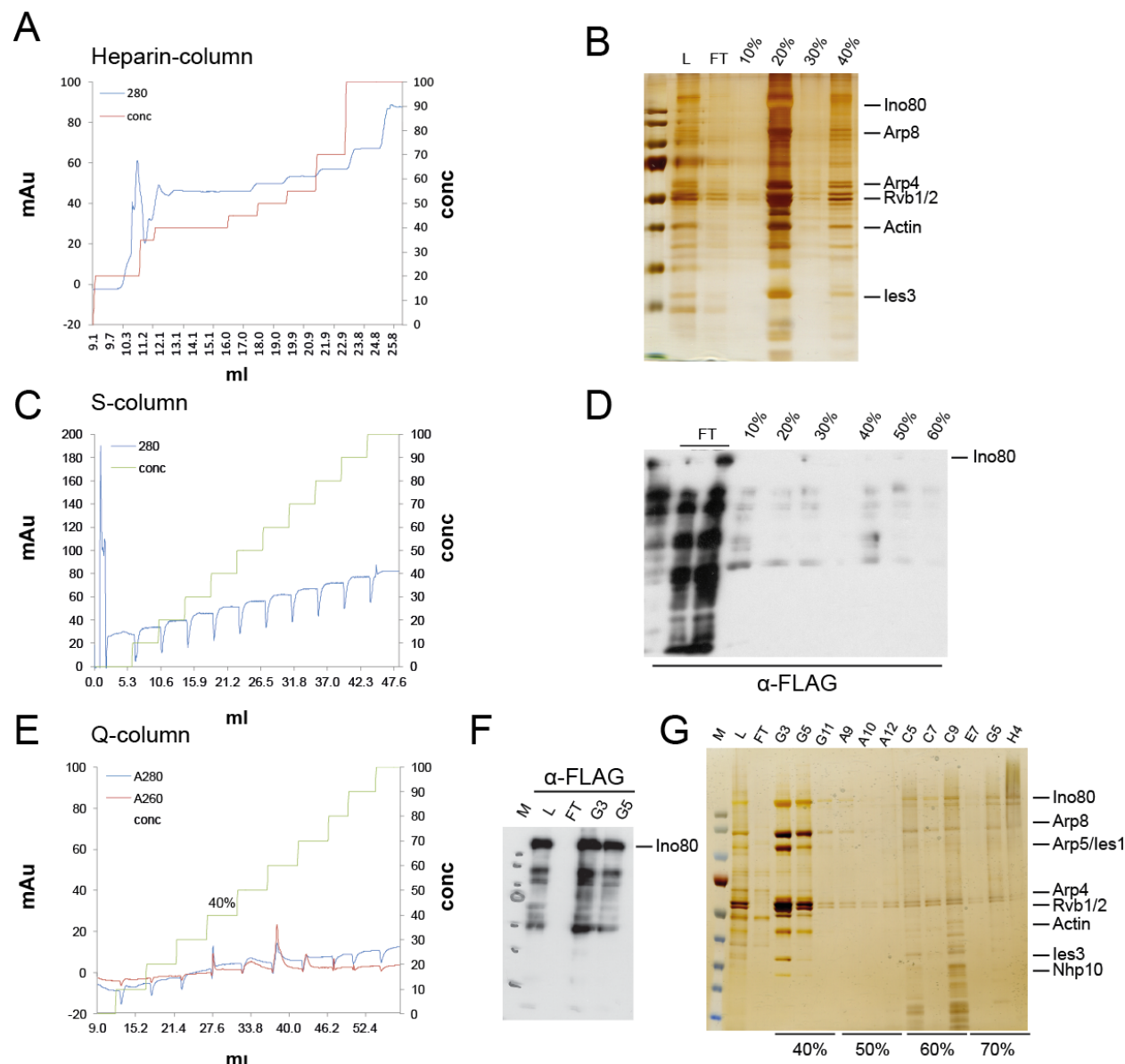


Figure 6 Testing Heparin, cation- and anion-exchange chromatography to improve purity of INO80. A and B) INO80 was applied (L = load) onto a Heparin column and was eluted by stepwise increasing the KCl concentrations in 10% steps (10%=280 mM KCl; 20%=360 mM KCl; 30%=440 mM KCl; 40%=520 mM KCl; 50%=600 mM KCl and 60%=680 mM KCl). INO80 eluted from the Heparin column at 360 mM KCl (20%). The early elution prevented stringent washing to remove contaminants, hence INO80 showed a heterogeneous composition. Fractions were analyzed by SDS-PAGE and silver-staining. C and D) INO80 did not bind quantitatively to S-material. Consistently, INO80 was detected in the flow-through (FT). Fractions were analyzed by Western-blot and an antibody was used against the FLAG-tag of the Ino80 subunit. E- G) INO80 bound to the Q material and eluted from it at 520 mM KCl (40%). DNA contaminated INO80 eluted at 680 mM KCl (60%, fractions C5-9). Thus DNA free INO80 could be separated from chromatin bound INO80. Smear bands are an indication for DNA contaminations. (G). Fractions were analyzed by SDS-PAGE and Western-blot.

The final protocol included a washing step with 400 mM KCl before elution of INO80 with 600 mM KCl from the anion exchange material (Figure 7A). In order to optimize the

concentration of INO80, the elution peak was separated in smaller 60 μ l fractions. The 680 mM salt concentration step (60%) contained chromatin associated INO80 and consequentially a heterogeneous INO80 sample (Figure 6G). In conclusion, this stepwise gradient not only removed contaminations and separated INO80 from INO80 bound to DNA, but also concomitantly yielded highly concentrated INO80 without using centrifugal concentrators.

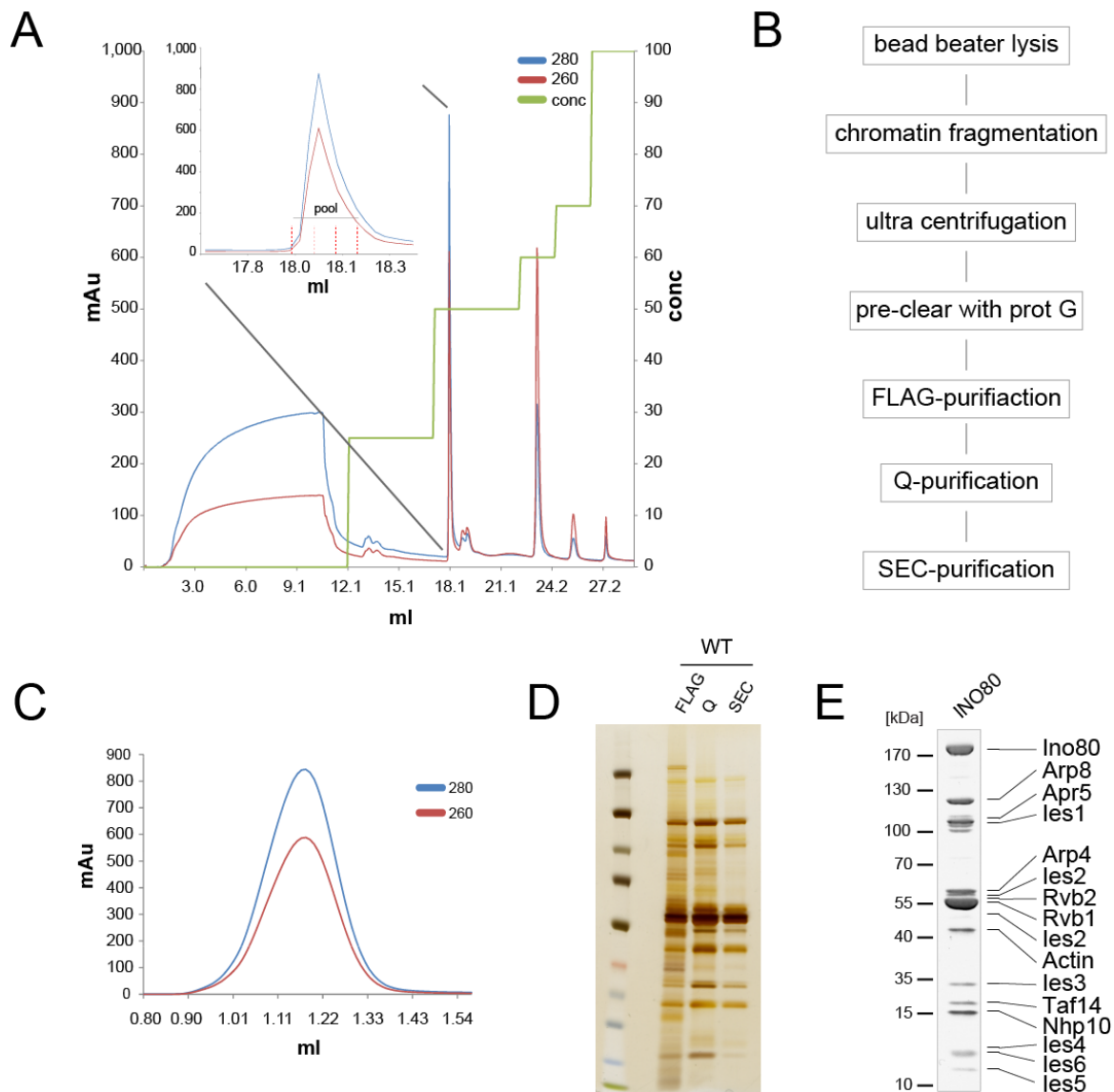


Figure 7 Optimized purification protocol of the INO80 complex. A) Typical elution profile of INO80 from a MonoQ column. Prior to elution INO80 was washed with 25% high salt buffer containing 400 mM KCl. INO80 eluted at 600 mM KCl (50%) in a sharp peak. Fractionation in 60 μ l steps allowed collection of all INO80 containing fractions without losing the concentration effect. B) Workflow of novel purification protocol: INO80 was purified by FLAG immunopurification, anion-exchange (Q) and size exclusion (SEC) chromatography. C) INO80 was directly applied to a Superose 6 column and eluted in a symmetric and monodisperse peak. D and E) INO80 purified by FLAG, Q and SEC were analyzed by SDS-PAGE and silver- and colloidal Coomassie staining. All subunits of INO80 were present and could be assigned to the respective bands.

For cross-linking and mass spectrometry analysis it is a prerequisite to have a monodisperse sample. Otherwise it is impossible to differentiate between cross-links between two complexes that were linked due to aggregation or cross-links found within one complex. Therefore, INO80 was further purified by size exclusion chromatography (Figure 7B and C). INO80 eluted from the anion exchange column was directly applied to a small size exclusion column with a bed volume of 2.4 ml (Figure 7C). INO80 eluted in a single symmetric peak and did not contain any aggregated INO80.

INO80 was highly enriched by FLAG, anion-exchange and size exclusion chromatography (Figure 7D). All INO80 subunits were present with the reported stoichiometry (Shen et al., 2000). However, a quantification of subunits was not possible due to the different sizes of INO80 members (13 -171 kDa) and Coomassie staining of protein is dependent on the size and amino acid composition.

To stabilize INO80 for EM, INO80 was mildly cross-linked with glutaraldehyde. The cross-linked INO80 was then again applied on a size exclusion chromatography and eluted once more in a monodisperse peak with no sign of aggregation. Covalent linking of all subunits was accomplished as INO80 did not separate in a SDS-PAGE.

In summary, this novel purification enabled a preparation of INO80 to near homogeneity with high concentrations within two days.

4.3 Nanobodies against the INO80 complex

Antibodies from *Camelidae* are composed of only one heavy chain and they recognize the antigen via the variable domain known as, nanobody or V_HH (Hamers-Casterman et al., 1993). The lack of the light chain marks them as the smallest integer antigen-binding-fragment (Muyldermans et al., 2001). The heavy-chain-only antibody is easy to clone, can be expressed in *Escherichia coli* and has similar antigen binding affinities as conventional antibodies (Arbabi Ghahroudi et al., 1997). The aim was to generate a nanobody against INO80 to purify INO80

without any tag from wild-type yeast, which is accessible in large amounts for low costs. In addition, the nanobodies are planned to be used to assist crystallization of sub-complexes or even the whole complex (Rasmussen et al., 2011).

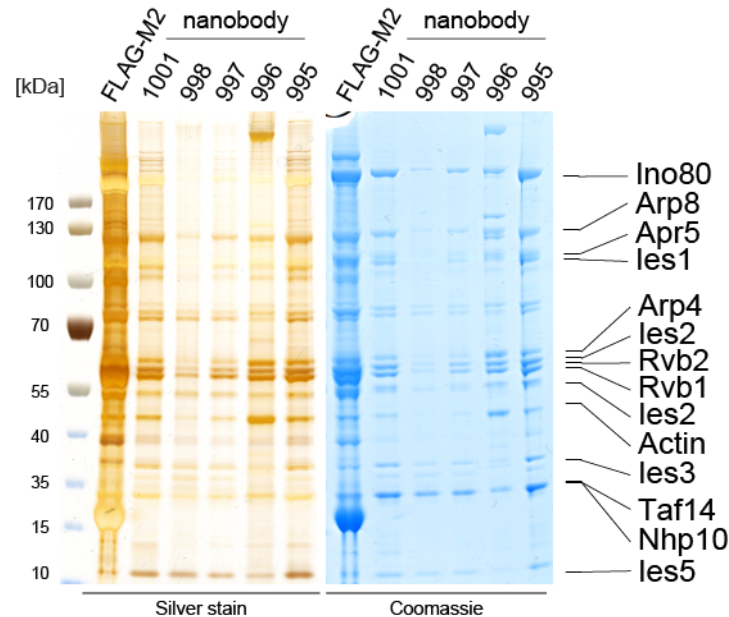


Figure 8 Nanobodies specifically pull out the INO80 complex. INO80 was immunoprecipitated from an *Ino80-FLAG* cell lysate by the commercial available FLAG-M2 agarose or by different clones of nanobodies (1001, 998, 997, 996 and 995) that have been shown to be positive in ELISAs. The INO80 complex was eluted from the beads and was analyzed by SDS-PAGE and silver- and Coomassie staining.

Nanobodies against INO80 have been obtained by immunization of alpacas with glutaraldehyde fixed INO80, Arp8-Arp4-Act-les4-HSA^{Ino80}, Nhp10-les3-les5, yeast Arp5-les6, human Arp8 (38-624) and Arp5-les6. Binders were panned by INO80 and selected by ELISA (enzyme-linked immunosorbent assay) screening. Six positive clones were obtained and tested against binding to Arp8-Arp4-Act-HSA^{Ino80}, yeast Rvb1/2 and Arp5-les6 by ELISA. If at all Arp5-les6 showed a weak signal. In order to characterize the binding of the nanobody candidates to the INO80 complex, the nanobodies were tested for immunoprecipitation of INO80 from an *Ino80-FLAG* strain. In the first trial, all six nanobodies pulled-out the INO80 complex with the same composition and stoichiometry of subunits as the commercial available FLAG-M2 agarose (Sigma-Aldrich) (Figure 8). Although the binding appeared to be less strong compared to the FLAG-M2 beads, the nanobodies pulled-out INO80 with a higher purity (especially clone 1001

and 995). Due to different coupling efficiency of the nanobodies to the beads, the immunoprecipitated quantity of INO80 is not really comparable between the nanobodies and the FLAG-M2 agarose. But decreased amounts pulled out with nanobodies can easily be compensated by simply using more nanobody coupled beads, because of the low production price.

In summary, nanobodies have been obtained that specifically immunoprecipitate an entire and stoichiometric INO80 complex. In future this can be used to adapt the purification protocol and circumvent the use of commercial FLAG-M2 agarose beads and genetically modified yeast. This brings several advantages including cheaper purification, usage of large wild-type cell amounts and they might promote crystallization of sub-complexes and of INO80. Furthermore, INO80 purified by nanobodies even shows a higher degree of purity. Future studies will show, if INO80 could be purified in large amounts from an endogenous source by nanobodies to have enough material to thoroughly screen for proper crystallization conditions.

4.4 Assessment of the activity of the purified INO80

To test, whether the novel purification preserved the activity of INO80, remodeling assays and ATPase were performed (Tosi et al., 2013). INO80 was shown to mobilize and equally space nucleosomes (Shen et al., 2003; Udugama et al., 2011). INO80 acts at *INO* genes; therefore we used nucleosomes reconstituted with a DNA sequence based on *INO1* (Ford et al., 2007). Indeed, INO80 could re-distribute octamers along the *INO1* DNA with increasing concentrations of INO80 (Figure 9A). This reaction was ATP-hydrolysis dependent as INO80 failed to mobilize nucleosomes in the presence of the non-hydrolysable ATP analog AMP-PCP or the transition state analog ADP-BeF_x.

INO80 was reported to have DNA and nucleosome induced ATPase activity and the nucleosome stimulated the ATPase activity two-fold more than DNA (Shen et al., 2000; Udugama et al., 2011). However, Shen et al. had to treat their samples with DNase before DNA stimulation was observed, as their prepared INO80 contained contaminating DNA. Our purified

INO80 showed basal ATPase activity (Figure 9B). A 356 bp long DNA fragment that was used to reconstitute INO1 nucleosomes stimulated the ATP hydrolysis rate about 4-fold more. INO1 nucleosomes resembling native chromatin even increased the ATPase activity 2-fold more than DNA stimulated complex (Tosi et al., 2013).

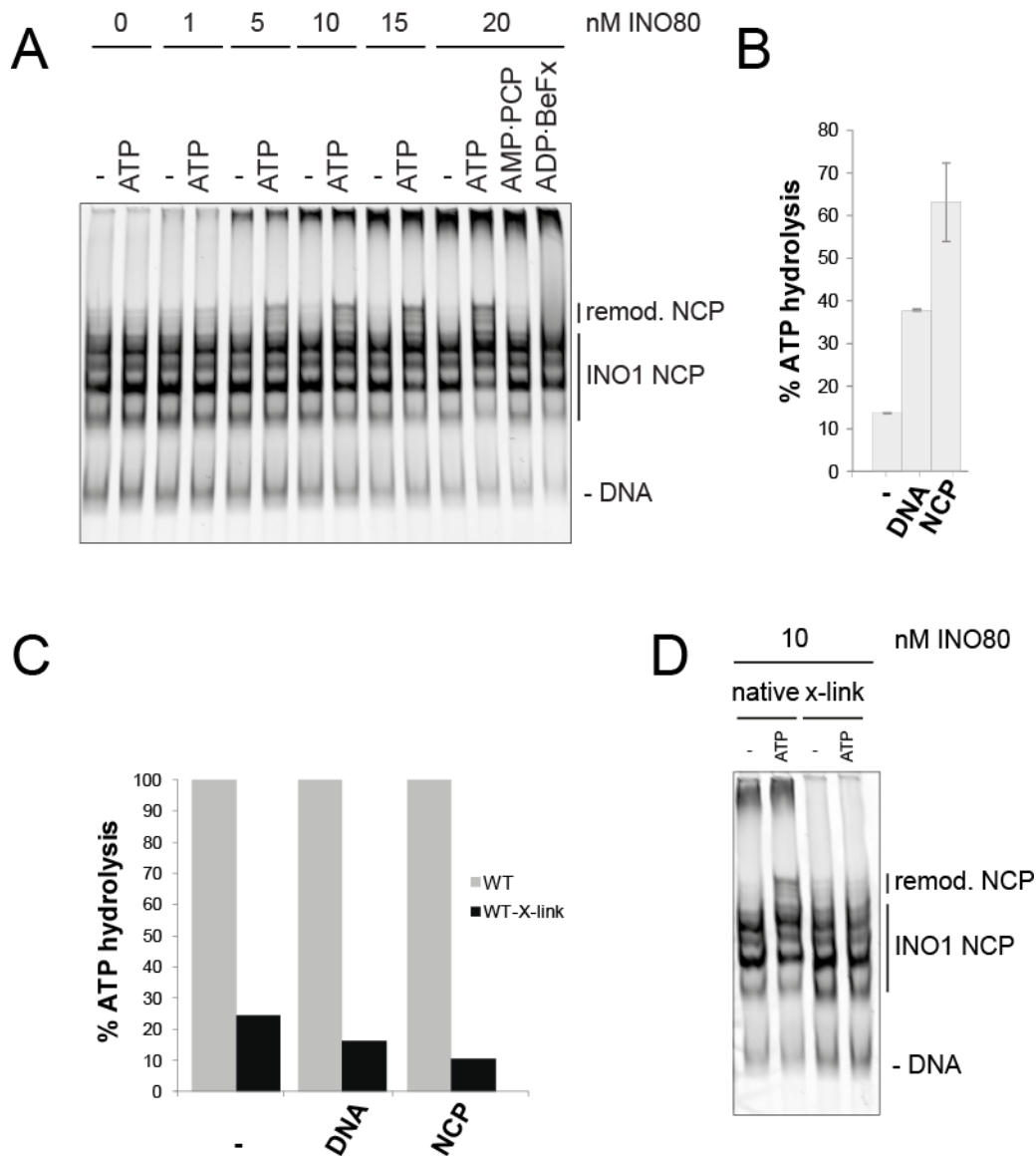


Figure 9 Purified INO80 exhibited ATPase and nucleosome remodeling activity. A) INO80 was able to mobilize nucleosomes of INO1 chromatin in the presence of ATP. Remodeling efficiency was concentration dependent. Non-hydrolysable ATP (AMP-PCP) or transition state (ADP-BeFx) analogs prevented nucleosome re-distribution. Remodeling reactions were analyzed by native PAGE. B) ATPase assay showed that INO80 had basal ATP hydrolysis activity, which was stimulated by DNA and INO1 nucleosomes (NCP). ATPase reactions were quantified and presented relative to ATPase hydrolysis rates of alkaline phosphatase. Data are represented as mean standard deviation. C and D) Fixation with glutaraldehyde reduced but not abolished ATPase and remodeling activity by INO80.

To test if cross-linking of INO80 with glutaraldehyde influenced native activity of INO80, we tested remodeling and ATPase activity of fixed INO80. Unexpectedly, cross-linking was not completely abolishing ATPase and remodeling activity (Figure 9 C and D). Glutaraldehyde reacts majorly with lysines and therefore potentially might distort the active site of enzymes (Migneault et al., 2004). The residual ATPase activity might originate from any of INO80's ATPase.

The novel purification procedure of INO80 yielded highly active and DNA free INO80 that is suitable for structural and biochemical characterization.

4.5 Chemical cross-linking and mass spectrometry analysis of the INO80 complex

4.5.1 Mapping of subunit interactions by cross-linking and mass spectrometry

The architecture of INO80-type remodelers was only based on genetic studies and was not complete. In order to increase the resolution and unravel the entire topology of INO80, we used the XL-MS analysis (Figure 10) (Tosi et al., 2013). The appropriate concentration of the isotopically labeled cross-linker DSS was assessed by a titration of the cross-linker to INO80 (Figure 11A). We analyzed four experiments and cross-linked INO80 with 1.5x, 3x, 3.5x DSS. This resulted in 534 intra-links and 217 inter-links, whereas 212 and 116 unique intra- or inter-links could be assigned (Tosi et al., 2013).

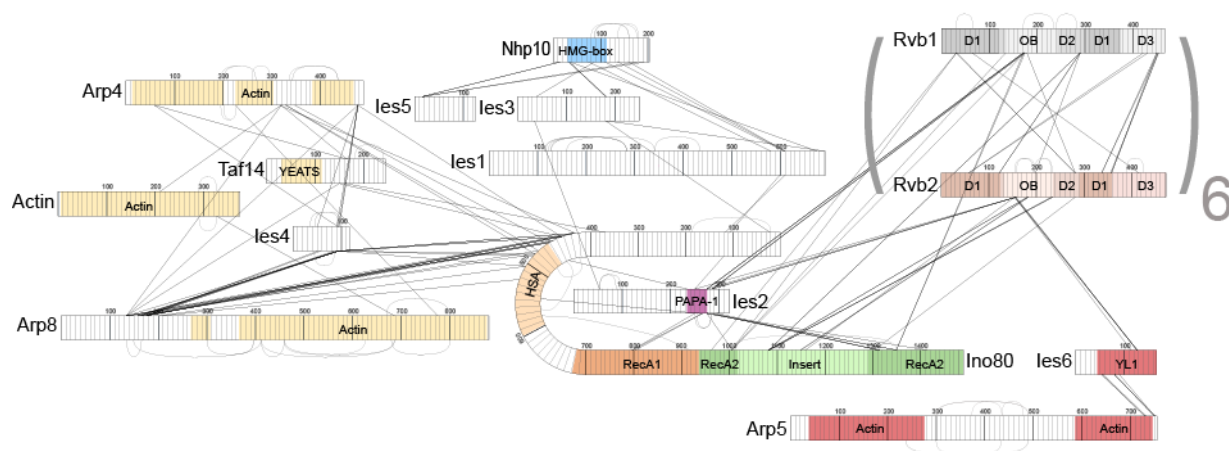


Figure 10 Interaction map of the INO80 complex. XL-MS revealed the topology of INO80. Intra-links with a minimum of 30 amino acids are depicted in grey. Ino80 (HSA (dark yellow), RecA1 (orange), insertion and RecA2 (light and dark green)) and les2 (pink) were a scaffold for Nhp10-les1-les3-les5 (blue), Arp8-Arp4-Act-les4-Taf14 (yellow), Rvb1/2 (grey and coppery) and Arp5-les6 (red) sub-complexes. The Figure was adapted from (Tosi et al., 2013).

The cross-linker can be understood as a molecular ruler and the Euclidean distance of a cross-link pair is measured between C_{α}^- C_{α} . The distance restraint for DSS was reported to be ≤ 30 Å (Herzog et al., 2012; Jennebach et al., 2012; Leitner et al., 2012b; Leitner et al., 2010). To validate the cross-linking approach, distances were estimated in available crystal structures, however structural information on INO80 subunits is limited. Atomic coordinates of yeast Actin (Vorobiev et al., 2003), Arp4 (Fenn et al., 2011) and human and yeast Arp8 (Gerhold et al., 2012; Saravanan et al., 2012) were accessible. The crystal structure of human full-length Rvb1 was available (Matias et al., 2006). Yeast and human Rvb1 share a sequence identity of almost 70%. The atomic coordinates of yeast Rvb1 and Rvb2 were modeled based on the crystal structure of human Rvb1. The sequence coverage of paralogous yeast Rvb1 and Rvb2 was only about 40%, nevertheless, the modeled yeast Rvb2 matches almost perfectly the OB-fold deleted structure of human Rvb2 (3UK6) (Petukhov et al., 2012) with a root mean square deviation (rmsd) of 0.791 Å. In general, the ATPase motor domains of Snf2 enzymes are highly conserved. To estimate the cross-links in the Ino80 Swi2/Snf2 domain crystal structures of *Danio rerio* (*Dro*) (Thoma et al., 2005) and *Sulfolobus solfataricus* (Durr et al., 2005) Rad54 were compared with each other. *Dro* and *Sso* Rad54 share a sequence identity of only ~28% to each other and also to the Snf2 domain of Ino80. However, the corresponding lobes of *Dro* and *Sso* individually matched with good rmsds of ~1.05 Å (Tosi et al., 2013).

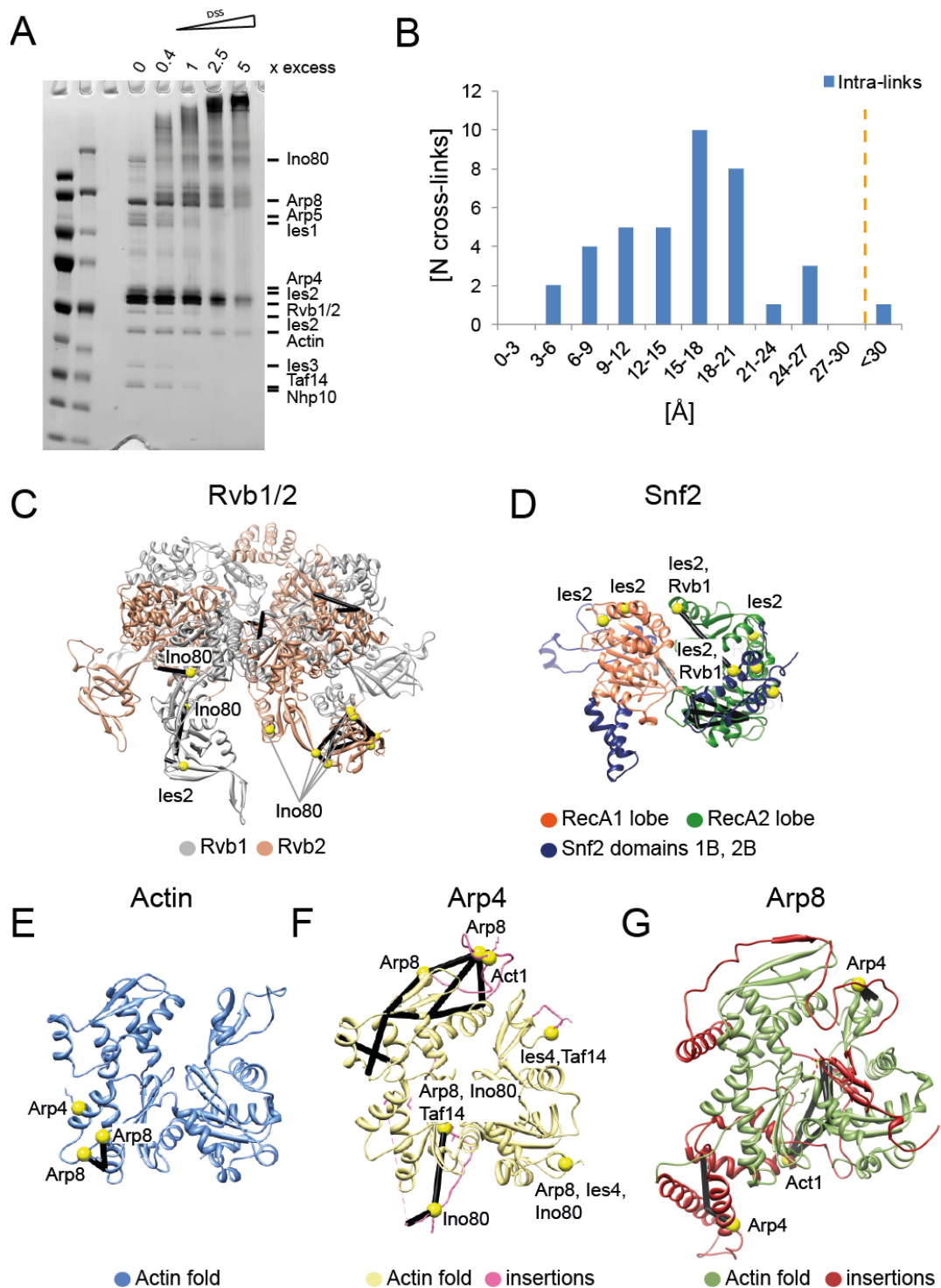


Figure 11 Titration of the cross-linker and assignment of intra-links. A) INO80 was incubated with increasing molar excess of DSS over concentration of lysines. Cross-linked and untreated complexes were separated by SDS-PAGE and visualized by silver staining. INO80 was cross-linked and analyzed by MS with DSS 1.5x - 3.5x over lysines. B) Euclidean distances of intra-links were measured in modeled yeast Rvb1/2 (C), homologous DroRad54 (Durr et al., 2005) (D) and available crystal structures: yeast Actin (Vorobiev et al., 2003) (E), Arp4 (Fenn et al., 2011) (F) and Arp8 (Saravanan et al., 2012) (G). Non-redundant cross-links were categorized in distance ranges. C-G) Intra-links were depicted in black and interface residues and corresponding interaction partners are colored in yellow. The Figure was adapted from (Tosi et al., 2013).

In general, the intra-links measured in available crystal and modeled structures were fulfilled (Figure 11B - G) (Tosi et al., 2013). Both crystal structures of *Dro* and *Sso* Rad54 fulfilled the distant restraints of the intra-links. Most cross-links averaged between 15 - 18 Å. A similar distance was observed before to be suitable for linking formation (Leitner et al., 2012b). However, one link in Arp4 was over the introduced distance cut-off of 30 Å (Herzog et al., 2012; Leitner et al., 2012b) with 32.1 Å, but corresponding residues were situated in a loop just before a crystallographic unresolved region.

The majority of the intra-links satisfied distance constraints of the cross-linker validating the XL-MS approach.

4.5.2 Subunit topology and structural modules of INO80

All subunits of INO80 were assigned by XL-MS. Interestingly, cross-links clustered within four sub-complexes: Rvb1/2, Arp5-les6, Nhp10-les1-les3-les5 and Arp8-Arp4-Act-les4-Taf14 assembled at the scaffolds les2 and Ino80 (Figure 10) (Tosi et al., 2013).

It was well established that Rvb1/2 form a stable complex (Cheung et al., 2010; Gorynia et al., 2011; Gribun et al., 2008; Lopez-Perrote et al., 2012; Niewiarowski et al., 2010; Petukhov et al., 2012; Puri et al., 2007; Torreira et al., 2008) and indeed they were highly interconnected. The C-terminus of Arp5 exclusively cross-linked to the YL-1 domain of les6, which in turn cross-linked to the OB-fold of Rvb2. Deletion of Rvb2 consistently resulted in the loss of Arp5 in purified INO80 deletion mutants (Jonsson et al., 2004). Rvb1/2 cross-linked to the RecA2 and to the insertion loop of Ino80 as well as to the uncharacterized PAPA-1 domain. Linkages were mostly found in the domain 2 of Rvb1/2. In agreement with this, complexes of Rvb1/2 and Arp5-les6 could be recombinantly expressed and purified (Figure 12 A).

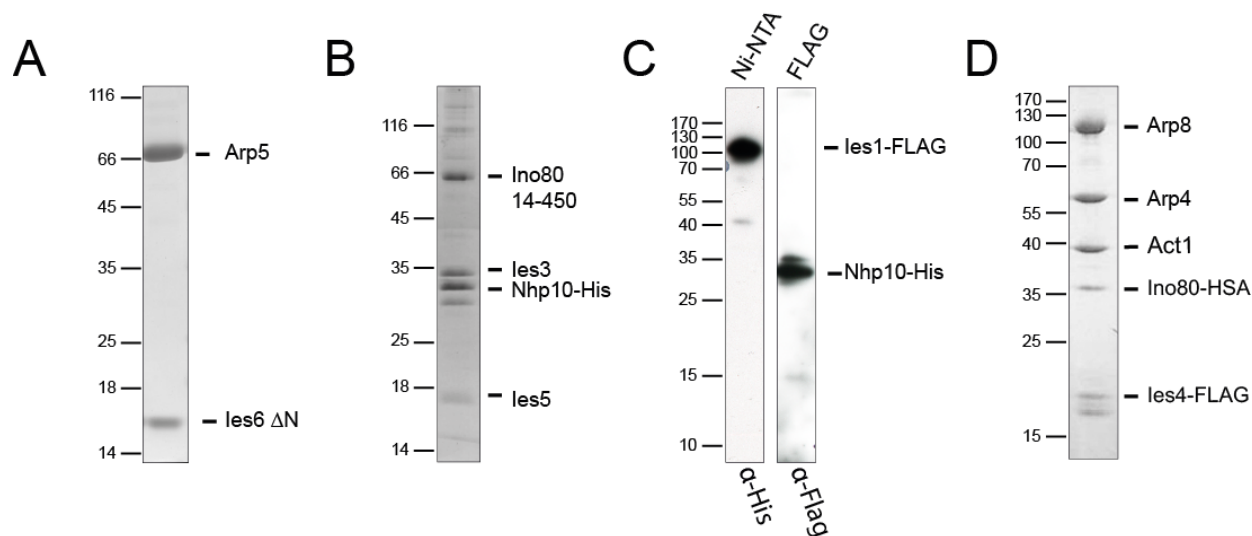


Figure 12 XL-MS completed sub-complex assignment. Recombinantly expressed and purified sub-complexes were analyzed by SDS-PAGE and Western-Blot analysis. A stable sub-complex consisting of Arp5-les6 (A) and Nhp10-les3-les5-Ino80¹⁴⁻⁴⁵⁰ could be purified and visualized by Coomassie staining. C) Nhp10-les3-les5-Ino80¹⁴⁻⁴⁵⁰ recruited les1 and vice versa shown by Western-blot analysis. D) Arp8, Arp4, Act, HSA and les4 formed a stable complex. Figure was adapted from (Tosi et al., 2013).

The Nhp10 sub-complex consists of Nhp10, les1, les3 and les5, which in turn cross-linked to the N-terminus of Ino80 (Figure 10). In agreement, les1 formed a complex with the N-terminus of Ino80 (Ino80¹⁴⁻⁴⁵⁰) and Nhp10-les3-les5 (Figure 12B and C (also see section 4.11.1). Nhp10, les1, les3 and les5 are yeast specific subunits, but the N-terminus of metazoan Ino80 was shown to interact analogously with non conserved, metazoan specific subunits (Chen et al., 2011).

The Arp8 sub-complex contains Arp8, Arp4, Act, Taf14 and les4 (Figure 10). Subunits of the Arp8 sub-complex cross-linked to the N-terminal part of the previously defined HSA patch (Szerlong et al., 2008). Indeed, the complex of Arp8-Arp4-Act was only formed stably when the HSA^{Ino80} was included (Figure 12D). Cross-link data indicated that les4 is a novel member of the Arp8 sub-complex. Consistently, les4 was recruited to an Arp8-Arp4-Act-HSA^{Ino80} complex (Figure 12D). Cross-links are indicative for interfaces and most of inter-links were found in the insertion domains apart from the Actin cores in Arp4 and Arp8. Especially the HSA^{Ino80} domain, les4 and Arp4 cross-linked to the N-terminus of Arp8 that is so far not structurally described.

Ies2 cross-linked to the N-terminus, HSA and RecA1 and RecA2 folds of INO80. The cross-links of Ies2 along the Ino80 polypeptide clustered especially in the PAPA-1 domain. Ies2 is very small, indicating that Ino80 is not extended within INO80 but rather adopts a bent conformation.

For the first time the XL-MS analysis of INO80 provided interaction studies with motif resolution of a large chromatin remodeler. This extended prior interaction studies as was performed on human INO80 (Chen et al., 2011) and now allows for a detailed structural interpretation.

4.6 Validation of INO80's modules *in vivo*

XL-MS indicated that INO80 has a modular organization, as cross-links clustered within sub-complexes. However, a lack of information is no gain of knowledge. Therefore, strains were created with $\Delta arp5$, $\Delta arp8$ and $\Delta nhp10$ in an *Ino80-FLAG* background. INO80 was purified from those deletion strains and the composition was analyzed by SDS-PAGE and MS (Figure 13A and B) (Tosi et al., 2013).

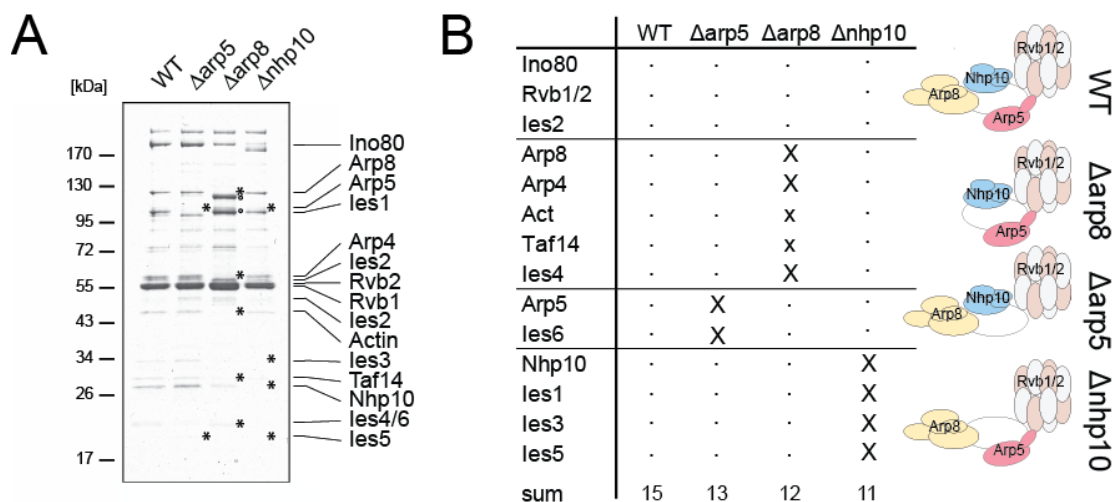


Figure 13 INO80 is organized in modules. A) SDS-PAGE of purified wild-type (WT), INO80($\Delta arp5$), INO80($\Delta arp8$) and INO80($\Delta nhp10$) complex. Asterisks indicate lost or reduced subunits and circles indicate degraded Ino80. B) Summary of composition of INO80 deletion mutants. Loss of subunits (X) and reduced levels (x) were indicated. This figure was adapted from (Tosi et al., 2013).

INO80 purified from $\Delta nhp10$ strains lacked Nhp10 and additionally les1, les3 and les5. INO80($\Delta arp8$) was omitted of Arp8, Arp4 and les4 and showed reduced levels of Act and Taf14. INO80($\Delta arp5$) exclusively lacked les6.

Reduction or loss of subunits has already been indicated by XL-MS analysis that strongly validated our approach, but further showed that INO80 is built up by four modules also *in vivo*: Rvb1/2, Arp5-les6, Nhp10-les1-les3-les5 and Arp8-Arp4-Act-les4-Taf14 next to an Ino80-les2 scaffold (Tosi et al., 2013).

4.7 Structure of the INO80 complex

4.7.1 Electron microscopy of INO80

In order to provide structural information of an INO80-type remodeler, we determined the structure of INO80 (Tosi et al., 2013). Electron micrographs of negatively stained and cryo preserved INO80 were recorded. Particles were manually selected and classified by reference-free class averaging using EMAN2 and ISAC (iterative and stable alignment and clustering) (Tang et al., 2007; Yang et al., 2012). Common line reconstruction and refinement resulted in 3D negative stain and cryo structure of INO80 with 22 Å and 17 Å, respectively (Figure 14A and B) (Tosi et al., 2013). Negative stain and cryo EM revealed that INO80 is an embryo-shaped particle with a head-neck-body architecture. The globular head has a diameter of ~120 Å and is connected to the residual neck-body-foot cone.

Class averages of negatively stained INO80 were in good agreement with projections. However, a small subset of classes could not be assigned and showed rather back bent or closed conformations (Figure 14C). In agreement, the cryo structure of INO80 showed a lower resolution in the foot strongly suggesting conformational flexibility in the foot (Tosi et al., 2013). However, we were not able to visualize stable bent intermediate or end states arguing for a continuum of conformations of INO80 (Tosi et al., 2013).

INO80 is an elongated particle, which has no obvious nucleosome binding cleft as it was observed in large SWI/SNF remodelers (Asturias et al., 2002; Chaban et al., 2008; Dechassa et al., 2008; Leschziner et al., 2005; Leschziner et al., 2007; Skiniotis et al., 2007; Smith et al., 2003). Closing of the foot could be part of a nucleosome recognition and binding procedure.

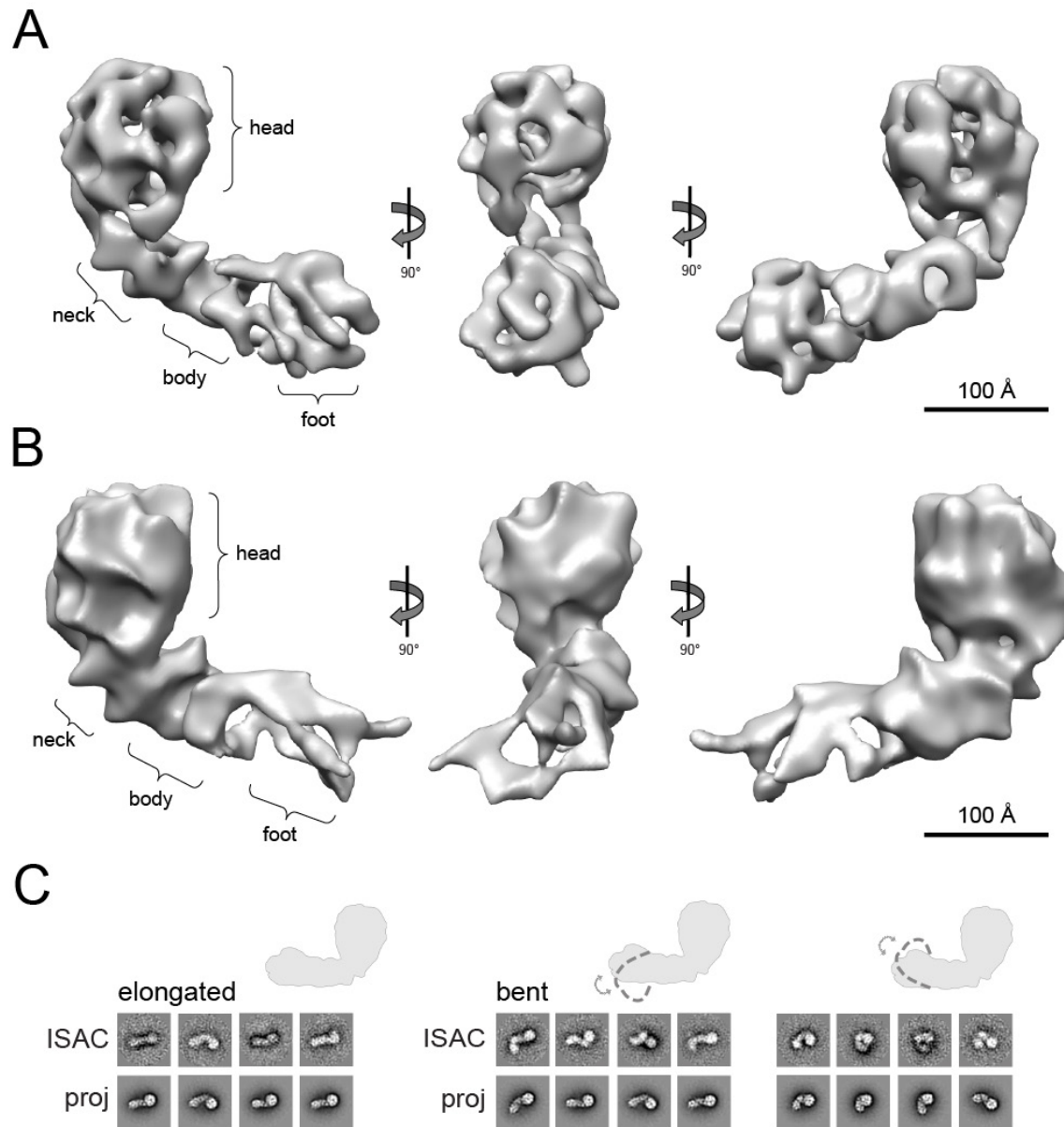


Figure 14 EM structure of the INO80 complex. A) Different views of the 3D structure of INO80 from negative stained INO80. INO80 is an embryo-shaped particle with a head-neck-body-foot architecture. The bar represents 100 Å. B) Cryo structure of INO80. C) Class averages from ISAC were largely in good agreement with the elongated structure and its projections. But a subset of classes could not be attributed to corresponding projections (first panel). In these classes the foot of INO80 was rather back bent (middle panel) or closed (last panel). This figure was adapted from (Tosi et al., 2013).

4.7.2 Towards a crystal structure of INO80

The novel purification protocol yielded INO80 at concentrations high enough (up to 6 mg/ml) for crystallization without an extra concentration step being required. Commercial screens were set up in 96-well format and nanoscale free interface diffusion. Promising spherulites and micro crystals were yielded that need to be analyzed further.

4.8 Rvb1/2 form a hetero-dodecamer

4.8.1 Rvb1/2 is composed of two hexameric rings in INO80

Rvb1/2 were extensively characterized in the isolated state by EM and crystallography (Cheung et al., 2010; Gorynia et al., 2011; Lopez-Perrote et al., 2012; Matias et al., 2006; Petukhov et al., 2012; Puri et al., 2007; Torreira et al., 2008), however, a structure in the native context was missing. The structure of INO80 was one of the first structures of Rvb1/2 within a native complex (Nguyen et al., 2013; Tosi et al., 2013). Human Rvb1 and domain II deleted Rvb2 were crystallized as homo-hexamers (Matias et al., 2006; Petukhov et al., 2012), but Rvb1/2 with a truncated domain II was crystallized in a hetero-hexameric state (Gorynia et al., 2011). EM structures could also not clarify the question, if Rvb1/2 is a homo- or hetero-hexamer as the resolution of available structures were too low to differentiate between the two similar proteins (Cheung et al., 2010; Gorynia et al., 2011; Lopez-Perrote et al., 2012; Puri et al., 2007; Torreira et al., 2008). Further biochemical analysis on isolated Rvb1/2 could also not clarify the oligomeric state. EM structures of human and yeast Rvb1/2 suit the volume of two hexamers (Cheung et al., 2010; Lopez-Perrote et al., 2012; Puri et al., 2007; Torreira et al., 2008), but biochemical analysis and structural data also suggest the formation of hexamers (Gribun et al., 2008) or even other oligomeric states as dimers, trimers or higher molecular species than dodecamers (Niewiarowski et al., 2010). The first step to analyze the oligomeric state and composition of Rvb1/2 in INO80 was to localize the hexameric rings. Since AAA+-ATPases in general and Rvb1/2 in particular have been shown to form hexameric complexes; a six-fold symmetry was searched in INO80 (Tosi et al., 2013). Indeed, a six-fold symmetry axis was found in the head of the negative stain and cryo structure of INO80 that was quasi parallel to the

residual cone (Figure 15A and B). The symmetry axis proved that Rvb1/2 was situated in the head. The averaged volume of head is composed of two rings indicating that Rvb1/2 is composed of two hexamers in INO80 (Figure 15C). Indeed, the volume and shape is suitable to accommodate two rings of Rvb1/2 (Figure 15D). The reported dodecameric structures of Rvb1/2 had a height of either 130 Å (Torreira et al., 2008) and 160 Å (Puri et al., 2007) and the Llorca group could resolve a closed and a stretched conformation of Rvb1/2 with a height of 130 Å and 145 Å (Lopez-Perrote et al., 2012). The height of the averaged head volume of INO80 is around 120 Å (Figure 15C) and is thus the most compact version of Rvb1/2 reported so far.

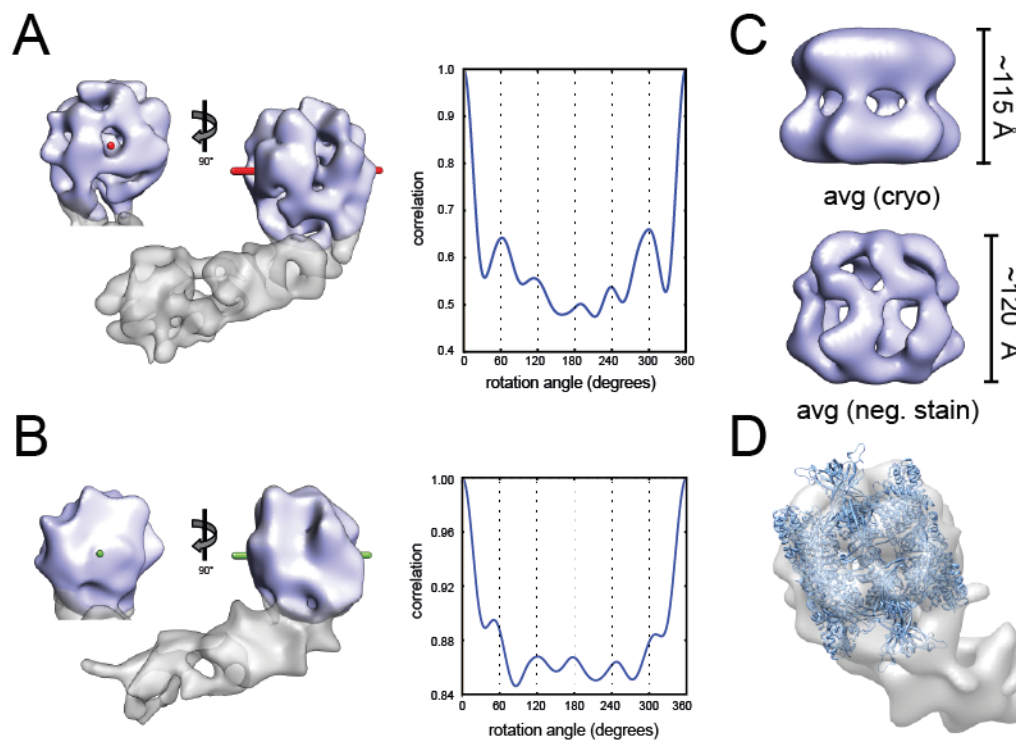


Figure 15 The head of INO80 contains a Rvb1/2 dodecamer. A and B) Six-fold symmetry axes were located in the head that is quasi parallel to the cone of INO80 in the negative stain (A) and cryo (B) EM structures. Cross-correlation plots rotated along the axis showed six maxima spaced by 60°. C) Averaged volumes of the head of the cryo and negative stain EM structure of INO80 showed two ring like structures stacked on top of each other. D) The volume and the shape of INO80's head was suitable to accommodate two human Rvb1 rings (2C9O (Matias et al., 2006)). This figure was adapted from (Tosi et al., 2013).

4.8.2 Rvb1/2 assemble as hetero-hexamers interacting via the domain 2 within INO80

In order to analyze, if the double-ring is composed of two hetero-hexamers of Rvb1 and Rvb2 or of two homo-hexamers, inter-links of Rvb1/2 were evaluated (Tosi et al., 2013). In principal, the

inter-links were assigned to homo- or hetero-hexameric models of Rvb1/2 rings (Figure 16A). Rvb1 and Rvb2 share the same domain organization in which the domain 1 and 3 form together the AAA+-ATPase core and the domain 2 is folding back to form the oligo-nucleotide binding (OB)-fold. 9 inter-links between Rvb1 and Rvb2 were found: Five links between AAA+ domains 1/3 of Rvb1 and Rvb2, one link between domains 1/3 of Rvb1 and 2 of Rvb2, one link between domains 1/3 of Rvb2 and 2 of Rvb1, and two links between domains 2 of Rvb1 and Rvb2. These links and therefore distance restraints could exclusively be fulfilled by a hetero-hexamer (Figure 16A) (Tosi et al., 2013).

In general, Rvb1 and Rvb2 rings can interact via the domains: (i) 2-2, (ii) 2-1/3 or (iii) 1/3-1/3 (Figure 16A). Previously published EM structures of isolated Rvb1/2 could not clarify the stacking arrangement unambiguously. Most of the structures strongly promote an interaction via domain 2-2 (Cheung et al., 2010; Lopez-Perrote et al., 2012; Torreira et al., 2008). However, the human Rvb1/2's EM shape from Puri et al. would also fit a Rvb1/2 complex interacting via domain 1/3-1/3 or 2-1/3 (Puri et al., 2007). Furthermore, Rvb1 and Rvb2 either one or both lacking OB-folds could be assembled as dodecamers indicating that domain 2 is not essential for the formation of a dodecamer (Niewiarowski et al., 2010). In order to elucidate Rvb1/2 stacking, mono-linking was analyzed (Tosi et al., 2013). Mono-links are indicative for solvent-exposure. Nine lysines were mono-linked and 2 were non-linked at the convex side (domain 1/3) (Figure 16C). In contrast, only one mono-link and 8 non-modified lysines were found at the concave side (domain 2) strongly suggesting that this site is protected. In addition, the head of INO80 is less dense in the middle of the equatorial plane. If Rvb1/2 was interacting via the AAA+-ATPase domains, this region would be high in mass confirming a domain 2-2 interaction of the rings. Fitting of the human Rvb1 crystal structure into the average volume of the head in a fashion that the rings stack via domain 2-2 resulted in slightly higher cross-correlation coefficients (0.62 and 0.56) compared to the other version (0.55 and 0.5). All arguments together strongly suggest that Rvb1/2 rings interact via domains 2.

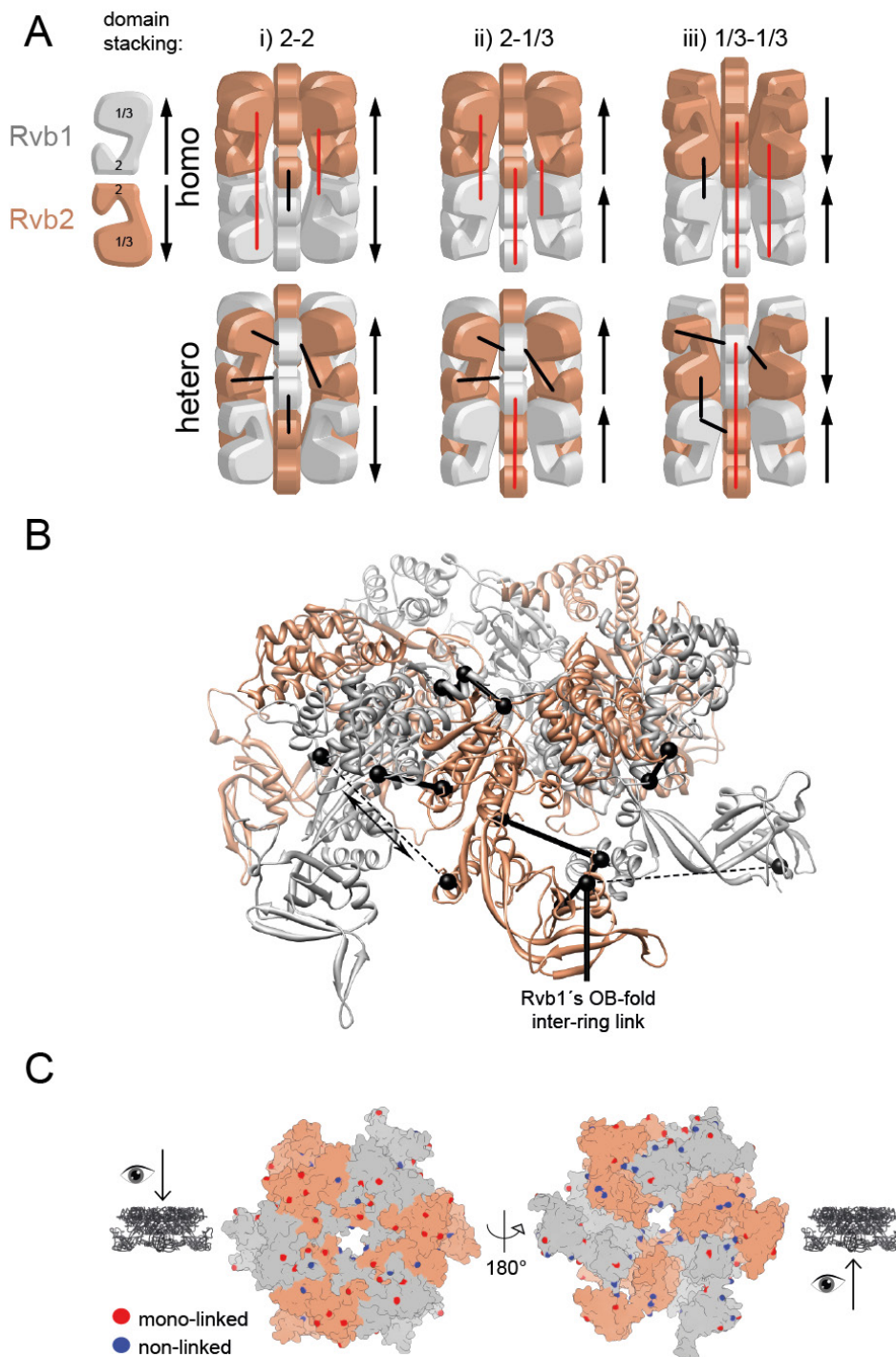


Figure 16 Rvb1/2 is composed of two hetero-hexameric rings stacked via domains 2. A) Theoretically possible stacking variants of Rvb1 and Rvb2. The rings could interact via domains: 2-2 (i), 2-1/2 (ii) or 1/3-1/3. Distance restraints were not fulfilled (red link), if rings are composed of homo-hexamers. But cross-links were satisfied (black), if rings contained both Rvb1 and Rvb2 (hetero). B) Cross-links were assigned in the modeled yeast Rvb1/2 hetero-ring structure. Links fulfilling the distant restraint of 30 Å were shown as a black line. Links violating the restraint were depicted as dashed lines. Arrow indicates that the link could be fulfilled, if the putative flexible N-terminus of Rvb1 moved towards the domain 2 of Rvb2. C) Mono-links (red) were found at the convex side indicating surface exposure, whereas the lysines at the concave side were protected (blue). This figure was adapted from (Tosi et al., 2013).

4.9 The catalytic core of INO80

4.9.1 The Swi2/Snf2 domain of INO80

The Swi2/Snf2 ATPase of Ino80 is the active core of the INO80 complex as a mutation in the Walker A motif results in a decrease of the ATPase activity to only 5% compared to WT complex (Shen et al., 2000). The Swi2/Snf2 fold of Ino80, especially the RecA2 domain was highly inter-linked with Rvb1 and Rvb2 (Tosi et al., 2013). Rvb1/2 is situated in the head of INO80. Thus, the Swi2/Snf2 fold has to be in spatial proximity to the head. Swi2/Snf2 helicases have a characteristic two-lobed structure (Durr et al., 2006). A density patch in the neck of INO80 resembles this typical shape (Tosi et al., 2013). The docking of the homologous DroRad54 (Thoma et al., 2005) resulted in a cross-correlation coefficient of over 0.8 (Figure 17) (Tosi et al., 2013). The orientation was further constrained as the RecA2 domain exclusively cross-linked to Rvb1/2. The density connecting the head and the neck could accommodate the insertion loop of the Ino80 ATPase domain that would protrude out of the top of the RecA2 domain. The insertion cross-linked to the domain 2 of Rvb1/2. In this position all cross-links would be full-filled.

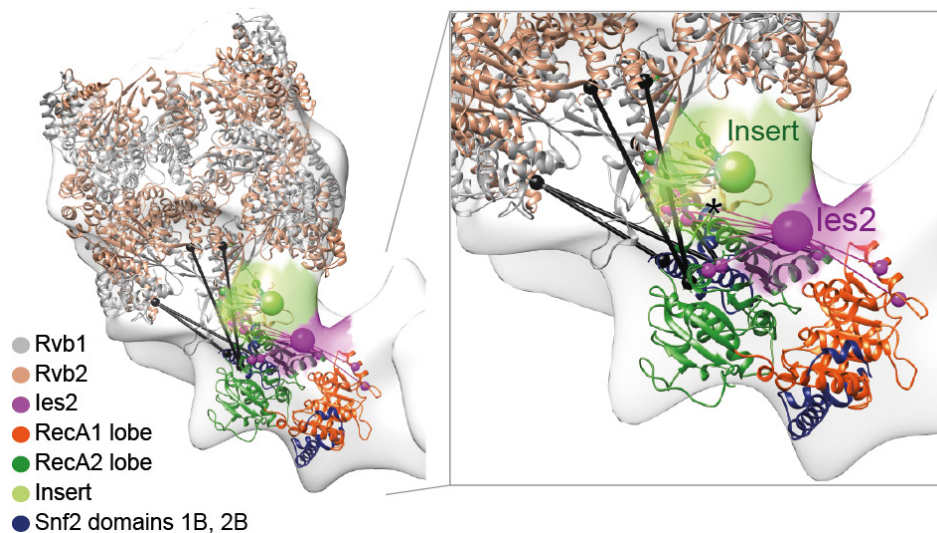


Figure 17 Docking of the catalytic core of INO80. The crystal structure of the homologous Swi2/Snf2 (Thoma et al., 2005) was docked into the neck of INO80 and further oriented by cross-links between Rvb1/2 and the RecA2 fold of the Swi2/Snf2 domain (black). Cross-linked lysines are depicted as small spheres. The insertion loop protrudes out at the top of the RecA2 fold (asterisk) and can be accommodated in the density patch connecting the head and the neck (large light green sphere). Cross-links of Rvb1/2 to the insertion would support this localization. Ies2 (large pink sphere) could be placed at the top of the Swi2/Snf2 domain. The cross-links track the way of cross-linked lysines along the C-terminus of Ies2 and from the top of the RecA1 to the RecA2 fold. This figure was adapted from (Tosi et al., 2013).

Remaining density at the top of the Swi2/Snf2 domain is sufficient to accommodate les2 (Figure 17). Interestingly, cross-linked lysines along the top of the Swi2/Snf2 domain towards the RecA2 fold follow cross-linked residues of les2 in the C-terminal direction indicating that les2 lies on top of the RecA folds (see discussion part 5.6).

In summary, we could localize the Swi2/Snf2 domain with its insertion loop and les2 in the neck region of INO80.

4.9.2 Expression and purification studies of the ATPase domain of Ino80 with les2 and Rvb1

XL-MS indicated that les2 and the OB-folds of Rvb1/2 are interacting with the Swi2/Snf2 ATPase of Ino80 (Tosi et al., 2013). Since expression of any Ino80 constructs including the ATPase was not successful so far, constructs of Ino80 were tried to be co-expressed with les2 and the OB-folds of Rvb1. Therefore, coding sequences of Ino80, les2 and Rvb1 were cloned from *S. c.* and *Chaetomium thermophilum* (*C. t.*) into vectors for expression in bacteria and insect cells. The Ino80 ATPase including the insertion loop as well as only the RecA1 and RecA2 domains were tried to express. Unfortunately, reasonable expression of soluble Ino80 could not be achieved. Certainly, the expression should be optimized in future studies.

4.10 Localization of the Arp8-, Arp5- and Nhp10-module

Localization of other INO80-modules based on inference was not possible. Therefore, DID-tagging (Flemming et al., 2010) of representative subunits of each module was performed. DID-labeled INO80 complexes were purified and visualized by negative stain EM (Tosi et al., 2013).

In order to localize the Arp8-module, INO80 complexes with DID-labeled Arp4 were visualized and the DID-tag was found to protrude out of the foot of INO80 (Figure 18A). Arp4 is a member of the Arp8-module indicating that the Arp8-module is localized in the foot. In

addition, a distal position agrees with that the Arp8-module is not cross-linking to any other module.

To position the Nhp10-module, Nhp10 DID-labeled INO80 complexes were purified and visualized. The DID-tag at Nhp10 protruded out of the body close to the neck of INO80 suggesting that Nhp10 is localized in the body (Figure 18A). This position is in agreement with a cross-link between les2 and les3 (Figure 10).

To validate the position of les2 in the neck, which was inferred from XL-MS and EM results, les2 DID-tagged INO80 was visualized. Indeed, the DID-tag protruded out of the neck close to the head (Figure 18A).

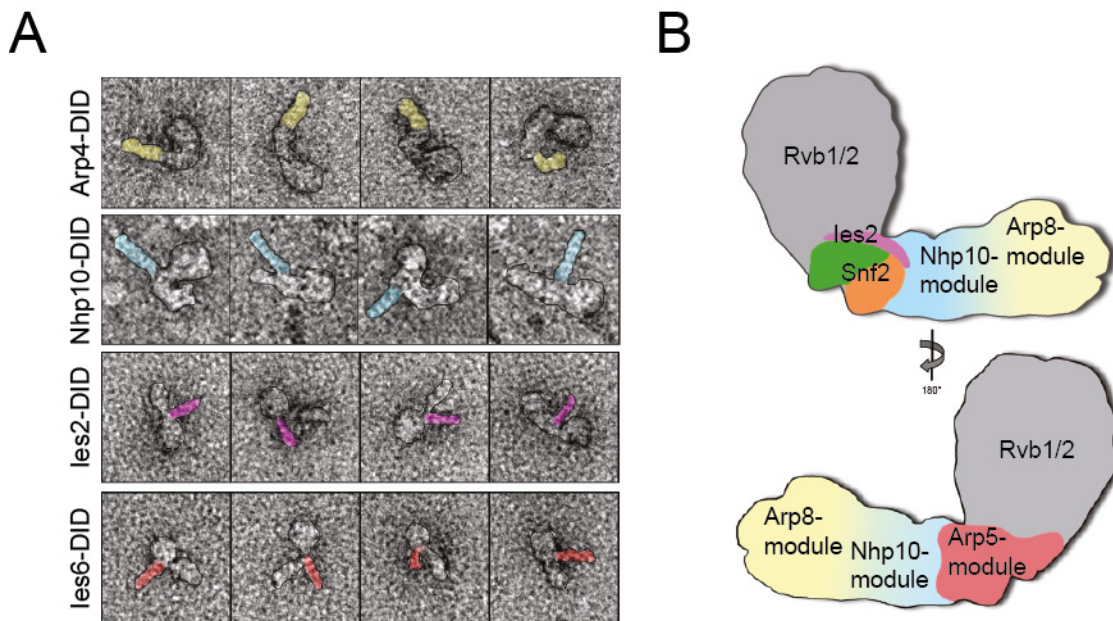


Figure 18 Assignment of INO80-modules. A) Purification and visualization of DID-labeled INO80 complexes by EM allowed localization of INO80-modules. Gallery of single particles of purified DID-Arp4 (first panel), DID-Nhp10 (2nd panel), DID-les2 (3rd panel) and DID-les6 (last panel). The DID-tags were colored in the color of the respective module: Arp4 yellow, Nhp10 blue, les2 pink and les6 red. B) Modules were assigned in the INO80 density. Rvb1/2 is situated in the head, Snf2-les2 and the Arp5-module in the neck, the Nhp10-module in the body and the Arp8-module in the foot. This figure was adapted from (Tosi et al., 2013).

Arp5-les6 exclusively cross-linked to Rvb1/2 in the head of INO80. The DID-tag at les6 protruded also out of the neck (Figure 18A), which is consistent with the cross-links. Moreover,

at the back of the localized Snf2 domain in the neck there is a density patch that resembles an Actin fold, which could accommodate Arp5 (Tosi et al., 2013).

In summary, all INO80-modules could be localized. Rvb1/2 is situated in the head connected to the neck, which contains the Swi2/Snf2-les2 and backed by Arp5-les6 (Figure 18B) (Tosi et al., 2013). The cone comprises the Nhp10-module in the body and the Arp8-module in the foot. We could not exclude that parts of Arp8 reach over to the body. Still, this is the first positioning of domains and modules into a large remodeler.

4.11 The Nhp10-module

4.11.1 Reconstitution of the Nhp10 module: Nhp10-les1-les3-les5-Ino80 (N-terminus)

An interaction between Nhp10 and les3 was already indicated in the literature (Morrison et al., 2004; Shen et al., 2003) and a stable complex formation between Nhp10, les3 and les5 was established in the lab (unpublished data from Sebastian Fenn, AG Hopfner). Nhp10-les3-les5 was expressed in insect cells and purified via an N-terminal His-tag on Nhp10 and anion exchange and size exclusion chromatography (Figure 19A and B). Nhp10-les3-les5 formed a stable complex on gel filtration, but run with a much higher molecular weight than expected. Crystallization screens of Nhp10-les3-les5 did not yield any promising hits and treatment with proteases (Trypsin and Chymotrypsin) in the drop did not promote crystallization.

Nhp10 was degraded in the Nhp10-les3-les5 complex to a stable degradation product Nhp10 1-164 (Nhp10-ISNI), which was identified by MS analysis (Figure 19B). This heterogeneity in the preparation could have prevented crystallization. Therefore, a construct of Nhp10 ISNI-les3-les5 was expressed and purified (Figure 20A). However, this Nhp10 construct was unstable, the yield was significantly reduced compared to full-length Nhp10 and did not improve crystallization.

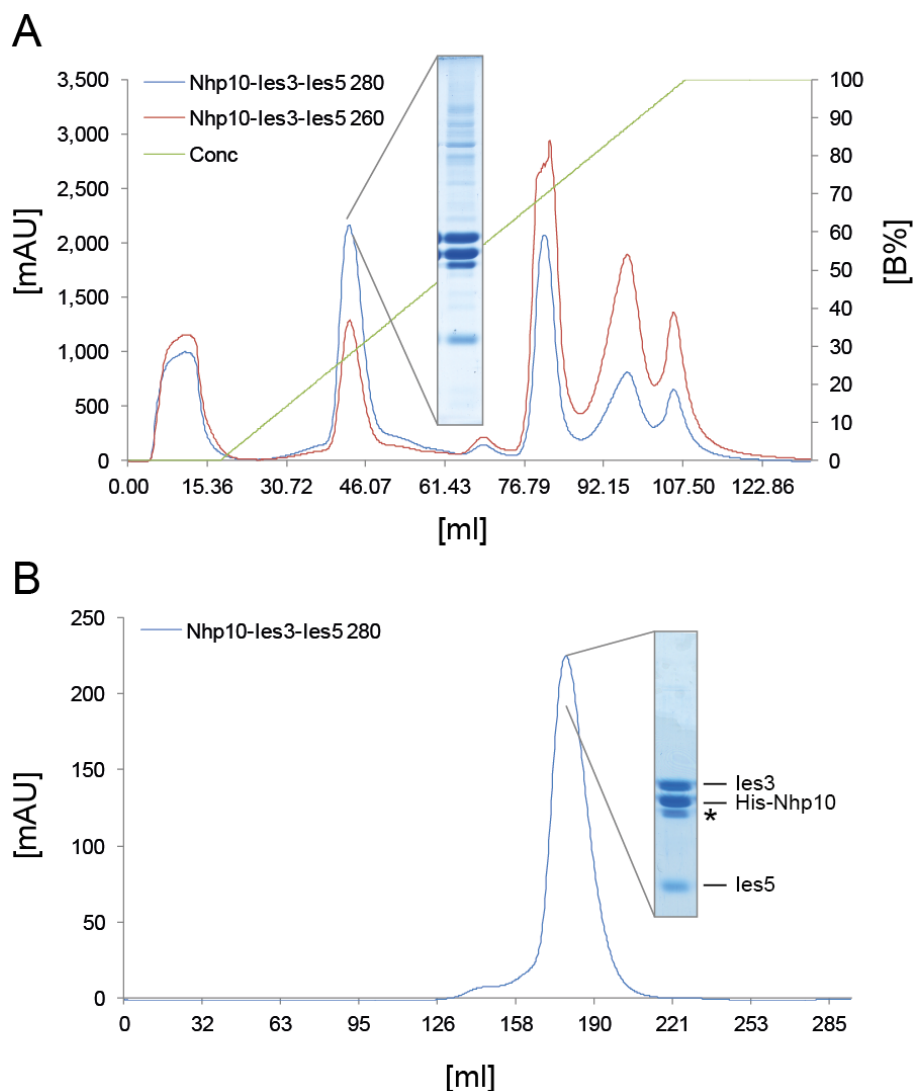


Figure 19 Purification of Nhp10-les3-les5. A) Nhp10-les3-les5 was expressed in insect cells and purified by Ni-NTA agarose. DNA free Nhp10-les3-les5 eluted from anion exchange chromatography at approximately 250 mM KCl and was analyzed by SDS-PAGE. The UV absorption at 260 or 280 nm is indicated to track protein-DNA ratios. B) Nhp10-les3-les5 was further purified via size exclusion chromatography. Nhp10-les3-les5 eluted at a higher molecular weight than expected (66 kDa) corresponding to about 250 kDa.

To facilitate crystallization of the Nhp10 sub-complex binding partners were searched that stabilize the complex. XL-MS analysis showed that the Nhp10-module consists of Nhp10, les1, les3 and les5 interacting with the N-terminus of Ino80 (Figure 10). Therefore, N-terminal constructs of Ino80 containing amino acids: 1-152, 1-213, 1-258, 14-450 were cloned into the Nhp10-les3-les5 containing vector and were purified (Figure 20B). All constructs were expressed, soluble and could be co-purified together with Nhp10-les3-les5 or Nhp10 ISNI-les3-

les5. Nhp10-les3-les5 formed a stable complex with Ino80 14-450 that could be purified by size-exclusion (Figure 20C). This complex additionally interacted with les1 (Figure 12C).

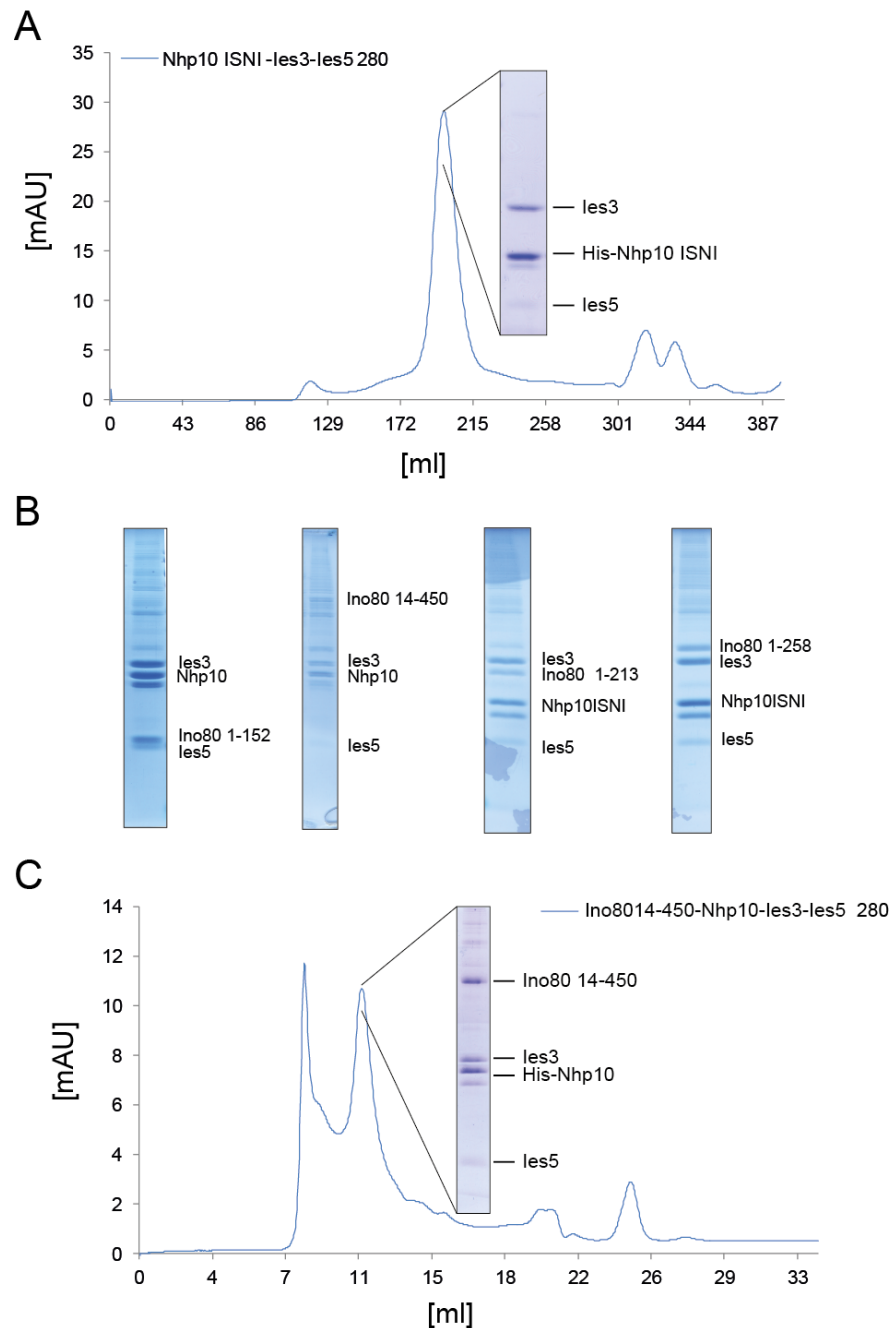


Figure 20 Nhp10-les3-les5 form a stable complex with the N-terminus of Ino80. A) Nhp10 ISNI (1-164) was purified by Ni-NTA, anion exchange and size exclusion chromatography. The gel filtration profile and the corresponding SDS-PAGE are shown. B) N-terminal constructs of Ino80 were expressed with Nhp10-les3-les5 and purified via Ni-NTA. Ino80 containing the amino acids 1-152, 14-450, 1-213 and 1-258 interacted with Nhp10-les3-les5. C) Nhp1-les3-les5-Ino80 14-450 could be purified by IMAC, anion exchange and size exclusion chromatography. The UV absorption at 280 nm is indicated to track protein.

A complex consisting of Nhp10-les1-les3-les5-Ino80 (N-terminus) was identified that could facilitate crystallization and proves once more the modular organization of INO80 inferred from XL-MS.

4.11.2 The Nhp10 sub-complex forms a stable DNA complex

Nhp10 is composed of two DNA binding domains (HMG boxes) and Nhp10 has been shown to interact favorably with structured DNA (Ray and Grove, 2009, 2012). Therefore, DNA binding of Nhp10-les3-les5 to different structured DNAs was assessed. Mammalian HMGB and Nhp10 were shown to prefer a distorted 37 bp long DNA with loops introduced by tandem mismatches separated by 9 bp (Grove et al., 1996). Nhp10 alone showed increased affinity to a DNA that is 50 bp long, but with the same features of mismatches (Ray and Grove, 2009). Binding to both types of DNA duplexes was tested by EMSAS (Figure 21A). Nhp10 in complex with les3 and les5 bound preferentially to the longer 50 bp tandem mismatch substrate.

INO80 is involved in the proper restart of stalled replication forks (Morrison et al., 2007; Papamichos-Chronakis and Peterson, 2008; Shimada et al., 2008), thus DNA duplexes resembling replication forks (Guy and Bolt, 2005) were also tested for binding. The INO80 complex binds and acts on nucleosomes therefore a DNA was designed that shows a curvature (Goodsell and Dickerson, 1994). Indeed, Nhp10-les3-les5 showed high binding affinity to fork and curved DNA substrates (Figure 21B). In addition, Nhp10-les3-les5 formed stable complexes with all tested DNA substrates on a gel filtration column (Figure 21D - F).

Nhp10-les3-les5 in complex with curved DNA formed a stable complex that could be separated from unbound DNA by size exclusion chromatography. Therefore, this complex was screened for crystallization and promising crystalline precipitation or micro crystals were among initial hits, which should be refined in future.

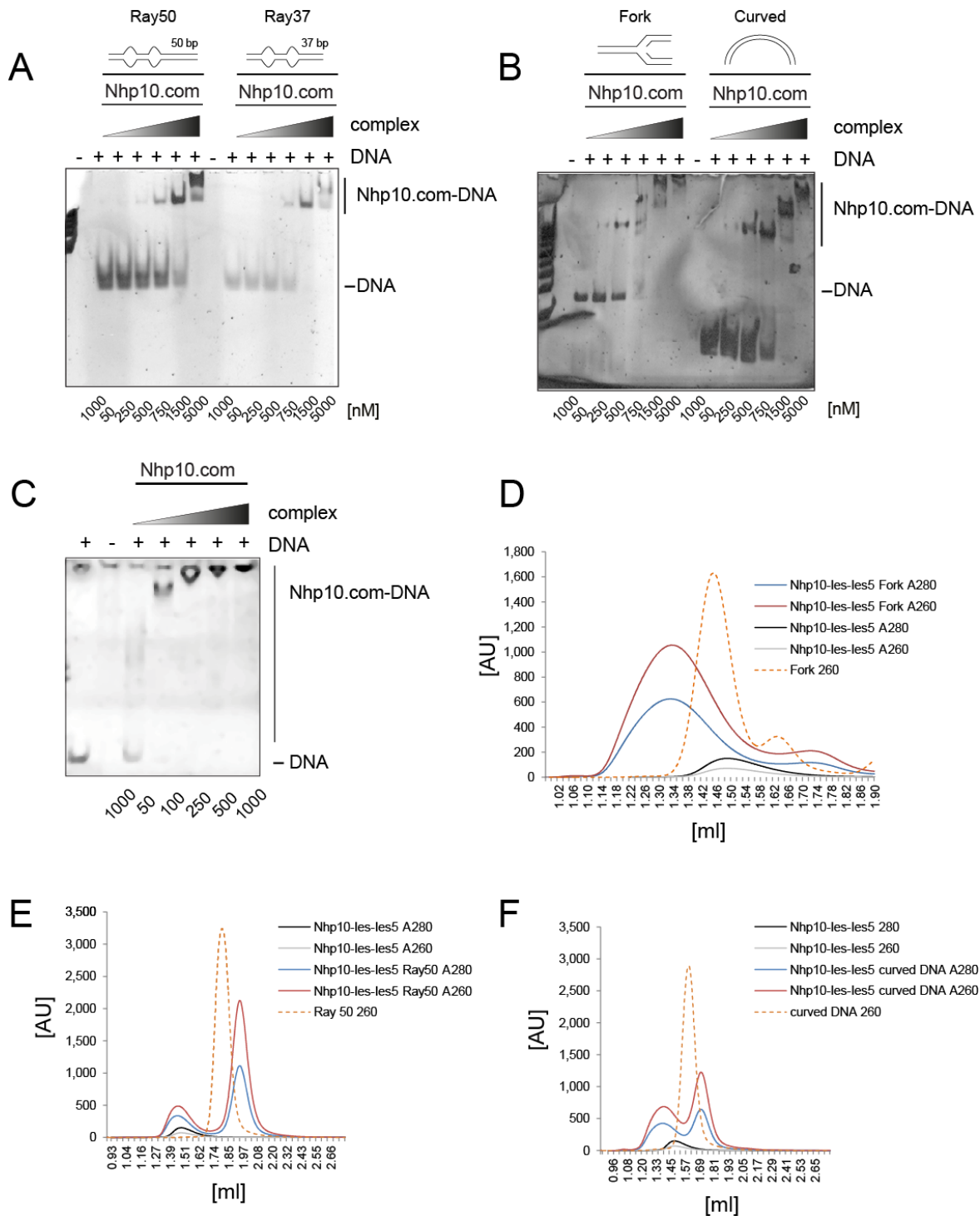


Figure 21 Nhp10-les3-les5-DNA complexes. A and B) Binding of 50 bp and 37 bp long duplex DNAs with tandem mismatches (Ray50 or Ray37) (Ray and Grove, 2009, 2012), fork DNA (Guy and Bolt, 2005) and curved DNA created by phased AGGAGAG sequence to Nhp10-les3-les5 was tested by EMSA. Increasing amounts of Nhp10-les3-les5 were incubated with structured DNAs. C) Nhp10-les3-les5 bound also to a 187 bp long DNA oligo containing the 601 positioning sequence (Lowary and Widom, 1998). D - F) Nhp10-les3-les5 in complex with fork DNA (D), Ray50 (E) and curved DNA (F) were analyzed on a size exclusion column. DNA containing complexes were shifted towards a higher molecular weight compared to Nhp10-les3-les5 or DNA alone. The UV absorption at 260 or 280 nm is indicated to track protein-DNA ratios.

4.12 Dissecting the function and activity of INO80-modules

4.12.1 Functional characterization of IN080-modules

INO80 binds preferentially to nucleosomes with long extranucleosomal DNA (Udugama et al., 2011). In order to functionally characterize INO80-modules EMSAs with DNA, nucleosomes and remodeling assays as well as ATPase assays were performed (Tosi et al., 2013). Deletion of the Arp8-, Nhp10- or Arp5-modules from INO80 did not completely abolish binding to DNA (Figure 22A and B). In principal, DNA binding, remodeling and ATPase activity of these mutants were tested earlier (Shen et al., 2003). However, we could expand the analysis by for instance testing for ATPase stimulation by DNA in addition to nucleosomal stimulation.

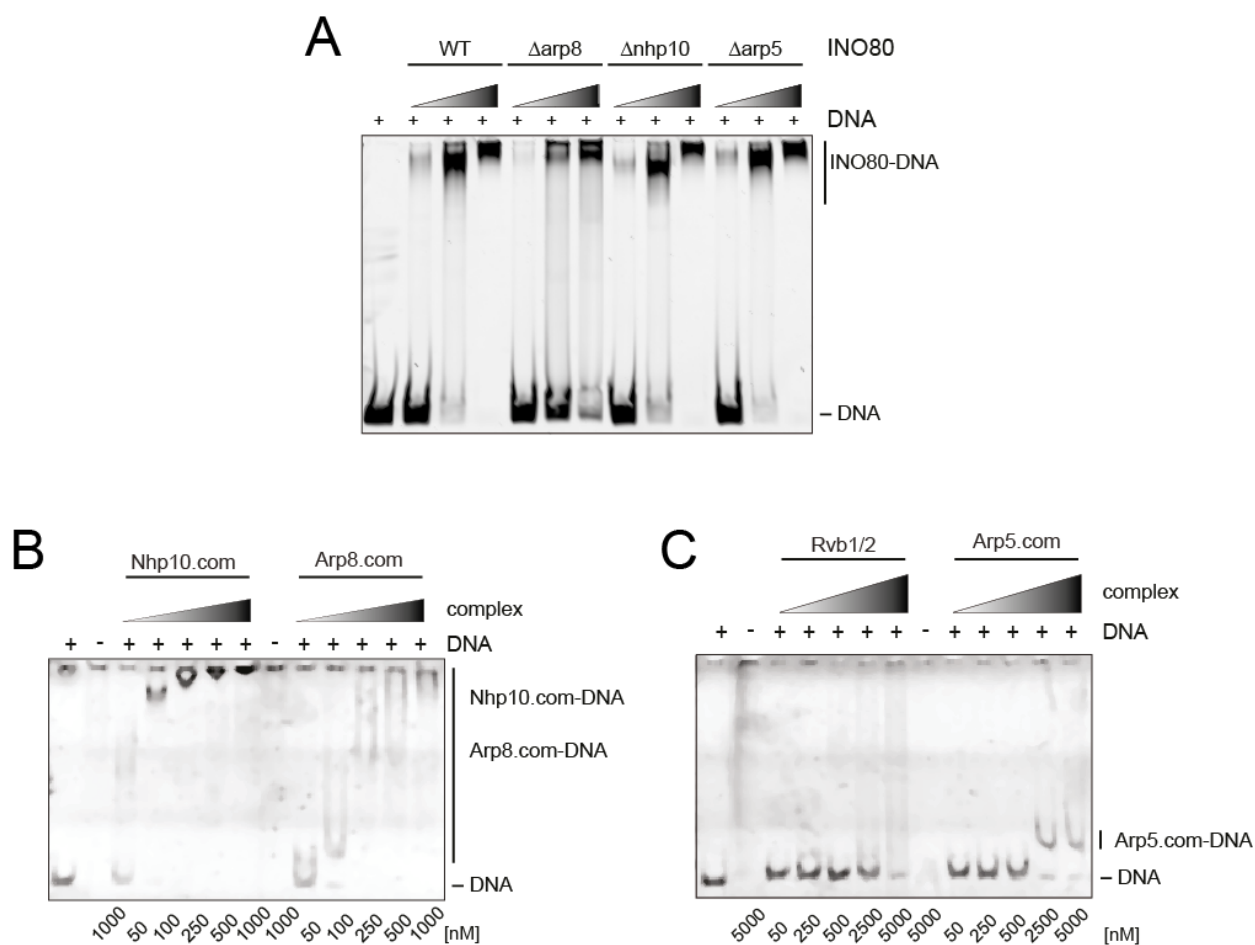


Figure 22 The Nhp10- and Arp8-sub-complex are responsible for DNA binding. A - C) Increasing amounts of WT INO80, INO80(Δ arp8), INO80(Δ nhp10) and INO80(Δ arp5) (A) and recombinantly expressed and purified Nhp10-les3-les5 (Nhp10.com), Arp8-Arp4-Act-HSA^{INO80} (Arp8.com) (B), Rvb1/2 or Arp5-les6 (Arp5.com) (C) were incubated with 187 bp DNA including the 601 nucleosome positioning sequence and were analyzed by native PAGE. This figure was adapted from (Tosi et al., 2013).

INO80(Δ nhp10) showed decreased DNA binding affinity compared to wild-type (WT) complex (Figure 22A and B). Reciprocal experiments with recombinantly expressed sub-complexes showed that Nhp10-les3-les5 bound strongly to DNA (Figure 21 and 22A and B). In agreement with Shen et al., 2003, deletion of the Nhp10-module did if at all slightly negatively affect remodeling rates, but had no negative influence on the ATPase activity (Figure 23A and B) (Tosi et al., 2013).

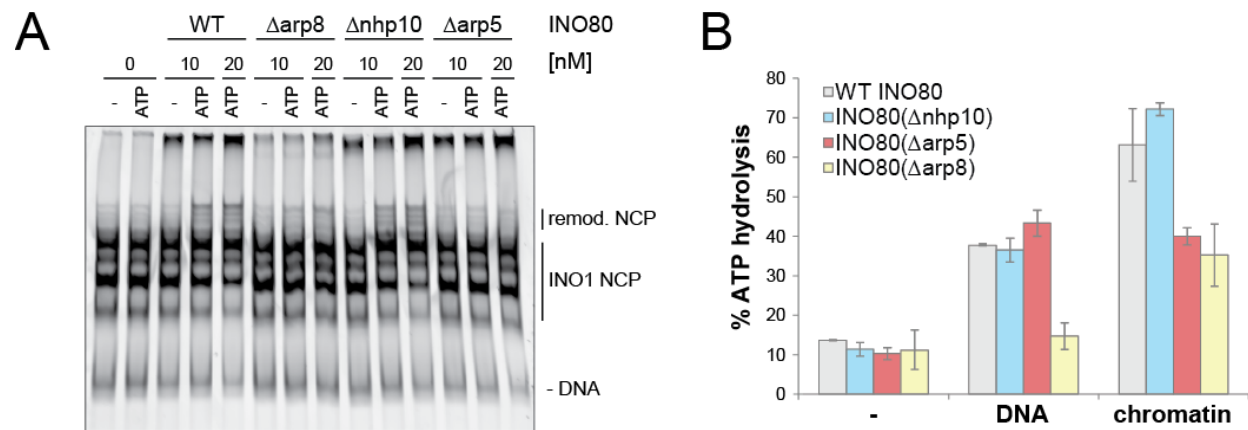


Figure 23 Deletion of INO80-modules influenced remodeling and ATPase activity. A and B) The ability to re-distribute nucleosomes along a 359 bp long *INO1* DNA by WT INO80, INO80(Δ arp8), INO80(Δ nhp10) or INO80(Δ arp5) was analyzed by native PAGE. D) The ATPase activity of WT and mutants INO80 complexes was analyzed by radioactive ATP hydrolysis assays. The ATPases were either measured with no stimuli (-) or was stimulated with 359 bp long *INO1* DNA (DNA) or *INO1* nucleosomes (chromatin). ATP hydrolysis was quantified and presented relative to ATPase hydrolysis rates of alkaline phosphatase. Data was represented as mean standard deviation. This figure was adapted from (Tosi et al., 2013).

INO80(Δ arp8) bound less efficiently to DNA and remodeling was decreased compared to WT complex (Figure 22A and 23A). However, the binding was not completely abolished as published earlier (Shen et al., 2003). Arp8-Arp4-Act-HSA^{INO80} bound DNA, but less efficiently compared to Nhp10-les3-les5 (Figure 22B). Both Nhp10-les3-les5 and Arp8-Arp4-Act-HSA^{INO80} oligomerized on DNA (Figure 21 and 22B). DNA failed to stimulate ATPase hydrolysis rates of INO80(Δ arp8) (Figure 23B). Nucleosomes stimulated the ATPase activity of INO80(Δ arp8) to DNA stimulated WT levels (Tosi et al., 2013).

Deletion of the Arp5-module did not affect DNA binding capabilities of INO80(Δ arp5) (Figure 22A). Arp5-les6 did not bind the nucleosome, but DNA was shifted at mM concentrations (Figure 22C). Consistent with previous work (Shen et al., 2003) INO80(Δ arp5)

failed to mobilize nucleosomes on INO1 chromatin (Figure 23A). In agreement, the ATPase activity of INO80(Δ arp5) failed to be simulated further by the histone entity of INO1 nucleosomes (Figure 23B). However, DNA activated the ATPases activity to similar rates as the WT complex (Tosi et al., 2013).

In summary, the Arp containing modules (Arp8 and Arp5) are essential for providing the catalytic activity, whereas the Nhp10- and the Arp8-module are responsible for binding and recruitment to the substrate.

4.12.2 Interaction and visualization of an INO80-nucleosome complex

The Nhp10- and Arp8-module are nucleosome and DNA binders (Shen et al., 2003; Tosi et al., 2013). To map directly the interaction sites of the INO80 subunits on the histones, INO80-nucleosome complexes were reconstituted and analyzed by XL-MS (Tosi et al., 2013). The appropriate DSS concentration was titrated (Figure 24A). Ten cross-link experiments with different molar ratios of the nucleosome to INO80 and different ATP analogs identified 52 inter-links between histones and INO80 subunits (Figure 25A - D) (Tosi et al., 2013). 35 cross-links were formed to histone tails that are unstructured (Luger et al., 1997) and thus only offer loose distant constraints (Figure 25B). 17 inter-links were to structured histone core folds and thus provide tight distant restraints (Figure 25A).

Inter-links between histones and INO80 modules were equally distributed: 12 cross-links were found to the Rvb1/2 head, 14 to the Ino80 ATPase, les2 and Arp5-les6 neck, 10 to the Ino80 N-terminus and Nhp10-les1-les3-les5 body and 16 to the tail containing the Arp8-Arp4-Act-les4-Taf14-HSA^{Ino80} (Figure 25A and B).

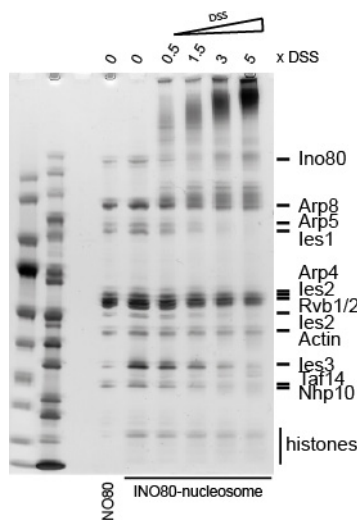


Figure 24 Titration of cross-linker of an INO80-nucleosome complex. INO80 was incubated with nucleosomes and then was cross-linked with increasing molar excess of DSS over concentration of lysines. Cross-linked and untreated complexes were separated by SDS-PAGE and visualized by silver staining. INO80-nucleosome complexes were cross-linked and analyzed by MS with DSS 1.5x - 3.5x over lysines. This figure was adapted from (Tosi et al., 2013).

Rvb1/2 cross-linked to the N- and C-termini of H2A (Figure 25C and D). The OB-folds of Rvb2 cross-linked to the $\alpha 2$ helix of H2B and to the N-termini of H3 and H4. The AAA+ ATPase of Rvb2 moreover cross-linked to the L1 of H4. Rvb1 cross-linked to the N-termini of H2B and H3. Interestingly, residues in the AAA+ ATPase domain (Rvb1₃₁) and in the domain 2 of Rvb2 (Rvb2₁₅₄ and Rvb2₂₃₃) and Rvb1₂₉₀, which cross-linked to the N- and C-terminus of H2A are 70 Å apart from each other. A similar distance (74 Å) is the cross-linking N- and C-terminus of H2A (H2A₁₃, H2A₁₂₂) apart. This makes it perfectly suitable to dock the Rvb1/2 dodecamer on one side of the nucleosome.

The Ino80 ATPase sitting in the neck region of INO80 cross-linked to the loop L2 of H2A. All cross-links in les2 to histones clustered in the short PAPA-1 domain (Figure 25 C). les2 cross-linked to the $\alpha 1$ of H3 and to αC of H2B as well as to the N-termini of H2A and H2B (Figure 25D). Cross-linking sites of Arp5 and les6 were in the insertion between the actin folds and in the YL-1 domain, respectively (Figure 25D). Arp5-les6 cross-linked to αC of H2B, to L1 of H4 and to the N-terminus of H3.

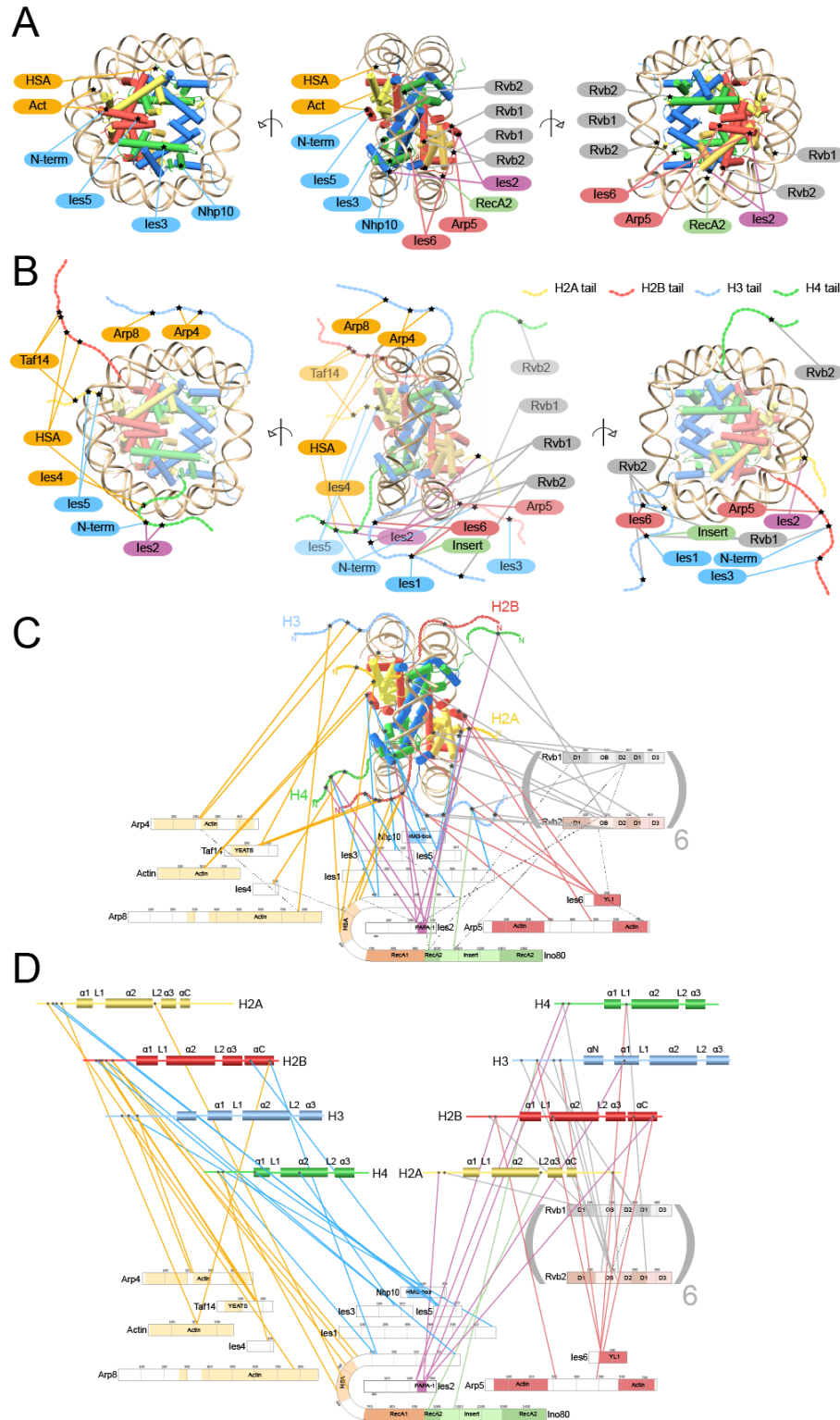


Figure 25 INO80-nucleosome interaction map. A-D) Different depictions of inter-links formed between nucleosome (2pyo, (Clapier et al., 2008)) and INO80 subunits. Inter-links to structured histone folds provide tight restraints (A) and inter-links to flexible histone tails offer loose restraints (B). (C) All INO80 modules are involved in nucleosome cross-links. Interfaces already represented in the apo-INO80 and were also found in INO80-nucleosome complexes were indicated with dashed lines. D) Histones were depicted as secondary structures.

The subunits in the head and neck of INO80 clustered at the H2A/H2B dimer and therefore blocked one complete side of the nucleosome (Figure 25C). This is in particular interesting as the H2A/H2B dimer is the part to be exchanged by INO80 and accordingly the product state.

The Nhp10-module cross-linked to the $\alpha 1$ and $\alpha 2$ helices of H4, αC of H2B and to all the N-termini of histones (Figure 25D). The Arp8-module was cross-linking to the αC helix of H2B, to the L2 loop of H2A and to the N-termini of all histones. Cross-linking sites between histones and the body and foot module were also covering one the side of the nucleosome (Figure 25C).

The head-neck and the body-foot modules occupied each one side of the nucleosome strongly arguing for a central position of the nucleosome (Figure 25C). However, it could not be excluded that more than one nucleosome was bound to INO80. The distant restraint of DSS (30 Å) could not be fulfilled by only a rigid body fitting of the nucleosome into a central position of INO80. A closure of the foot would lead to a compact packing of the nucleosome (Figure 14) and could be part of the nucleosome recognition (Tosi et al., 2013).

Some of the lysines in histones situated near the DNA entry/exit site that cross-linked to Ies6, Ies2 and Rvb2 were not accessible in an intact nucleosome and would require a partial unwrapping of the DNA. Exactly at this site the Swi2/Snf2 fold and catalytic essential Arp5 were located that could provide the mechanical force to generate access (Tosi et al., 2013).

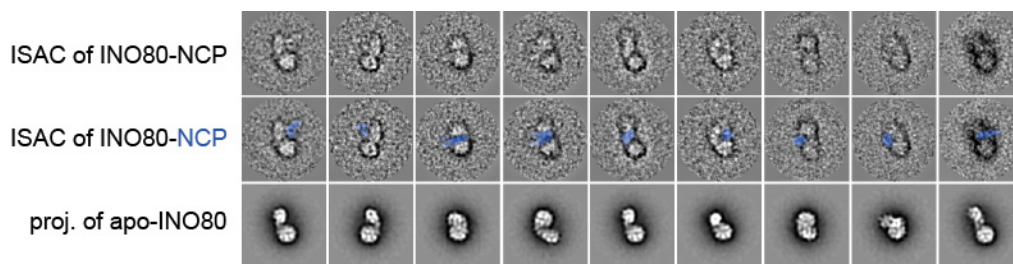


Figure 26 Visualization of INO80-nucleosome complexes. Class averages of INO80-nucleosome gained by ISAC (first and middle panel). Extra density in the central groove is stained blue. Extra density could not be assigned in the respective projections of apo-INO80 (last panel).

To confirm the central location of the nucleosome, INO80-nucleosome particles were visualized by negative stain EM (Figure 26) (Tosi et al., 2013). Indeed, extra density was observed in the central groove that could not be assigned in projections of empty INO80.

4.13 INO80 forms a stable complex with the Mec1 complex

INO80 is phosphorylated by Mec1 and Tel1 (ATR and ATM in mammals) and is a functional part of the DNA damage signaling cascade (Morrison et al., 2007). Mec1 and the obligatory partner LCD1 named ATR and ATRIP (ATR-interacting protein) in mammals respectively were co-purified with INO80 (Figure 27 and Table 2).

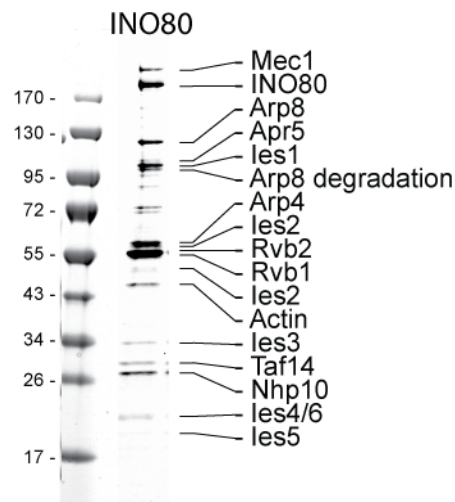


Figure 27 INO80 interacts with the Mec1 complex. Analysis of the composition of FLAG and anion exchange purified INO80 by SDS-PAGE showed that Mec1 interacted stably with INO80.

In future studies INO80-Mec1 complex will be purified and analyzed by XL-MS to identify the interaction architecture of an ATR-ATRIP complex in complex with its native substrate. There is also no structure available of ATR alone or in complex with its substrate; therefore EM will be used to determine the structure of the 1.5 MDa complex.

Ies4 is progressively phosphorylated by Mec1 upon treatment with the DNA damaging agent methyl methanesulfonate (MMS) (Morrison et al., 2007). In addition, *Ino80* mutants are

sensitive to hydroxyurea (HU) that inhibits ribonucleotide reductase and causes thus stalling of replication forks (Papamichos-Chronakis and Peterson, 2008). Thus, it will be tested, if MMS and HU increase the association between Mec1 and INO80.

Table 2 Identified subunits of the INO80 complex. The composition of the FLAG-purified INO80 complex and the interacting proteins were analyzed by LC-MS/MS. Hit Nb: Number of found protein; Protein Id: abbreviation of protein; Protein description: name of protein; Score: Mascot score; Mass: molecular weight of protein in Da; Coverage %: calculated from length and the set of peptides assigned to the protein. Proteins identified with a score below 100, where manually validated. INO80 core subunits are highlighted in grey and novel identified subunits of the Mec1 complex in orange.

<i>Hit Nb</i>	<i>Protein Id</i>	<i>Protein description</i>	<i>Score</i>	<i>Mass [Da]</i>	<i>Coverage %</i>
1	Ino80	Putative DNA helicase INO80	3688	171863	29.5
2	Rvb2	RuvB-like protein 2	2949	51694	43.3
3	Rvb1	RuvB-like protein 1	2549	50593	39.7
4	Arp8	Actin-like protein ARP8	1472	100604	26.6
5	Mec1	Serine/threonine-protein kinase MEC1/ATR	1168	275108	13.3
6	Ies1	Ino eighty subunit 1	1084	78932	25.7
7	Arp4	Actin-related protein 4	1040	55197	34.6
8	Act	Actin	754	41891	28
9	Nhp10	Non-histone protein 10	694	23956	38.4
10	Hsp71	Heat shock protein SSA1	545	69786	24.3
10	Hsp72	Heat shock protein SSA2	462	69599	24.3
11	Arp5	Actin-related protein 5	532	87677	14.3
12	Ies2	Ino eighty subunit 2	513	36189	22.2
13	Ies4	Ino eighty subunit 4	509	13084	50.9
14	Hsp75	Heat shock protein SSB1	499	66732	17
14	Hsp76	Heat shock protein SSB2	495	66668	17
15	6p21	6-phosphofructo-2-kinase 1	422	93587	13.5
16	Taf14	Transcription initiation factor TFIID subunit 14	370	27423	16.8
17	Lcd1	DNA damage checkpoint protein LCD1/ATRIP	334	86712	15.5
18	Ef1a	Elongation factor 1-alpha	316	50400	14.8
19	Ies3	Ino eighty subunit 3	295	28225	18.8
20	Ksp1	Serine/threonine-protein kinase KSP1	286	117351	6.7
21	Rpa34	DNA-directed RNA polymerase I subunit RPA34	264	26916	18.5
22	Ies6	Chromatin-remodeling complex subunit IES6	258	18579	30.1
23	Rs3	40S ribosomal protein S3	249	26543	18.8
24	Ltn1	E3 ubiquitin-protein ligase listerin	224	181270	6.3
...
57	Ies5	Ino eighty subunit 5	95	14303	32

5 Discussion

5.1 Hybrid view on INO80

Large chromatin remodelers are multi subunit complexes. The remodeling mechanism especially of macromolecular complexes is scarcely understood. Overall shapes have been reported of all families of remodelers except the INO80/SWR1 family (Asturias et al., 2002; Chaban et al., 2008; Leschziner et al., 2005; Leschziner et al., 2007; Skiniotis et al., 2007; Smith et al., 2003). Molecular topologies of large remodelers are known partially and most of the data was based on genetic studies. For INO80 it was indicated that Nhp10-Ies3, Rvb1/2-Arp5 and Arp8-Arp4-Act-HSA^{INO80} form sub-complexes with each other. Using XL-MS the interaction map of the INO80 complex could be unraveled and all INO80 subunits could be associated to the respective modules. So far interaction data was used to indentify networks, to map additional interacting proteins on homology models or to clarify the topology of complexes (Ciferri et al., 2008; Herzog et al., 2012; Jennebach et al., 2012; Leitner et al., 2012a). The XL-MS approach indicates interfaces between proteins and thus dissects with motif resolution. This is in particular strong in combination with low resolution EM structures that do not go under subnanometer resolution. In the case of INO80 this allowed building up a partial atomic fitting of available crystal structures in the head and neck region of INO80. Large complexes as INO80 are often dynamic and thus exhibit conformational heterogeneity. Crystal and EM structures only provide us with snapshots and therefore flexible under-represented conformational states or bound ligands are lost. The XL-MS technique allowed identifying the histone interaction sites in respect to INO80 subunits. A separation of for instance INO80-nucleosome or INO80-Mec1 complexes from apo-INO80 would allow analyzing the effect on the INO80 architecture in response to ligand binding.

5.2 The chromatin remodeler INO80

EM revealed that INO80 is an elongated particle (Tosi et al., 2013) and thus has complete difference appearance compared to the globular shaped, large RSC or SWI/SNF remodelers (Asturias et al., 2002; Chaban et al., 2008; Dechassa et al., 2008; Leschziner, 2011; Leschziner et al., 2005; Leschziner et al., 2007; Skiniotis et al., 2007; Smith et al., 2003). The foot of INO80 could undergo large conformational rearrangements that could be part of nucleosome recognition (Tosi et al., 2013). INO80 also looks remarkably different from SWR1 (Nguyen et al., 2013). The most striking molecular difference is probably that SWR1 contains only a hetero-hexamer compared to INO80's dodecamer (see below).

We solved the molecular architecture of INO80 by an integrated approach combining XL-MS, EM, subunit tagging and localization (Tosi et al., 2013). Four modules could be assigned within the INO80 complex next to the Ino80-Ies2 scaffold: Rvb1/2, Arp5-Ies6, Nhp10-Ies1-Ies3-Ies5 and Arp8-Arp4-Act-Ies4-Taf14. Rvb1/2 was localized in the head, the Arp5-module in the neck with the Swi2/Snf2 ATPase and Ies2, the Nhp10-module in the body and the Arp8-module in the foot (Figure 28). The modules will be separately discussed in more detail below.

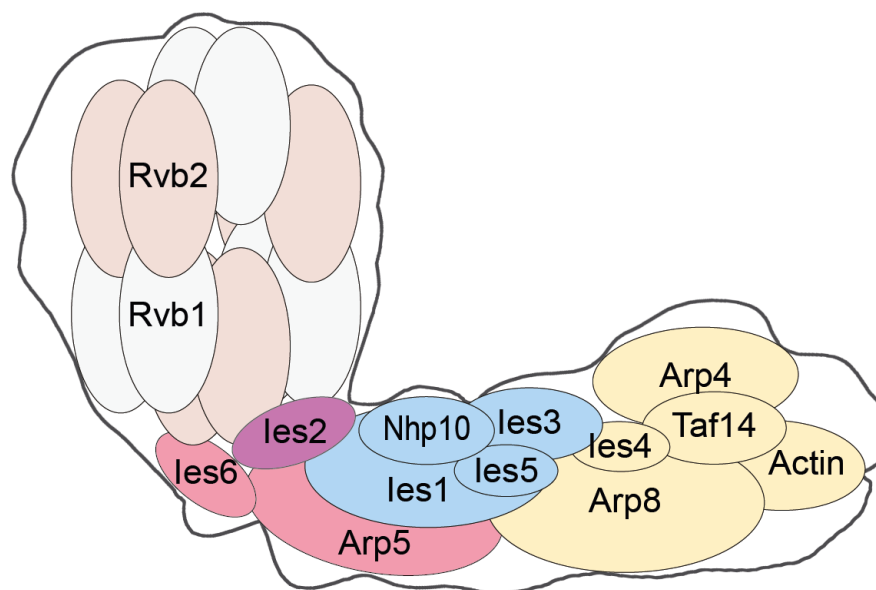


Figure 28 Model of the subunit architecture of INO80. Rvb1/2 was localized in the head of INO80 with a hetero-dodecameric organization. The Snf2 ATPase and Ies2 sit in the neck with Arp5-Ies6 in the back. Nhp10-Ies1-Ies3-Ies5 was localized in the body and Arp8-Arp4-Act-Ies4-Taf14 in the foot.

5.3 Structure of Rvb1/2 in the INO80 complex

The Rvb1/2 complex is a prominent feature of INO80 and there was no structure of an Rvb1/2 within its native complex. The structures of isolated Rvb1/2 could not clarify (i) if Rvb1/2 is a hexamer or a dodecamer; (ii) if the rings are homo- or hetero-oligomeric and (iii) how the rings interact with each other.

The INO80 complex is among the first structure containing the Rvb1/2 in a native context. However, conclusions gained about INO80's Rvb1/2 are not necessarily applicable to Rvb1/2 in other complexes or in an isolated state, if there is one. In the majorities of isolated structures, Rvb1/2 is dodecameric (Lopez-Perrote et al., 2012; Puri et al., 2007; Torreira et al., 2008), but Rvb1/2 was even be found in other oligomeric states (Cheung et al., 2010; Gorynia et al., 2011; Niewiarowski et al., 2010). Endogenously purified yeast Rvb1/2 in complex with the chaperone Hsp90 has been shown to be hetero-hexameric (Cheung et al., 2010). Rvb1/2 in the native INO80 environment adopts a dodecameric state, comprised of two hexameric rings (Tosi et al., 2013).

The resolution of the isolated Rvb1/2 EM structures was too low to differentiate Rvb1 from Rvb2; consequently the composition of the rings could not directly be abbreviated (Lopez-Perrote et al., 2012; Puri et al., 2007; Torreira et al., 2008). However, antibody labeling suggested that the rings could be composed of one species (Torreira et al., 2008). In addition, there are crystal structures of homo-rings composed of either Rvb1 (Matias et al., 2006) or Rvb2 (Petukhov et al., 2012), and hetero-hexameric rings (Gorynia et al., 2011), but this structures has a deleted domain 2. The distance restraints determined by XL-MS exclusively allow a hetero-hexameric composition of Rvb1/2 in INO80 (Tosi et al., 2013).

The stacking of the rings has been under debate as well. Yeast and human structures from the Llorca lab could easily interpreted as a domain 2-2 stacking (Lopez-Perrote et al., 2012; Torreira et al., 2008), but the stacking could not be unambiguously determined in the structure from the Tsaneva lab (Puri et al., 2007). A following work from the same lab showed that the deletion of domain 2 of Rvb1 destabilizes the dodecamer and they thus concluded that this argues against a domain 2-2 interaction of the rings (Niewiarowski et al., 2010). However, a

complete deletion of the domain 2 resulted in insoluble protein. Therefore Niewiarowski et al., deleted only the external part, the OB-folds and thus leaving the internal part of domain 2, which then can mediate the interaction (Niewiarowski et al., 2010). The volume and shape of the head of INO80 were sufficient to accommodate two rings of Rvb1 (Matias et al., 2006; Tosi et al., 2013). However, the diameter of the head was only ~ 120 Å. Thus, it was the most compact version compared to any isolated Rvb1/2 structure. Movements in the domain 2 were shown to mediate between the stretched (145 Å) and compact (130 Å) form of human isolated Rvb1/2 (Lopez-Perrote et al., 2012). Our dodecameric model of Rvb1/2 was based on the crystal structure of the hetero-dodecameric Rvb1/2 (Gorynia et al., 2011). In this structure, it was indicated that the two rings form a complex via the internal domain. But the electron densities of Gorynia et al. as well as of Matias et al. showed poor coverage in this region impeding a detailed analysis of interaction interphases (Gorynia et al., 2011; Matias et al., 2006). The compact packing of Rvb1/2 in INO80 would bring the internal domains 2 of the two opposing rings in such a close proximity principally enabling an interaction between them (Tosi et al., 2013). This would also explain why the deletion of the external OB-folds did not split the dodecameric version of Rvb1/2 (Niewiarowski et al., 2010).

In our model, the domain 2 of the same sort (Rvb1 or Rvb2) would interact with each other. This makes it likely that the hetero-hexameric composition promotes a dodecameric complex formation.

The six-fold axis in the head of INO80 enabled a placement of Rvb1/2 (Tosi et al., 2013). However, a closer inspection revealed that it is not a strict six-fold symmetry axis. The main deviation from a stringent six-fold symmetry was found in the region where the neck-body-foot cone is inserted. Such an insertion could be mediated by the insertion loop of Ino80 that was shown to recruit Rvb1/2 to SWR1 (Wu et al., 2005). In theory, if every Rvb1/2 pair in the dodecamer could bind an Ino80 insertion loop, three Ino80s could be inserted resulting in a tripod like structure. However, insertion at one site could influence the symmetry and the EM density indicated that the insertion of Ino80 resulted in an opening of the rings (Tosi et al., 2013). This would generate tension in the rings that may prevent further insertions of Ino80.

A similar hybrid approach as we performed on INO80 was applied on SWR1. SWR1 is more compact and the authors inferred that it contains a single hetero-hexameric ring (Nguyen et al., 2013). Both remodelers belong to the same family of remodelers, but SWR1 is composed of a different sub-set of subunits as INO80. The insertion in the split ATPase is a common structural feature with Ino80, albeit is not conserved on a sequence level. The insertion was shown to recruit the Rvb1/2 complex in SWR1 (Wu et al., 2005). Consistently, different insertion loops could assemble a different kind of Rvb1/2 species: a hexamer in the case of Swr1 and a dodecamer in the case of Ino80. However, non-GraFix treated samples from the study on SWR1 contained particles resembling a two layered Rvb1/2 particle (Nguyen et al., 2013). The author also quantified the intensity of the Rvb1 and 2 from a SDS-PAGE of SWR1 and INO80. The observed stoichiometry was consistent with a hexamer in both complexes. However, a similar quantifications of our highly purified and structural integer INO80 preparation resulted in ratios of 1:5.4:5.5 (Ino80:Rvb1:Rvb2), which is in agreement with the dodecamer observed in the EM map (Tosi et al., 2013). Remarkably, Nguyen et al. also found fractions containing Rvb1/2 and Swr1 with a stoichiometry of 6:6:1 in their glycerol gradient strongly indicating that the purified SWR1 was composed of hexamers and dodecamers (Nguyen et al., 2013). In general, protein staining methods are highly dependent on the amino acid composition, which is why a simple quantification of bands of a SDS-PAGE is not suitable for proper analysis of stoichiometry. Instead structural methods as analytical ultracentrifugation or native MS should be applied.

In Archaea only one form of Rvb1/2 exists indicating that two sorts of Rvb have developed during evolution, maybe by gene duplication. Rvb1 has approximately 12,000 copies per cell, whereas Rvb2 was found with 3,000 molecules (Ghaemmaghami et al., 2003). The higher copy number of Rvb1 suggests that it is also associated in other complexes independent of Rvb2.

In summary, we could show that in the INO80 complex Rvb1/2 form a hetero-dodecamer that is stacked via domains 2.

5.4 The Nhp10-module

XL-MS and biochemical analysis of INO80 deletion mutants showed that the Nhp10-module consists of Nhp10-les1-les3-les5 and that this module assembles at the N-terminal part of Ino80 (Tosi et al., 2013). Metazoan complexes also contain species-specific subunits that also assemble at the N-terminal part of Ino80 (Chen et al., 2011). Indeed, the Nhp10 sub-complex could be recombinantly expressed and purified (Tosi et al., 2013). Association with les1 was not stable and the yields were low, when les1 was co-expressed from a separate vector. To increase expression yields, les1 coding sequence will be integrated into one vector containing Nhp10-les1-les3-les5-Ino80^{N-term}. The complex of Nhp10-les3-les5 alone did not yield any promising crystallization hits. However, stabilization with DNA improved the crystallization properties. The full Nhp10-module may stabilize the complex sufficiently to yield diffracting crystals.

The Nhp10-module was assigned to the body of INO80, adjacent to the neck containing the Swi2/Snf2 ATPase of Ino80 (Tosi et al., 2013). The Nhp10-module does not belong to the conserved subunits. In general, one might expect that the conserved subunits evolved together and therefore are localized in a similar sub-compartment. In contrast, the conserved Rvb1/2, the Swi2/Snf2 domain, les2 and the Arp5-module localize in the head and neck of INO80 (Tosi et al., 2013), whereas the conserved Arp8-module is positioned in the foot of INO80. Cross-links and inference (see 5.5) indicated that the Ino80 polypeptide folds back thereby placing the Nhp10-module next to the Swi2/Snf2 module (Tosi et al., 2013). Human, fly and fission yeast INO80 complexes include GLI-Kruppel family zinc finger containing subunits that are involved in DNA binding (Cai et al., 2007; Hogan et al., 2010; Klymenko et al., 2006; Wu et al., 2007). Conceivably, INO80 only requires a strong DNA binder that facilitates recruitment and remodeling and is thus integrated close to the neck region.

Nhp10 was shown to preferentially bind long distorted DNA (Ray and Grove, 2009, 2012). In general, one HMG box interacts with ~10 bp of duplex DNA (Love et al., 1995; Ohndorf et al., 1999; Wong et al., 2002; Yen et al., 1998). Since Nhp10 consists of two HMG boxes, it was predicted to bind to a 20 bp long DNA (Ray and Grove, 2009). But Nhp10 preferred far longer constructs and a 50 bp long duplex was even favored over 37 bp. On those substrates Nhp10-

les3-les5 was forming oligomers. The DNA could either serve as binding platform for one molecule or oligomerization could increase the binding affinity.

Nhp10-les3-les5 was found to bind structured and curved DNA and to be a high affinity nucleosome binder (Tosi et al., 2013). This renders the Nhp10-module a perfect candidate to stabilize reaction intermediates in the remodeling reaction or target the INO80 complex to sites of action.

5.5 The Arp8-module

The Arp8-module consists of Arp8-Arp4-Act-les4-Taf14-HSA^{INO80} (Tosi et al., 2013). Arp4 and Arp8 were shown to bind to histones and to DNA (Gerhold et al., 2012; Harata et al., 1999; Shen et al., 2003). Indeed, we found that INO80(Δ arp8) was compromised in DNA and nucleosome binding and remodeling. However, binding and remodeling of nucleosomes were not completely abolished in the case of INO80(Δ arp8) as was observed previously (Shen et al., 2003). We found that the structural integrity of INO80(Δ arp8) was diminished. Thus all assays had to be performed with freshly purified INO80(Δ arp8) as otherwise the complex was aggregated and failed to bind to its substrate.

The distant restraints gained by XL-MS analysis could be used to structurally model complexes by minimizing the constraint. Although crystal structures of yeast Arp4, Arp8 and Actin (Fenn et al., 2011; Gerhold et al., 2012; Saravanan et al., 2012; Schubert et al., 2013; Vorobiev et al., 2003), and the structure of the related complex of Arp7-Arp9-Rtt102-HSA^{Swi/Snf} were available an unambiguous modeling could not be achieved. Arp4 more closely resembles Arp7 on a sequence basis (Muller et al., 2005). Therefore, Arp4 could be placed in the position where Arp7 resides and Act could be modeled in the respective position of Arp9 in the Arp7-Arp9-Rtt102-HSA^{Swi/Snf} complex without significant steric clashes (Schubert et al., 2013). The inter-links in principle agreed with that fitting. However, the majority of the inter-links were found in loops inserted into the core actin folds. These insertions were mostly unstructured in the crystal structures indicating flexibility and thus prohibited reliable fitting. These loop

regions might be stabilized when the interface is formed within the Arp8-complex. Rtt102 was shown to bind in an extended form to a conserved region of the Arp7-Arp9 interface suggesting a stabilizing role (Schubert et al., 2013). This function could be fulfilled by for instance either Ies4 or Taf14 within INO80's HSA module. The C-terminal part of Taf14 was highly inter-linked within the Arp8-module (Tosi et al., 2013) and could thus stabilize the interface. The N-terminal part containing the YEATS-domain was not necessary for the association with chromatin remodelers, but rather may provide a regulatory platform outside of INO80 (Schulze et al., 2010). In summary, insufficient distant restraints in ordered parts and observed flexibility in the foot region of INO80 (Tosi et al., 2013) prohibited modeling of the Arp8-module with an unambiguous solution.

The HSA domain in the Arp7-Arp9-Rtt102-HSA^{Swi/Snf} complex adopts a largely extended α -helical structure (Schubert et al., 2013). This extended conformation of the HSA-domain could explain how Ino80 could span across the neck and the foot. This elongated form is also perfectly suitable to provide an interaction platform and structural rearrangements of the foot of INO80 could thereby mediate the complete mechanistic framework of INO80.

5.6 The nucleosome remodeler INO80

INO80 is an ATP-dependent nucleosome remodeler that catalyzes various DNA mediated processes such as exchange of histone variants or even evicting complete nucleosomes or sliding (Morrison and Shen, 2009; Shen et al., 2000). Therefore, it is of importance to study the holo-INO80 complex bound to a nucleosome. The interaction sites of INO80 to histones were determined by XL-MS and the nucleosome bound to INO80 was visualized by 2D EM. XL-MS of INO80-nucleosome complexes oriented the H2A/H2B dimer at the head and neck modules of INO80 (Tosi et al., 2013). EM revealed extra density corresponding to the nucleosome in the central groove of INO80. This central position of the nucleosome is also consistent with the placement of the INO80-modules. The nucleosome could be sandwiched between the head and

the foot (Figure 29). The different modules could thus approach the nucleosome from opposing sites imposing an asymmetry on the pseudo-symmetric nucleosome.

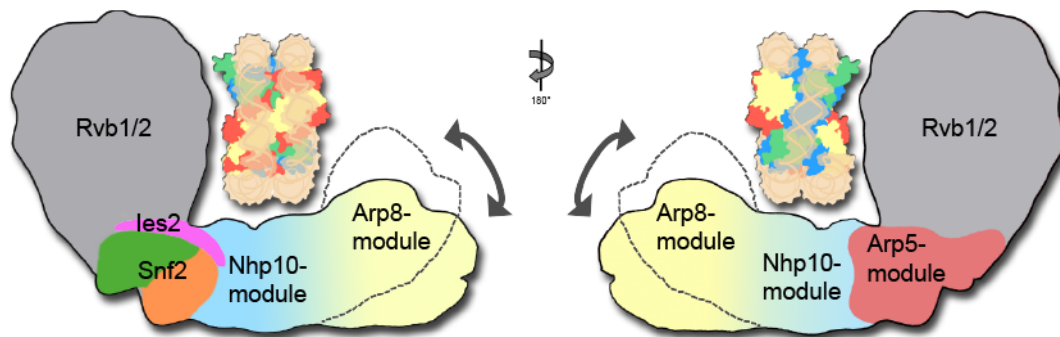


Figure 29 Model of an INO80-nucleosome complex. The nucleosome is sandwiched between the Rvb1/2 head module and the Arp8-module containing foot of INO80. The DNA could be contacted by the Nhp10-module in the body. The histones are flanked by the Snf2 domain, Ies2 and the Arp5-module in the neck and the Arp8-module. The observed conformational flexibility of the foot could explain how INO80 engulfs the nucleosome.

Both the Swi2/Snf2 domain of Ino80 and Arp5-Ies6 in the neck, which are both required for INO80's catalytic activity, are in close proximity to the H2A/H2B dimer (Tosi et al., 2013). It is of particular interest how INO80 interacts with the H2A/H2B dimer in the nucleosome, since this is the product state of an exchanged H2A.Z/H2B dimer. Intriguingly, the DNA binding OB-folds of Rvb1/2 are in proximity to the H2A/H2B dimer close to the DNA entry/exit site and to the RecA2 fold and Ies2 allowing a coordinated action. Rvb1/2 marginally bound to DNA and nucleosomes in shift assays (Tosi et al., 2013). However, Rvb1/2 was highly inter-linked with histones. A deletion of Rvb1/2 from INO80 results in a remodeling deficient complex (Jonsson et al., 2004). But the loss of Rvb1/2 is not necessarily the cause for remodeling deficiency as the Arp5-module, which is critical for remodeling was also lost together with Rvb1/2 (Jonsson et al., 2004; Shen et al., 2003; Tosi et al., 2013). Rvb1/2 showed no nucleosome or DNA binding, albeit was highly inter-linked with it. It is thus likely that Rvb1/2 plays a critical role in the catalytic mechanism of remodeling.

Ies2 covers the central cleft of the two Swi2/Snf2 ATPase lobes (Figure 30). Work on other Swi2/Snf2 ATPases, as the Chd1 and ISWI remodeler has shown that accessory domains influence the activity and provide negative autoregulation (Hauk et al., 2010; Narlikar et al., 2013). In general, the helicase motifs of Swi2/Snf2 ATPases have to align to be compatible with

ATP hydrolysis. In the case of Chd1, the chromodomains block the DNA binding site on the ATPase lobe 2 and prevent proper alignment of conserved helicase motifs thereby reducing the discrimination of naked DNA over nucleosomes (Hauk et al., 2010). ISWI's NegC lies across the two ATPase lobes bridging the cleft and inhibits coupling of the ATPase activity to DNA translocation (Clapier and Cairns, 2012).

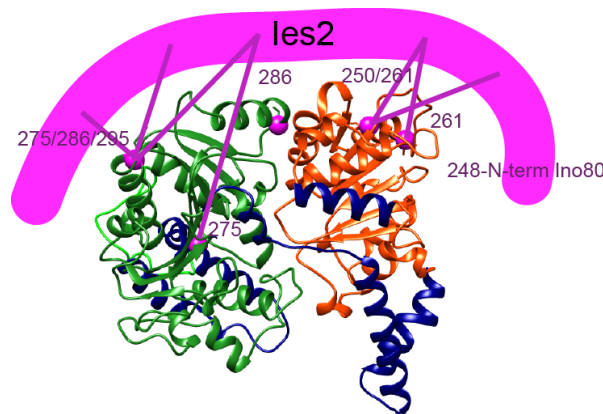


Figure 30 The PAPA-1 domain of Ies2 covers the Swi2/Snf2 ATPase lobes. Ies2 (pink) cross-linked to the Swi2/Snf2 fold of Ino80 (used homology model DroRad54 (PDB: 1Z3I (Thoma et al., 2005))) in a way that it would cover both RecA lobes. Residues that were cross-linking to Ies2 were marked as pink small spheres. Numbers indicate the cross-linking amino acid of Ies2.

Cross-links indicated that Ies2 is localized at the Swi2/Snf2 ATPase of Ino80 in a manner that it is crossing the two lobes from N- to C-terminus (Tosi et al., 2013). This involves only a short patch in Ies2, the PAPA-1 domain suggesting that this region is extended. In this position, Ies2 is perfectly situated to regulate the ATPase of Ino80 and therefore it could be an accessory subunit helping to discriminate between substrates and to regulate the Ino80 ATPase.

The Arp5-module sits together with the Swi2/Snf2 and Ies2 in the neck of INO80 (Tosi et al., 2013). Arp5-Ies6 was crucial for remodeling, but only marginally bound to DNA and nucleosomes (Shen et al., 2003; Tosi et al., 2013). ATP hydrolysis of INO80(Δ arp5) was stimulated by DNA, but the histone component in INO1 nucleosomes did not further increase ATPase activity. Ies6 has an YL-1 domain that is also found in Swc2, a subunit in the SWR1 remodeler, which has been shown to directly bind to H2A.Z-H2B (Wu et al., 2005). Swc2 recruits, positions and locks SWR1 on the +1 nucleosome (Ranjan et al., 2013; Watanabe et al., 2013; Yen et al., 2013). Deletion of Swc2 resulted in low and irregular recruitment of SWR1 and

substantial loss of H2A.Z (Yen et al., 2013). The counterpart of Swc2 in INO80, Ies6 could fulfill similar roles. Loss of Arp5 led to the retainment of H2A.Z at the +1 nucleosome and even led to increased occupancy of the variant. This suggests that Arp5-Ies6 could act as a histone chaperone that may bind to either the substrate or product state H2A or H2A.Z, respectively. This notion is additionally supported by the fact that the ATPase activity of INO80(Δ arp5) is not reacting anymore to the histone moiety. Moreover, human Arp5 has been shown to shuttle between the nucleus and cytoplasm (Kitayama et al., 2009) and yeast Arp5 fulfills functions outside from INO80 (Yen et al., 2012).

The Nhp10-module is situated in the body close to the neck of INO80. The central upright orientation of the nucleosome would thus allow the high affinity DNA binder, Nhp10-Ies3-Ies5 to fixate the substrate in the remodeling reaction (Tosi et al., 2013). Apart from just merely binding to the substrate, HMG-box proteins have been implicated in stimulating the remodeling activity (Stros, 2010; Ugrinova et al., 2009). It is plausible that Nhp10 can facilitate the reaction by binding to intermediate states or by bending DNA to distort histone-DNA contacts.

The structure of the INO80 complex is remarkably different from all other chromatin remodelers and the proposed clamping mechanism of how INO80 interacts with the nucleosome is unique for remodelers (Figure 29) (Tosi et al., 2013). INO80 embraces the nucleosome and has a large interface with its substrate, which is completely different to the limited contacts provided by the related SWR1 (Nguyen et al., 2013). All modules of INO80 cross-linked to the histones suggesting that they are all involved in the interaction with the nucleosome. Simple docking of the nucleosome particle into the concave groove of INO80 could not explain how all the subunits are able to contact it. Indeed large conformational changes with a flexible foot have been observed (Tosi et al., 2013). Such structural rearrangements could bring especially the subunits of the foot in touch with the nucleosome (Figure 30).

The proposed enclosure could explain how INO80 acts as a steric ruler in the nucleosome spacing reaction. In fact, INO80 spaces nucleosomes with extreme long linker DNA *in vitro* (168 bp) far more precisely than the hallmarked spacer, ISWI that rather randomize arrays with such a linker length (Gangaraju and Bartholomew, 2007; Kagalwala et al., 2004;

Udugama et al., 2011; Vary et al., 2003). One simple reason could be the bigger size of INO80 that enables a complete engulfment of the nucleosome including long linker DNA. In fact, SWR1 is not able to slide nucleosomes and showed to have limited contacts to its substrate (Nguyen et al., 2013). Remodelers that have large interfaces with its substrate have been shown to slide octamers (Chaban et al., 2008; Dechassa et al., 2008; Tosi et al., 2013). Thus, it could be speculated that extensive nucleosome contacts are required to compensate for unwound DNA states.

The closing and opening rearrangements of INO80 around a nucleosome could mediate partial disassembly of the nucleosome particle (Figure 29). Indeed, open nucleosome states have been identified ((Bohm et al., 2011), reviewed in (Andrews and Luger, 2011)). Those open intermediates exist in a minority of 0.2-3% under physiological conditions and could be promoted by remodelers such as INO80. INO80 regulates the high nucleosome turnover at +1 that could conceivably promote a partial disassembly of this nucleosome and the created accessible H3/H4 histones could then be removed by histone chaperones (Yen et al., 2013). Many cross-linking sites between subunits of INO80 and histones were found, which were not accessible in an intact nucleosome as observed in crystal structures (Clapier et al., 2008; Luger et al., 1997; Tosi et al., 2013). In fact, those cross-linked and buried residues were located at the DNA entry/exit site, which was contacted by the Swi2/Snf2 ATPase of Ino80 and further catalytically crucial subunits of INO80 that could in principal distort contacts between the DNA and histones. The chemo-mechanical force could be provided by the Swi2/Snf2 ATPase to create more accessible or partially unfolded states, and accessory subunits could stabilize those intermediates. Interestingly, at this position the C-terminal H2A.Z docking domain is located, which shows the highest sequence divergence to canonical H2A. It is conceivably that les2 or the putative histone chaperone les6 senses their substrate at this site. Strikingly, the location of the RecA2 cross-link at the H2A/H2B dimer coincides with the binding site of ISW2 on the nucleosome (Dang and Bartholomew, 2007). ISWI has been shown to contact DNA at an internal location of ~20 bp away from the dyad (SHL -2/+2). The Swr1 subunit containing the Swi2/Snf2 ATPase likewise cross-linked to a ~20 bp region that is 70 bp away from the dyad in CHIP-exo data (Yen et al., 2013). Ino80 was broadly distributed over the +1 nucleosome

consistent with a complete embracement of the nucleosome by INO80 (Tosi et al., 2013; Yen et al., 2013). Nonetheless, it is tempting to speculate that it is a common feature among Swi2/Snf2 remodeler that they act close to the SHL2 of nucleosomes.

Still, the overall mechanism of H2A.Z histone exchange is not clear. A plausible scenario might be that SWR1 is recruited to the distal H2A/H2B dimer at the +1 nucleosome via the NFR, histone acetylation and the Swc2 subunit (Luk et al., 2010; Ranjan et al., 2013; Yen et al., 2013). Then the exchange with a H2A.Z/H2B dimer takes place. To produce a homo-typic ZZ nucleosome (two copies of H2A.Z), the second H2A/H2B containing dimer must be exchanged. The structure of SWR1 with its limited nucleosome contact points provides though no clue how it could move to the other side of the nucleosome. Given the small interface SWR1 may bind very transiently and thus just hops randomly to the other side. INO80 could be recruited to the NFR and the sequence specific DNA binder Reb1, which is known to organize arrays could promote the binding (Badis et al., 2008; Hartley and Madhani, 2009; Yen et al., 2013). Reb1 typically resides approximately 70 bp upstream of the +1 nucleosome in the NFR (Badis et al., 2008; Yen et al., 2013). A nucleosome with a 70 bp long extranucleosomal DNA is the preferred substrate of INO80 (Udugama et al., 2011). Nhp10 and Ies5 mirror the occupancy of Reb1 and Arp8 might be the bridge to the +1 nucleosome core (Yen et al., 2013). It is therefore likely that the proximal H2A.Z/H2B dimer is evicted first. Consistently, the distal H2A.Z/H2B dimer is enriched at +1 nucleosomes. However, the genome wide occupancies of INO80 subunits do not correlate with a simply docking of the nucleosome into the structure of INO80 (Tosi et al., 2013; Yen et al., 2013). INO80 in contrast to SWR1 is able to remodel the nucleosome and thus could partially unfold or dismantle the nucleosomes (Tosi et al., 2013; Udugama et al., 2011).

5.7 Chromatin regulators facilitate transcription

The transcription machinery is probably assembled at the 5' NFR upstream of the +1 nucleosome (Pugh, 2013; Venters and Pugh, 2013). But how do all these involved factors access the DNA? Transcription factors and the polymerase need to contact and read the underlying

DNA sequence. Besides the accessible NFR and exposed major groove in the nucleosome, thermal fluctuations and DNA breathing might create accessibility of certain DNA regulatory elements (Polach and Widom, 1995). Access to DNA is also actively mediated by chromatin remodeling. Nucleosome sliding by RSC and SWI/SNF could distort histone-DNA contacts thereby creating unwrapped regions (Dechassa et al., 2008; Engeholm et al., 2009; Ulyanova and Schnitzler, 2005). Furthermore, nucleosome spacing by ISWI1a, Chd1 or INO80 could either open and close DNA sites or ISW1 and CHD1 could space nucleosomes after a partial disassembly and reassembling following transcription, which could be assisted by chaperones as FACT (facilitates chromatin transcription) or Spt6 (Bortvin and Winston, 1996; Narlikar et al., 2013; Orphanides et al., 1999). The +1 nucleosome can be additionally modified by histone variants, such as the incorporation of H2A.Z mediated by SWR1 (Kobor et al., 2004; Krogan et al., 2003; Mizuguchi et al., 2004). At activated genes, the -1 and +1 nucleosomes are modified by methylation and acetylation. Acetylated histones are recognized by bromodomain containing chromatin regulators including the SAGA histone acetyltransferase complex and the general transcription factor TFIID (Hassan et al., 2002; Jacobson et al., 2000; Pugh, 2013). TFIID and SWR1 share the bromodomain-containing factor 1, Bdf1 that recognizes acetyl histone marks (Ladurner et al., 2003; Pugh, 2013). INO80 contains Taf14 that is also found in TFIID. However, whether Taf14 in the context of INO80 could function together with TFIID remains to be elucidated (Schulze et al., 2010). SAGA and TFIID deliver TBP (TATA-binding protein) to promoters (Pugh, 2013; Sermwittayawong and Tan, 2006). TBP recruits TFIIB, which positions the polymerase II at the promoters (Bushnell et al., 2004; Hausner et al., 1996; Nikolov et al., 1995). Chromatin remodelers engage the same NFR and +1 nucleosome interface as the transcription machinery (Yen et al., 2013). Those sites are thus frequented crossroads for factors of chromatin regulation and transcription. How this tight traffic is controlled remains to be elucidated in future.

6 *Material and Methods*

6.1 *Materials*

For all methods described, deionized water, sterile solutions and sterile flasks were used. Unless otherwise mentioned, chemicals and reagents were obtained from Amersham-Pharmacia, Applied BioSystems, BioMol, BioNEER, BioRad, Difco, Fluka, Invitrogen, Kodak, Merck, New England BioLabs, Promega, Roth, Roche, Riedel de Haen, Serva, Sigma or Stratagene.

Oligonucleotides and enzymes were obtained from Fermentas (Thermo Scientific), Metabion and Eurofins MWG.

E. coli strains were cultivated in Luria broth (LB) medium containing 10 g bacto tryptone, 5 g yeast extract, 5 g NaCl and 1.3 ml 2 M NaOH per 1 L and the respective antibiotic (100 mg/ml ampicillin; 50 mg/ml kanamycin; 35 mg/ml chloramphenicol; 12.5 mg/ml tetracycline; 7.5 mg/ml gentamycin). Agar plates contained 15 g agar.

S. cerevisiae strains were cultivated in YPD medium containing 20 g bacto peptone, 10 g yeast extract and 20 g glucose per 1 L.

All purifications were performed on Äkta systems with appropriate chromatographic columns (GE Healthcare). Crystallization screens and tools were purchased from Jena Bioscience, Hampton Research or Nextal Biotechnologies (Qiagen).

6.2 Yeast strains

Table 3. Yeast strains used in this study

Strain	Genotype	Source
INO80-FLAG ₂	<i>MATa INO80-FLAG₂ his3Δ200 leu2Δ0 met15Δ0 trp1Δ63 ura3Δ0</i>	Shen et al., 2000
INO80Δarp5	<i>MATa INO80-FLAG₂ his3Δ200 leu2Δ0 met15Δ0 trp1Δ63 ura3Δ0 arp5Δ::KanMX6</i>	This study
INO80Δarp8	<i>MATa INO80-FLAG₂ his3Δ200 leu2Δ0 met15Δ0 trp1Δ63 ura3Δ0 arp8Δ::KanMX6</i>	This study
INO80Δnhp10	<i>MATa INO80-FLAG₂ his3Δ200 leu2Δ0 met15Δ0 trp1Δ63 ura3Δ0 nhp10Δ::KanMX6</i>	This study
Arp4-DID1	<i>MATa INO80-FLAG₂ his3Δ200 leu2Δ0 met15Δ0 trp1Δ63 dyn2Δ::KanMX6 Arp4-DID1::URA3</i>	This study
Nhp10-DID1	<i>MATa INO80-FLAG₂ his3Δ200 leu2Δ0 met15Δ0 trp1Δ63 dyn2Δ::KanMX6 Nhp10-DID1::URA3</i>	This study
les6-DID1	<i>MATa INO80-FLAG₂ his3Δ200 leu2Δ0 met15Δ0 trp1Δ63 dyn2Δ::KanMX6 les6-DID1::URA3</i>	This study
les2-DID1	<i>MATa INO80-FLAG₂ his3Δ200 leu2Δ0 met15Δ0 trp1Δ63 dyn2Δ::KanMX6 les2-DID1::URA3</i>	This study

6.3 Plasmid lists

Table 4. Plasmid list for expression in *E. coli* or insect cells used in this study.

Encoded sequence and construct name	Origin	Vector	Purpose, Tag and Source
Nhp10, les3, les5	<i>S. c.</i>		N-term His-tag Nhp10
Ino80 1-152, Nhp10, les3, les5	<i>S. c.</i>	pFBDM	N-term His-tag Nhp10
Ino80 1-213, Nhp10, les3, les5	<i>S. c.</i>	pFBDM	N-term His-tag Nhp10
Ino80 1-258, Nhp10, les3, les5	<i>S. c.</i>	pFBDM	N-term His-tag Nhp10
Ino80 14-450, Nhp10, les3, les5	<i>S. c.</i>	pFBDM	N-term His-tag Nhp10
les1	<i>S. c.</i>		N-term FLAG-tag
Ino80 707- C-term, les2	<i>S. c.</i>	pFBDM	N-term His-tag Ino80
Ino80 692-1021 + 1248- C-term, les2, Rvb1 130-248	<i>S. c.</i>	pFBDM	N-term His-tag Ino80
Ino80 692-1021 + 1248- C-term, les2	<i>S. c.</i>	pFBDM	N-term His-tag Ino80
Ino80 973-1278/1538-1705, les2	<i>C. t.</i>	pFBDM	N-term His-tag Ino80
Ino80 973-1705, les2	<i>C. t.</i>	pFBDM	N-term His-tag Ino80
Ino80 958-1278/1538-1705, les2	<i>C. t.</i>	pET Duet	N-term His-tag Ino80
Rvb1 122-240	<i>C. t.</i>	pRSF Duet	
Rvb1 122-240	<i>C. t.</i>	pFBDM	
H2A	<i>D. m.</i>	pFMP	
H2B	<i>D. m.</i>	pFMP	
H3	<i>D. m.</i>	pFMP	

H4	<i>D. m.</i>	pFMP	
H2A.v	<i>D. m.</i>	pET21	
Gentamicin	-	pFA6a	Kanamycin resistance marker for G418 selection (P. Wendler)
URA3 promoter and gene	-	pBluescript	URA3 auxotrophy marker for ura selection (K. Strässer)
DID1-Nup120	-	pProEx	DID tagging in yeast; fusion of DID1 to gene of interest (Flemming from E. Hurt)
PrA-TEV-DID1	-	pProEx	DID tagging in yeast; fusion of DID1 to gene of interest (Flemming from E. Hurt)
GST-FLAG-DID2	-	pProEx	DID tagging in yeast; DID2 is expressed in Rosetta(DE3) (Flemming from E. Hurt)
His6-Dyn2	-	pET	DID tagging in yeast; Dynein2 (Dyn2) is expressed in Rosetta(DE3) (Flemming from E. Hurt)

6.4 Oligonucleotide list

Table 5. Oligonucleotide list used in this study.

Primer name	5' – 3' Sequence	Vector/Purpose
Nhp10_Sall_for	AAAAAGTCGACATG AAA CATCATCATCATCATATAAAATGTCAGTTGAA GAAAAAAGCGCAGAC	pFBDM polh; N-terminal His-tag TAGzyme
Nhp10_NotI_bac	AAAAA GCGGCCGCTTAGTTAGAGGAACTAACTTCCATC	pFBDM polh
yles3_XhoI_fw	AAAAACTCGAGATGAAGTTCGAAGACCTCTTGGC	pFBDM p10
yles3_NheI_rv	AAAAAGCTAGCTTAAAGAAT GTTTTCCAAAAG GCC G	pFBDM p10
yles5_XhoI_fw	AAAAACTCGAGATGCCTAGTAAA GATCCA GAG	pFBDM p10
yles5_NheI_rv	AAAAA GCTAGCTTATGGTGTGTGCGTATC	pFBDM p10
ylo8-1-x_Sall_f	AAAAAGTCGACATGTCACTGGCAGTTCTAC	pFBDM polh
ylo8-1-152Not_r	AAAAAGCGCCGCTCAAAGCTCGTCTTCATCATC	pFBDM polh
ylo8-1-213Not_r	AAAAAGCGCCGCTCATCCATTAAACAGTAACAACAG	pFBDM polh
ylo8-1-258Not_r	AAAAAGCGCCGCTCATCCATTTTCTTCCTCG	pFBDM polh
ylo8-1-450Not_r	AAAAAGCGCCGCTCACAACCCGTGTCTAGTG	pFBDM polh
ylo8_14-xSal_f	AAAAAGTCGACATGATATCTGATTTTCAAAG	pFBDM polh
KanB rev	CTGCAGCGAGGAGCCGTAAT	check G418 cassette in Δ strain
KanC for	TGATTTTGATGACGAGCGTAAT	check G418 cassette in Δ strains
Arp8 up for	GAACAACTCTCGAACAAGG	amplify arp8 Δ box
Arp8 down rev	GCTACGGGGTATTGTCTC	amplify arp8 Δ box
Arp8 up check for	AGAGTGGAAGTAACAAACAGAAC	check for right locus of deletion
Nhp10 up for	GTGATAGTCGGCAAAGG	amplify nhp10 Δ box

Nhp10 down rev	GTGATATTAGGAATCGTCTG	amplify nhp10 Δ box
Nhp10 up check for	GATCATCATTACTATCTACCATG	check for right locus of deletion
Arp8 del L2 rev	GGGGATCCGTCGACCTGCAGCGTACCATGTTAGGTGCGATTGTATCC	deletion of ARP8 KanMX6, upstream of START rev
Arp8 del L3 for	AACGAGCTCGAATTCATCGATGATATGAGATATGCATATGGAAGTTTTTG	Deletion of Arp8 with KanMX6, downstream of STOP
L1 Arp5 up for	GAAGGTGACAATATAGAAGGG	amplify of deletion box
L4 Arp5 down rev	GGGTGTCAATCCAAAAG	amplify of deletion box
Arp5 up check for	TACCAAAATGTGTGCAGG	check for right locus of deletion
L2 Arp5 del rev	GGGGATCCGTCGACCTGCAGCGTACCATTATACGTCTTATGTTTCAGAGTCC	deletion with KanMX6, upstream of START rev
L3 Arp5 del for	AACGAGCTCGAATTCATCGATGATATGAGGAGACAGCAAAGTAAAC	deletion with KanMX6, downstream of STOP
L1 les1 up for	AAAAGACCACTACTGTTATGACA	amplify of Δ box
L4 les1 down rev	GGATAACGCTGAAGGTCA	amplify of Δ box
L1 les3 up for	GAGAACTTGTTCCTTCGC	amplify of Δ box
L4 les3 down rev	GGAGGTTGAGTTCGAGAAC	amplify of Δ box
L1 les5 up for	CACGTTGCGGACTAAAC	amplify of Δ box
L4 les5 down rev	ACGCAGTGAAGGAGATTAC	amplify of Δ box
L1 Dyn2 up for	CCGACGAATGGATTATTATC	amplify of Δ box
L2 Dyn2 del rev	GGGGATCCGTCGACCTGCAGCGTACCATTTTGGTTTTAATTGCTCTTC	Deletion with KanMX6, upstream of START rev
L3 Dyn2 del for	AACGAGCTCGAATTCATCGATGATATGAATAGTGTCTTCAATAGTTAATCG	deletion with KanMX6, downstream of STOP
L4 Dyn2 down rev	CTACCCTCTCTTGCAAAGTCT	amplify of deletion box
yRecA1_692_fw	AAAAAGTCGACGGTGAAATAACCATCGAGC	pFBDM
yRecA1_707_fw	AAAAAGTCGACAAAGAATATCAGCTCAAGGG	pFBDM
yRecA1_1021_rv	GATGGCATTGATATGTTGGAATCTGCCCTTTCAAAAAGATCC	pFBDM
yRecA2_1248_fw	GGATCTTTTTGAAAGGGCAGATTCCAACATATCAATGCCATC	pFBDM
yRecA2_C_rv	AAAAAGCGGCCGCTCATGCCAATGCACTTGC	pFBDM
ctRecA2_1538_fw	GTTTGAGCGTGCCGACACAAATATCACGGTCCCG	pET Duet/ pFBDM
ctRecA1_1705_rv	AAAAAGCGGCCGCTTAACCAGTACCAGTGATGAC	pET Duet/ pFBDM
ctRA1_973_BamH1_duet fw	AAAAAGGATCCgAAAGAATACCAGTTGAAAGGTC	pET Duet
CtR1_958_BamH1_duet fw	AAAAAGGATCCgACCGAATTCGAGGTTG	pET Duet
Ray_50nt_CT-9-AA-fw	ACAGTGGAGTAGGCTACACCTACTCTTTGTAAGAATTTTGCAAAAAGTAC	Oligo for DNA binding
Ray_50nt_CT-9-AA-rv	TGTCACCTCATCCGATGTGCTTGAGAAACAACTTAAACGTTTTTCATG	Oligo for DNA binding

Ray_37nt_CT-9-AA-fw	TGGAGTAGGCTACACCTACTCTTTGTAAGAATTTTGC	Oligo for DNA binding
Ray_37nt_CT-9-AA-rv	ACCTCATCCGATGTGCTTGAGAAACAACTTAAACG	Oligo for DNA binding
Guy_fork_3_1	CAACGTCATAGACGATTACATTGCTACATGGAGCTGTCTAGAGGATCCGA	Oligo for DNA binding
Guy_fork_3_2	GTCGGATCCTCTAGACAGCTCCATGATCACTGGCACTGGTAGAATTCGGC	Oligo for DNA binding
Guy_fork_3_3	TGCCGAATTCTACCACTGCCAGTGAT	Oligo for DNA binding
Guy_fork_3_4	TAGCAATGTAATCGTCTATGACGTT	Oligo for DNA binding

6.5 Buffer list

Table 6. Buffers used for protein purification used in this study.

Buffers	
Buffer name	Ingredients
Protease Inhibitor	500 μ M pepstatin A, 100 μ M phenylmethanesulfonylfluoride (PMSF), 66 μ M leupeptin, 270 mM benzamidine in ethanol
Resuspension buffer	20 mM HEPES KOH pH 8.0, 5% glycerol (v/v), 1.2% PVP-40, 1x protease inhibitor
Lysis buffer	25 mM HEPES KOH pH 8.0, 500 mM KCl, 10% glycerol (v/v), 0.05% NP40 (v/v), 1 mM EDTA, 1 mM DTT, 4 mM $MgCl_2$, 1x protease inhibitor
H-0.5 FLAG	25 mM HEPES KOH pH 8.0, 500 mM KCl, 10% glycerol (v/v), 0.05% NP40 (v/v), 1 mM EDTA, 1 mM DTT, 4 mM $MgCl_2$
H-0.2 FLAG	30 mM HEPES KOH pH 8.0, 200 mM KCl, 10% glycerol (v/v), 0.05% NP40 (v/v), 1 mM DTT, 4 mM $MgCl_2$
Elution buffer	30 mM HEPES KOH pH 8.0, 200 mM KCl, 10% glycerol (v/v), 0.05% NP40 (v/v), 1 mM DTT, 4 mM $MgCl_2$, FLAG peptide
H-0.2 Q	25 mM HEPES KOH pH 8.0, 200 mM KCl, 7% glycerol (v/v), 0.05% NP40 (v/v), 1 mM DTT, 4 mM $MgCl_2$
H-1 Q	25 mM HEPES KOH pH 8.0, 1000 mM KCl, 7% glycerol (v/v), 0.05% NP40 (v/v), 1 mM DTT, 4 mM $MgCl_2$
H-1 SEC	25 mM HEPES KOH pH 8.0, 200 mM KCl, 3% glycerol (v/v), 0.05% NP40 (v/v), 1 mM DTT, 4 mM $MgCl_2$
H-0.1 Nhp10	25 mM HEPES KOH pH 8.0, 100 mM KCl, 10% glycerol (v/v), 2 mM β -mercaptoethanol, 4 mM $MgCl_2$
H-0.1 Q Nhp10	25 mM HEPES KOH pH 8.0, 100 mM KCl, 7% glycerol (v/v), 2 mM β -mercaptoethanol, 4 mM $MgCl_2$
H-1 Q Nhp10	25 mM HEPES KOH pH 8.0, 1000 mM KCl, 7% glycerol (v/v), 2 mM β -mercaptoethanol, 4 mM $MgCl_2$
H-0.1 SEC Nhp10	25 mM HEPES KOH pH 8.0, 100 mM KCl, 3% glycerol (v/v), 2 mM β -mercaptoethanol, 1 mM $MgCl_2$

Sau-0	40 mM NaOAc pH 8.0, 8 M Urea, 5 mM β -mercaptoethanol, 5 mM lysine
Sau-1000	40 mM NaOAc pH 8.0, 8 M Urea, 5 mM β -mercaptoethanol, 5 mM lysine, 1000 mM NaCl
Sau-200	40 mM NaOAc pH 8.0, 8 M Urea, 5 mM β -mercaptoethanol, 5 mM lysine, 200 mM NaCl
Histones-0 Q	15 mM Tris HCl pH 8.0
Histones-2 Q	15 mM Tris HCl pH 8.0, 2 M NaCl
Unfolding buffer	20 mM Tris HCl pH 7.5, 7 M guanidine hydrochloride, 10 mM DTT
Refolding buffer	10 mM Tris HCl pH 7.5, 2 M NaCl, 5 mM β -mercaptoethanol, 1 mM EDTA
NCP buffer-0	20 mM Tris HCl pH 7.5, 10 mM DTT
NCP buffer-2000	20 mM Tris HCl pH 7.5, 10 mM DTT, 2000 mM KCl
Remodeling buffer	25 mM Hepes KOH pH 7.6, 50 mM NaCl, 10% glycerol, 0.05% NP-40, 0.1 mM EDTA, 4 mM $MgCl_2$, 1 mM DTT

6.6 Molecular biology methods

6.6.1 Cloning in bacteria

In principal, cloning was performed with standard protocols. Polymerase chain reactions (PCR) were performed using a premixed reaction and a primer concentration of 0.5 μ M to generate constructs listed in table 4. The annealing temperatures were adapted to primers listed in table 5. PCR reactions were analyzed by a 1% agarose gel electrophoresis. The insert and vector DNA were digested with appropriate restriction enzymes and according to instructions from the manufacturer. The vector was subsequently dephosphorylated by alkaline phosphatase. Cleavage reactions were purified by agarose gel electrophoresis. The digested insert was ligated into the linearized vector using DNA ligase. Multiple genes were cloned in one vector using the pFBDM vector system (Berger et al., 2004). The pFBDM vector has two cloning cassettes that can be inserted multiple times enabling the expression of several subunits from one vector. Ligated products were transformed into chemical competent *E. coli* XL1 blue cells by heat shock. After generation of antibiotic resistance mediated by the plasmid, cells were selected on LB agar plates containing the appropriate antibiotic. Amplified plasmids from an overnight

culture were purified using plasmid extraction kits. Positive clones were verified by test restriction cleavage or sequencing.

6.6.2 Cloning in yeast

In order to clone deletion mutants and tag subunits, the respective open reading frame was replaced by a KanMX6 resistance cassette (pFA6a KanMX6, Amp^r, AG Wendler) created by PCR (Reid et al., 2002). DID1-tags (Flemming et al., 2010) were C-terminally inserted at the endogenous locus together with URA3 marker (pRS316, Amp, Strässer) for selection. Deletions strains were generated, either by amplification of the deletion box from gene disruption yeast library strain by PCR (Table 5) or by the amplification of the *KanMX6* cassette with primers flanking regions homologous to regions of targeted gene. The integration of the G418 (Sigma-Aldrich) marker occurred by transformation of the purified PCR product into the INO80-FLAG strain leading to a deletion of the respective ORF. For DID1-tagging, a PCR product was amplified such that the STOP codon was inserted behind the DID-tag, URA3 was inserted in the terminator of the gene of interest.

Yeast transformation was performed according to (Gietz and Woods, 2002). Cells grown to an OD₆₀₀ of 0.5 to 0.8 were resuspended in a buffer containing 0.1 M LiAc, 40% PEG 4000, salmon sperm carrier DNA and DNA to be transformed. Cells were heat shocked at 42°C for 10 min and after a rescue step selected on the appropriate antibiotic or minimal media plate.

6.7 Protein expression and purification

6.7.1 Protein expression in *E. coli*

For overexpression of proteins in *E. coli*, BL21(DE3), BL21(DE3)-star or Rosetta (DE3) strains were transformed with the plasmid containing the gene of interest. In general, protein expression in *E. coli* was performed as described before. Protein expression was induced by supplementing the media with the galactose analogous IPTG (Isopropyl-β-D-Thiogalactopyranoside) at late logarithmic phase. Protein expression was allowed for either 4 h at 37°C or over night at 18°C. Cells were harvested by centrifugation.

6.7.2 Protein expression in insect cells

The use of *E. coli* as an expression host is limited as many eukaryotic large polypeptides fail to express in bacteria. Expression in insect cells offer several advantages (Berger et al., 2004): (i) the multiplication module in the pFBDM vector allows the insertion of several genes encoding components of multiprotein complexes in one vector under two different promoters. (ii) Recombinant baculoviruses produce high expression levels. (iii) The expression in a eukaryotic organism facilitates the production of difficult gene products and allows a similar post-translational modification state as in the original host.

Genes of interest were cloned into the pFBDM vector. The insertion into the MultiBac baculoviral DNA is mediated via the Tn7 transposition sequence upon transformation in DH10MultiBac *E. coli* cells (Berger et al., 2004; Fitzgerald et al., 2006). The antibiotic resistance propagated by the pFBDM vector and the adjacent LacZ gene on the MultiBac DNA that enables blue/white screening allow selection of positive clones on agar plates containing (X- α -galactose; 100 μ g/ml, tetracycline and kanamycine). Recombinant bacmid DNA was isolated with standard Mini and Midi plamid isolation kits. 2 ml of Sf21 (*Spodoptera frugiperda*) (Gibco, Invitrogen) insect cells with 0.4 mio/ml were transfected with 2 μ g DNA with 3 μ l transfection reagent (FuGene, Promega) in serum-free medium (Gibco). Baculoviral particles were amplified at 27.5°C for four days and the supernatant of the attached cells was used to infect 10 ml of SF21 cells with 1 mio/ml in a suspension culture for four days. The Cells were harvested and the supernatant containing the virus were steril-filtered. The virus was amplified for another generation before it was used for infection of High Five (*Trichopulsia ni*) (Gibco, Invitrogen). High Five cells with 1 mio/ml were infected with appropriate virus titer for recombinant protein expression.

6.7.3 Culturing of yeast

To prepare large-scale yeast fermentation, yeast cultures were cultivated stepwise. First, 10 ml of YPD media supplemented with 50 mg/ml ampicillin were inoculated with colonies from a freshly grown plate and cultivated at 30°C for 8 h. A 200 ml culture was inoculated with the

10 ml pre-culture and was cultivated over night. This culture was used to inoculate a 2 L culture with 50 ml and subsequently cultivated for 8 h. The media for either a 100 or 200 L fermenter was supplemented with tetracycline (12.5 mg/ml), ampicillin (100 mg/ml) and 200 ml antifoam per 200 L and the pH was titrated to 6.8 – 6.9. The fermenter was inoculated with a starting OD of 0.0115. The fermentation was performed at 30°C with 250 rpm and 85 NL/h air-flow for 13 h. At a final OD₆₀₀ of 5 – 7 the cells were harvested.

Mutant strains were grown in 10 L buckets heated to 30°C in a water bath. The ventilation was accomplished by pumping air through an aquarium air stone. YPD media was supplemented equivalent to the large scale fermentation.

Cells were harvested by centrifugation, washed first with water, then with lysis buffer (Table 6) and subsequently were aliquoted and frozen in liquid nitrogen.

6.7.4 SDS-PAGE and Western blot analysis

Proteins were separated according to their size by SDS polyacrylamide gel electrophoresis (SDS-PAGE), as described earlier (Laemmli, 1970). INO80 complex was analyzed by pre-casted gradient gels either 4-12% (Invitrogen) in MOPS buffer or 10-20% (BioRad). Recombinant sub-complexes and histones were denatured with 4xLaemmli buffer (50% v/v glycerol, 250 mM Tris-HCl pH 6.8, 7.5% w/v SDS, 5 mM EDTA, 10 mM DTT, 0.5% w/v bromphenol blue) and analyzed on 15% or 18% polyacrylamide gels with 4% stacking gels (Table 7), respectively. After separation of the proteins by electrophoresis, the gels were stained with colloidal Coomassie staining solution (Invitrogen) or silver staining.

Table 7 Gel components for 2 gels with 15% or 18% resolving gel and 4% stacking gel.

Resolving gel			Stacking gel	
Reagent	15%	18%	Reagent	4%
	Volume [ml]	Volume [ml]		Volume [ml]
Water	5.7	3.7	Water	12
Acrylamide/Bis Solution 37,5:1 (30 % w/v)	9.3	11.3	Acrylamide/Bis Solution 37,5:1 (30 % w/v)	6
Lower 3 M Tris, pH 8.5	5	5	Upper 0.5 M Tris, pH 6.8	30
10% APS	100 μ l	100 μ l	10% APS	0.048
TEMED	10 μ l	10 μ l	TEMED	0.45

6.7.5 Silver staining

Silver staining was performed as in principal described before (Sasse and Gallagher, 2009). Gels were washed shortly with water and were then fixed (10% acetic acid, 45% methanol) twice for 10 min. Gels were then treated twice with 50% ethanol for 10 min and once with 30% ethanol. Gels were sensitized in 0.8 mM $\text{Na}_2\text{S}_2\text{O}_3$ for 60 sec and then washed in water for 3x 20 sec. Bands were then stained with 2 g/l AgNO_3 , 0.026% formaldehyde for 20 min. Silver solution was washed off with water 3x 20 sec. Bands were visualized with 6% Na_2CO_3 , 0.0185% formaldehyde and 16 μM $\text{Na}_2\text{S}_2\text{O}_3$. Developing was then quenched with 10% acetic acid.

6.7.5.1 Immunoblotting – Western Blotting

In order to detect proteins with specific antibodies after SDS-PAGE, they were transferred onto a polyvinylidene difluoride (PVDF) membrane in a wet (tank) blot system. To equilibrate and activate the PVDF membrane, it was plunged briefly in methanol. The blot was assembled as follows: two layers of 5 MM Whatman soaked in Transfer buffer (50 mM Tris/HCl pH 8.3, 0.19 M glycine, 0.1 (w/v) % SDS and 20 % methanol) and enclosed the gel lying over the PVDF membrane. Blotting was performed for 1 h at a constant voltage of 100 V and 400 mA. Prior to incubation with the first antibody, unspecific binding sites were blocked by incubating the membrane for 20 min in 5% (w/v) milk in 1xTBS-T. The first antibody incubation of the membrane was performed with 1xTBS-T, 5% (w/v) milk and the required antibody in the

indicated dilution by shaking over night at 4°C. The blot was subsequently washed by shaking three times for 10 min in 1× TBS-T buffer. The membrane was incubated with the secondary, horse radish peroxidase coupled antibody in 1× TBS-T, 5% (w/v) milk for 1 h at room temperature. The blot was again washed as described above. To visualize the immunodetected proteins, 10 ml ECL solution was freshly supplemented with 3 µl H₂O₂, 25 µl cumaric acid and 50 µl luminol and incubated for 1 min at room temperature with the membrane by shaking. The signal was then detected by exposure to film (Biomax Light, Maximum Resolution or Maximum Sensitivity film, Kodak) and subsequent developing by Kodak X-Omat 2000 processor in the dark room.

6.7.6 Purification of histones and reconstitution of nucleosomes

In principal, histones were purified as described before (Dyer et al., 2004; Huynh et al., 2005). Coding sequences of *D. m.* histones H2A, H2B, H3 and H4 are codon optimized in expression vectors (Peter Becker's group). Coding sequence of *D.m.* H2A.v was cloned into pET21 vector. Histones were expressed in BL12 Star (DE3) cells. Cells were resuspended in Sau-200 buffer (Table 6) and subsequently sonicated with an output control of 5 and a duty cycle of 40%. The lysate was cleared by centrifugation at 20,000 rpm for 20 min at 4°C. The supernatant was filtered through Mira-cloth and 0.45 µm filter. The filtrate was loaded online onto a HiTrap SP HP 5 ml column (GE Healthcare) using a 50 ml injection super loop. The histones were eluted from the column as follows: (i) wash with 20% Sau-2000 for 3 column volumes, (ii) wash with 25% Sau-2000 for 5 column volumes and (iii) elution with a gradient of 20-60% and 60-100% of Sau-2000 for 6 and 3 column volumes, respectively. Proper fractions were pooled and dialyzed against 3 L of ddH₂O for 30 min, over night and again for 1 h at 4°C. Subsequently, histones were loaded on a HiTrap Q FF 5 ml column (GE Healthcare) in Histones-0 Q buffer (Table 6). The histone containing flow through were collected and concentration was determined by NanoDrop photospectrometer (Thermo Scientific) and SDS-PAGE. Histones were aliquoted, frozen and lyophilized overnight.

Histones were dissolved yielding a concentration of 4 mg/ml in Unfolding buffer (Table 6). Histones were unfolded for 30 min – 3 h. The octamer was reconstituted by mixing the four histones in 120% H2A and H2B to 100% H3 and H4 equimolar ratio. The octamer was dialyzed against 3x 2 L of refolding buffer (Table 6). The precipitation was removed by centrifugation and the octamer was concentrated using Amicon centrifugal filters (Merck Millipore). The octamer was finally purified on size exclusion chromatography column S200 26/60 (GE Healthcare). The stoichiometry and purity was controlled by SDS-PAGE and the octamer was stored in 50% glycerol (w/v).

Various DNAs were used to reconstitute nucleosomes. INO1 nucleosomes were reconstituted using genomic sequence covering +1 - +359 of the *INO1* gene. 147 bp, 187 long (with 20 bp on each side or 40 bp overhang) DNAs were based on the Widom 601 positioning sequence (Huynh et al., 2005).

In brief, 147 bp and 187 bp long DNAs were cloned into a pFMP vector. Plasmids were amplified in bacteria and isolated. Purified plasmids were digested with respective restriction enzymes. Digested DNA was purified on native 8% acrylamide gels. DNA was isolated by electroelution from the gel. DNA was purified by phenol/chloroform-isoamyl alcohol and ethanol precipitation.

For INO1 nucleosomes, the DNA was amplified by PCR (Table 5). 2 ng of template DNA was amplified in 50 µl PCR reactions containing 5 µl 10x Taq buffer, 5 µl dNTPs (FIRMA), 2.5 µl 10 µM forward and reverse primer and 1 µl Taq polymerase with following settings: 2 min at 94°C; 30 cycles with 15 sec 94°C, 15 sec 56°C, 30 sec 72°C; 5 min at 72°C. DNA was purified on a 1.2% agarose gel with a Gel Extraction Kit (QIAquick®) and by ethanol precipitation. 1/10 (v/v) NaOAc and 2.5 volume 100% ethanol were added and incubated at -20°C over night. The DNA was pelleted at 4°C with 15.000 g for 30 min and washed with 70% ethanol. The purified DNA was dissolved in Tris EDTA buffer (10 mM Tris and 1 mM EDTA) to a final concentration of 5-7 µg/µl. The DNA concentration was determined on a NanoDrop photospetrometer (Thermo Scientific).

In order to avoid high concentrations of free DNA in the nucleosome preparations, the proper DNA concentration had to be titrated. Various molar ratios of DNA to octamer were mixed together and transferred to small dialysis chambers. The salt concentration was slowly reduced by linear salt gradient dialysis with following steps: (i) 7h 0.2 ml/min, (ii) 16h 0.4 ml/min and (iii) 7h 1ml/min. the final salt concentration was 50 mM KCl in the nucleosome reconstitution. The quality of nucleosomes was assessed by 5% native PAGE and measuring DNA absorption at 260 nm.

6.7.7 Establishment of an INO80 purification protocol

The endogenous purification of INO80 from *S. cerevisiae* was based on earlier purification protocols (Shen, 2004; Shen et al., 2000). The modified protocol improved quality and homogeneity of INO80 and allowed a comprehensive structural analysis.

6.7.7.1 Cell lysis

6.7.7.1.1 Cryogenic disruption of yeast cells

For small-scale purifications cells were disrupted using a planetary ball mill on frozen cells (Alber et al., 2007). Yeast strains were grown to an OD₆₀₀ of 0.5 – 1.5. Cells were harvested by centrifugation and were washed with water and resuspension buffer (Table 6). Cell paste was pressed through a syringe into liquid nitrogen producing frozen noodles. These noodles were then cryogenically disrupted using a planetary ball mill (PM 100, Retsch). Disrupted frozen cells were then resuspended in lysis buffer (Table 6).

6.7.7.1.2 Bead-beater

Large-scale yeast disruption was accomplished with bead-beaters (BioSpec). The bead-beaters were used after instructions of the manufacturer. The chamber was filled with 200 ml glass beads (0.5 mm, Roth) and 150 ml cell pellet resuspended Lysis buffer (Table 6). Cells were lysed

for 1.15 h with 1 min intervals. Residual cell lysate was washed from the beads with 200 ml lysis buffer.

6.7.7.2 Chromatin fragmentation

In the course of assessing appropriate chromatin fragmentation, MNase (Roche) treatment and sonication was tested. For MNase digestion, 400 µl cell lysate was incubated with 45 U of MNase in lysis buffer containing 10 mM CaCl₂ for either 1 h at 4°C or 10 min at 37°C. Digestion was stopped by adding EDTA. In the standard protocol, chromatin was fragmented with a polytron homogenizer (Kinematica; Fisher Scientific) for four rounds for 30 s at 16.000 rpm/min and then by sonication (Branson) for seven round for 30 s with a duty cycle of 4, an output control of 5 and output yield of 60% on ice. For DNA isolation 500 µl of diluted lysate were mixed with 500 µl phenol and phases were separated by centrifugation at 15.000 g for 5 min. The aqueous phase was recovered and mixed with 460 µl chloroform-isoamylalcohol. 400 µl were recovered and DNA was precipitated by 2.5 volumes -20°C 96% ethanol and 1/10 (v/v) 3 M NaAc pH 5.2 for at least 3 h at -80°C. The precipitated DNA was washed twice with -20°C cold 70% ethanol. The pelleted DNA was dried at room temperature and dissolved in 10 µl H₂O. RNA was digested with 1 µl RNase (Fermentas) for 30 min at 37°C. DNA length was analyzed by gel electrophoresis using 1% agarose gels.

6.7.7.3 FLAG purification of the INO80 complex

In order to remove debris and unbroken cells, the lysate was centrifuged with 14,000 rpm for 30 min at 4°C (rotor SLA 1500; Thermo Scientific). The supernatant was removed and further centrifuged in an ultra centrifuge at 40,000 rpm for 90 min at 4°C (Ti45; Beckmann and Coulter). The fatty layer on top was removed and supernatant was gently collected. To remove sticky proteins, a pre-clearing step was performed with 200 µl protein G beads (Invitrogen) equilibrated in lysis buffer for 30 min on a nutator. Beads were removed by centrifugation at 3,000 g (Hettich centrifuge) for 10 min. Immunopurification was performed with 2 ml of M2 FLAG-beads (Sigma-Aldrich) for 1.5 h on a nutator at 4°C. Beads were collected by

centrifugation at 1,000 g (Hettich centrifuge) for 10 min. The supernatant was not quantitatively removed and the beads were resuspended in residual liquid and transformed to gravity flow column. Unbound proteins were removed by washing with 10 column volumes of H-0.5 buffer and 5 column volumes of H-0.2 buffer (Table 6). INO80 was eluted from FLAG-beads by adding subsequently elution buffer (Table 6) either containing 0.1 mg/ml or 0.2 mg/ml FLAG peptide. FLAG peptide (Sigma Aldrich) was dissolved in buffer containing 10 mM HEPES pH 8.0, 100 mM KCl and 2 mM $MgCl_2$ to yield a final concentration of 5 mg/ml. Elution was performed as follows: (i) 15 min incubation with 2 ml of 0.1 mg/ml FLAG peptide containing buffer and collection of elution by gravity flow, (ii) 10 min incubation with 1 ml of 0.1 mg/ml FLAG peptide containing buffer and collection of elution by gravity flow, (iii) 15 min incubation with 2 ml of 0.2 mg/ml FLAG peptide containing buffer and collection of elution by gravity flow, (iiii) 10 min incubation with 1 ml of 0.2 mg/ml FLAG peptide containing buffer and collection of elution by gravity flow and (iiiii) FLAG beads were washed with 2 ml of H-0.2 buffer. After elution FLAG-beads were re-incubated with the lysate over night on nutator. FLAG beads were collected and treated as described. Last washing step was complemented with 0.1 mg/ml FLAG peptide and beads were incubated for 15 min for elution. INO80 was further eluted by 2 ml of 0.2 mg/ml FLAG peptide containing buffer and elution was collected by gravity flow. Residual INO80 was collected by washing the beads with 1 ml of H-0.2 buffer (Table 6). INO80 purification was analyzed by SDS-PAGE and Western blot analysis.

6.7.7.4 Ion exchange chromatography

In the course of establishing purification protocol for INO80 diverse columns have been assessed: HiTrap Heparin HP 1 ml, Mini S 4.6/50 PE 0.8 ml and a Mono Q 5/50 1 ml (GE Healthcare) connected to a Micro Aekta system (GE Healthcare).

In principal, the pooled elution fractions from FLAG purification were loaded online onto the columns with a 10 ml super-loop (GE Healthcare) and H-01 Q buffer (Table 6). In the standard protocol the Mono Q column was used. For this, the sample was loaded with 0.125 ml/min onto the column. The washing and elution protocol was run with 0.4 ml/min.

Unbound proteins were washed away with 25% (400 mM KCl) of buffer H-1 Q (Table 6). INO80 complexes were eluted from resin at 50% (600 mM KCl) of buffer H-1 Q and elution was fractionated in 60 μ l. DNA containing proteins eluted at higher salt-concentrations.

6.7.7.5 Size exclusion chromatography

In order to exchange buffer and achieve a monodisperse sample, the elution fractions were pooled and directly applied to a Superose 6 PC 3.2/30 (2.4 ml) column (GE Healthcare) connected to Ettan Aekta system (GE Healthcare). The column was run with 0.04 ml/min of H-0.2 SEC buffer (Table 6) and was fractionated in 25 μ l.

To stabilize INO80 for the EM analysis, INO80 was cross-linked with 0.05% glutaraldehyde (EM grade, Sigma-Aldrich) at 20°C for 30 min. The reaction was quenched by adding 100 mM Tris pH 8.2 and incubation at 20°C for 15 min. Cross-linked samples were applied to another round of size exclusion chromatography to assess homogeneity.

6.7.8 Purification of the Swi2/Snf2 sub-complex

In brief, either coding sequences from *S. c.* or *C. t.* of the full Snf2 ATPase of Ino80 including the insertion fold or constructs coding only for the RecA1 and RecA2 folds without the insertion domain were cloned in either pFBDM vectors for expression in insect cells or pET duet vector for expression in *E. coli*. Ino80 constructs were tried to express with Ies2 alone or together with the OB-folds of Rvb1. All the Ino80 constructs contained an N-terminal His-tag that allowed immunopurification.

6.7.9 Purification of the Nhp10 subcomplex

S. cerevisiae Nhp10, Ies3 and Ies5 were cloned into pFBDM vector (Table 4). A coding sequence for a His₆-tag was fused N-terminal to Nhp10. Additional to Nhp10, Ies3 and Ies5, diverse N-terminal constructs of Ino80 were cloned into this vector. Furthermore, a vector containing the

coding sequence of *les1* fused to N-terminal FLAG tag was used to assess interaction with the Nhp10 sub-complex. Proteins were expressed accordingly (Fitzgerald et al., 2006). In brief, High five cells were infected with 1:100 Nhp10-*les3-les5* baculovirus or were co-infected with each 1:20 Nhp10-*les3-les5-Ino80* (NTD) and *les1*-FLAG viruses for 3 days. Cells were lysed by sonication on ice for 8x 40 bursts with a duty cycle of 4, an output control of 5 and output yield of 60%. The lysate was cleared by twice centrifugation at 18.000 rpm (SS-34, Thermo Scientific) for 30 min. Immunopurification of complex was performed with Ni-NTA beads. Unbound proteins and contaminations were washed off with buffers containing 20 mM, 40 mM or 1 M NaCl. Complexes were eluted with a buffer containing 300 mM imidazole. Ni²⁺-elution fractions were pooled and directly loaded onto HiTrap Q HP (GE Healthcare) column. Complexes were eluted by a linear gradient. Proper fractions were pooled and the complex was concentrated using Amicon centrifugal filters (Merck Millipore). Complexes were then applied on a size exclusion chromatography column S200 (GE Healthcare). Proteins were subsequently concentrated and analyzed by SDS-PAGE.

6.8 Generation of INO80 binding nanobodies

To generate nanobodies that target the INO80 complex an alpaca was immunized with 500 µg freshly purified and glutaraldehyde fixed INO80, 700 µg Arp8-Arp4-Act-HSA-*les4*, 700 µg yeast Arp5-*les6*, 700 µg Nhp10-*les3-les5*, 500 µg human Arp8 (38-624) and human 700 µg Arp5-*les6*. Peripheral blood lymphocytes were isolated; total RNA was extracted and written into cDNA. The phagemid library was generated by cloning the V_HH repertoire from the heavy-chain repertoire. Binders were selected after panning with ~400 µg INO80 followed by solid-phase ELISA screening. Positive clones were tested to bind to Arp8-Arp4-Act-HSA, yeast Rvb1/2 and Arp5-*les6*.

To validate the ability to immunoprecipitate INO80, binders covalently linked to agarose beads were incubated with cell lysate from an *Ino80-FLAG* strain. The same amount of FLAG-M2 beads (Sigma-Aldrich) was used as a reference. After the normal INO80 purification procedure,

the bound proteins were eluted from the beads with conventional Laemmli-buffer and were analyzed by SDS-PAGE visualized by silver and Coomassie staining. Nanobodies have been generated as described before (Rothbauer et al., 2006) and in collaboration with ChromoTek (Munich).

6.9 Cross-linking and mass spectrometry

6.9.1 *Titration of cross-linker*

A titration of the cross-linker, DSS (Creative Molecules) was performed to find appropriate cross-linking concentration. As lysines are the exclusive target for NHS esters, the cross-linker concentration was determined in respect to the lysine amount. It was assumed that 1 μg of protein contains 500 pmol of lysines. Based on this assumption the concentration was expressed and calculated as cross-linker over lysines. In general, 1 mg of an equimolar mixture of light and heavy labeled DSS was dissolved in dimethylformamide (DMF, Thermo Scientific) to a concentration of 25 mM. DSS was then further diluted to cross-linking concentration with H_2O . The samples were warmed up to room temperature and cross-linked by adding the diluted cross-linker and mixing. The samples were then incubated for 35 min at 30°C with 1000 rpm. After spinning the samples down, the reaction was quenched by adding 100 mM Tris pH 8.0 or ammonium bicarbonate. The samples were then incubated for 15 min at 30°C with 1000 rpm. To evaluate cross-linking efficiency 1 μg of complex was analyzed on pre-cast SDS-PAGE gradient gel 4-12% (Invitrogen). For the titration, 2 μg of freshly purified and monodisperse INO80 were cross-linked with 0.4x, 1x, 2.5x or 5x DSS over lysines and 1.5 μg of INO80-nucleosome complex were cross-linked with 0.5x, 1.5x, 3x and 5x DSS over lysines.

6.9.2 *Sample preparation for mass spectrometry analysis*

Cross-linking of samples was in principal performed as the titration, but with the difference that the dissolved cross-linker was directly added to the complex. We cross-linked 30, 40, 50, 84 μg of INO80 from different preparations with 3x, 3.5x, 1.5x and 3x DSS, respectively. For INO80-

nucleosome complexes, ten preparations of INO80 between 100 and 200 µg were incubated with a 1 to 5 fold molar excess of nucleosomes with either 187 bp off-centered or 147 bp DNA in absence or presence of ADP BeFx or AMP-PCP on ice for 30 min. INO80-nucleosome complexes were cross-linked with 1.5x or 3.5x DSS over lysines. Cross-linking and peptide preparations were in principal performed as described before (Herzog et al., 2012; Jennebach et al., 2012; Leitner et al., 2012b).

After quenching the cross-linking reaction, proteins were denatured with twice the volume of 8 M urea. Cysteines were reduced with 5 mM tris(2-carboxyethyl)phosphine (TCEP, Thermo Scientific) for 15 min at 37°C. Cysteines were further alkylated with 10 mM iodoacetamide (Sigma-Aldrich). Proteins were digested with 1:50 (w/w) of lysyl endopeptidase C (Wako) for 1 h at 37°C at 950 rpm. After diluting the sample to a urea concentration of 1 M, 1/50 (w/w) trypsin (Promega) was added and incubated at 37°C at 950 rpm over night. Samples were acetified with 1% (v/v) trifluoroacetic acid (TFA, Sigma-Aldrich) and peptides were enriched by solid-phase extraction using C18 cartridges (Sep-Pak, Waters). Elution was dried by vacuum centrifugation and dissolved in 18.5 µl of (3% ACN; 0.2% formic acid (FA)) at 37°C 1400 rpm. Cross-linked peptides were enriched by peptide size exclusion chromatography Superdex peptide PC 3.2/30 (GE Healthcare) with a mobile phase (70% H₂O, 30% ACN, 0.1% TFA). A peptide standard, insulin B oxidized (Sigma-Aldrich) helped to identify fractions containing cross-linked peptides. Fractions were dried and dissolved in 3% ACN; 0.2% FA for 1 h at 1400 rpm at 37°C.

Samples were analyzed on a liquid chromatography coupled to tandem mass spectrometry (LC-MS/MS), LTQ Orbitrap (Thermo) equipped with a standard nanoelectrospray source.

6.9.3 Sample analysis

In general, analysis and validation of cross-links was performed as described before (Herzog et al., 2012; Leitner et al., 2010; Walzthoeni et al., 2012). For the cross-link peptide search xQuest was used and FDR were determined by xProphet. Parameters were set as follows: maximum

number of missed cleavages = 2, peptide length = 4-45 amino acids, fixed modifications = carbamidomethyl-Cys (mass shift = 57.021460 Da), variable modifications = oxidation-Met (mass shift = 15.99491), mass shift of the light cross-linker = 138.068080 Da, mass shift of mono-links = 156.078644 and 155.096428 Da, MS1 tolerance = 15 ppm, MS2 tolerance = 0.2 Da for common ions and 0.3 Da for cross-link ions, search in ion-tag mode.

The experimental spectrum was assigned to theoretical candidate spectra and was scored according to quality of the match. The cross-link candidates were filtered by the mass error (-4 to +7 ppm) and the Δ score ($\geq 15\%$) that indicated relative scores between the next ranked match. All cross-links were manually validated. Manual validation included that each peptide had at least four bond cleavages in total or three in a series and a minimum length of six amino acids. Cross-links composed of one peptide with five amino acids that fulfilled filtering and manual criteria were included.

6.10 Analysis of subunit composition of INO80's knock-out mutants

INO80 complexes from subunit knock-out mutants were purified according to the WT. The composition and quantity of subunits of the INO80 mutants was determined by analysis of the FLAG-elutions using SDS-PAGE. The omission of subunits was verified by MS. To remove agents interfering with MS-analysis, the FLAG-elutions were shortly run on a SDS-PAGE. Entire lanes were cut out and subjected to in-gel trypsinization. The obtained mixtures of tryptic peptides were analyzed by LC-MS/MS using an OrbitrapXL instrument. In agreement with the genetic subunit deletions, corresponding INO80 protein subunits could not be identified in single band LC-MS/MS analysis. MS/MS spectra were searched with MASCOT using the yeast subset of the Swiss-Prot protein database. Proteins identified with a Protein score below 100, were manually validated.

6.11 Analysis of distant restraints

We assessed C_{α} - C_{α} distances of intra-links using available crystal structures from the RCSB protein data bank: *Dro* Snf2 (1Z3I, (Thoma et al., 2005)), yeast Actin (1YAG; (Vorobiev et al.,

2003)), yeast Arp4 (3QB0; (Fenn et al., 2011)), human and yeast Arp8 (4FO0 and 4AM6; (Gerhold et al., 2012; Saravanan et al., 2012)). Distant constraints in atomic coordinates were measured using the UCSF chimera package (Pettersen et al., 2004). All illustrations involving EM structures as well as crystal structures were acquired from UCSF chimera.

To determine whether hexameric Rvb1/2 rings are composed of hetero- or homo-hexamers, we modeled the 3D structure of yeast Rvb1/2 using SWISS MODEL (Kiefer et al., 2009). The model of the yeast Rvb1 and Rvb2 is based on the crystal structure of hexameric human Rvb1 (Matias et al., 2006; 2C9O). Human and yeast sequences were acquired from NCBI and were aligned using ClustalW (Larkin et al., 2007).

For analysis of INO80-nucleosome cross-links we used sequences acquired from NCBI and the atomic coordinates of the *D. melanogaster* nucleosome (2PYO) (Clapier et al., 2008).

6.12 Functional assays

6.12.1 Electrophoretic mobility shift assays

For electrophoretic mobility assays, increasing amounts of proteins were incubated with diverse structured DNA oligonucleotides. Each 50 nM of 50 bp and 37 bp long distorted DNA duplexes (Ray and Grove, 2009, 2012), 50 bp long fork structure (Guy and Bolt, 2005), 50 bp long curved DNA and 187 bp long 601 sequence (Huynh et al., 2005) were assessed for binding. The reaction buffer contained 5% glycerol (v/v) and total volume was 10 µl. The reactions were loaded on a 5% native polyacrylamide gel, which was pre-run before. After electrophoresis in 0.5x Tris-borate-EDTA (TBE) for 1.5-2 h at 100V at 4°C, the gel was stained with Sybr Green I (1:5000 in 0.5x TBE) for 30 min and scanned on a Typhoon scanner (GE Healthcare).

6.12.2 Remodeling assay

Remodeling assays contained 50 nM nucleosomes on a 359 bp long DNA (INO1 gene bp +1 to +359) were incubated with increasing concentrations of INO80 in a remodeling buffer (Table 6)

in absence or presence of 2 mM ATP or non-hydrolysable ATP analogs, AMP-PCP or ADP·BeF_x for 30 min at 30°C. Subsequently, 10 µl of the reaction were loaded onto 4% native polyacrylamide gels. After electrophoresis in 0.5x TBE buffer for 1.5-2 h at 100 V at 4°C, the DNA was visualized by Sybr Green I (1:5000 in 0.5x TBE) for 30 min.

6.12.3 ATP hydrolysis assays

An ATPase reaction (5 µL) was performed in remodeling buffer and contained 30 µM ATP and 20 nCi [γ -³²P]ATP. 20 nM INO80 complexes were either stimulated with 50 nM 359bp long DNA (INO1 gene bp +1 until +359) or nucleosomes or none. Reactions were incubated for 30 min at 30°C in a PCR machine. Reactions were separated by thin-layer chromatography with 1 M formic acid containing 0.5 M LiCl. TLC plates were subsequently incubated on storage phosphate screens for 30 min. Signals were scanned on a STORM scanner (GE Healthcare). In general, two experiments were quantified by Image J. ATP hydrolysis rates were calculated relative to complete ATP hydrolysis achieved by calf intestinal alkaline phosphatase treatment.

7 References

- Abbott, D.W., Ivanova, V.S., Wang, X., Bonner, W.M., and Ausio, J. (2001). Characterization of the stability and folding of H2A.Z chromatin particles: implications for transcriptional activation. *J Biol Chem* 276, 41945-41949.
- Alber, F., Dokudovskaya, S., Veenhoff, L.M., Zhang, W., Kipper, J., Devos, D., Suprpto, A., Karni-Schmidt, O., Williams, R., Chait, B.T., *et al.* (2007). Determining the architectures of macromolecular assemblies. *Nature* 450, 683-694.
- Alber, F., Forster, F., Korkin, D., Topf, M., and Sali, A. (2008). Integrating diverse data for structure determination of macromolecular assemblies. *Annu Rev Biochem* 77, 443-477.
- Allain, F.H., Yen, Y.M., Masse, J.E., Schultze, P., Dieckmann, T., Johnson, R.C., and Feigon, J. (1999). Solution structure of the HMG protein NHP6A and its interaction with DNA reveals the structural determinants for non-sequence-specific binding. *EMBO J* 18, 2563-2579.
- Andrews, A.J., and Luger, K. (2011). Nucleosome structure(s) and stability: variations on a theme. *Annu Rev Biophys* 40, 99-117.
- Arbabi Ghahroudi, M., Desmyter, A., Wyns, L., Hamers, R., and Muyldermans, S. (1997). Selection and identification of single domain antibody fragments from camel heavy-chain antibodies. *FEBS Lett* 414, 521-526.
- Arents, G., Burlingame, R.W., Wang, B.C., Love, W.E., and Moudrianakis, E.N. (1991). The nucleosomal core histone octamer at 3.1 Å resolution: a tripartite protein assembly and a left-handed superhelix. *Proc Natl Acad Sci U S A* 88, 10148-10152.
- Asturias, F.J., Chung, W.H., Kornberg, R.D., and Lorch, Y. (2002). Structural analysis of the RSC chromatin-remodeling complex. *Proc Natl Acad Sci U S A* 99, 13477-13480.
- Auger, A., Galarneau, L., Altaf, M., Nourani, A., Doyon, Y., Utley, R.T., Cronier, D., Allard, S., and Cote, J. (2008). Eaf1 is the platform for NuA4 molecular assembly that evolutionarily links chromatin acetylation to ATP-dependent exchange of histone H2A variants. *Mol Cell Biol* 28, 2257-2270.
- Badis, G., Chan, E.T., van Bakel, H., Pena-Castillo, L., Tillo, D., Tsui, K., Carlson, C.D., Gossett, A.J., Hasinoff, M.J., Warren, C.L., *et al.* (2008). A library of yeast transcription factor motifs reveals a widespread function for Rsc3 in targeting nucleosome exclusion at promoters. *Mol Cell* 32, 878-887.
- Ball, H.L., Myers, J.S., and Cortez, D. (2005). ATRIP binding to replication protein A-single-stranded DNA promotes ATR-ATRIP localization but is dispensable for Chk1 phosphorylation. *Mol Biol Cell* 16, 2372-2381.
- Bao, Y., and Shen, X. (2007). INO80 subfamily of chromatin remodeling complexes. *Mutat Res* 618, 18-29.
- Bao, Y., and Shen, X. (2011). SnapShot: Chromatin remodeling: INO80 and SWR1. *Cell* 144, 158-158 e152.
- Barbera, A.J., Chodaparambil, J.V., Kelley-Clarke, B., Joukov, V., Walter, J.C., Luger, K., and Kaye, K.M. (2006). The nucleosomal surface as a docking station for Kaposi's sarcoma herpesvirus LANA. *Science* 311, 856-861.
- Bauer, A., Chauvet, S., Huber, O., Usseglio, F., Rothbacher, U., Aragnol, D., Kemler, R., and Pradel, J. (2000). Pontin52 and reptin52 function as antagonistic regulators of beta-catenin signalling activity. *EMBO J* 19, 6121-6130.
- Berger, I., Fitzgerald, D.J., and Richmond, T.J. (2004). Baculovirus expression system for heterologous multiprotein complexes. *Nat Biotechnol* 22, 1583-1587.
- Bernstein, B.E., Liu, C.L., Humphrey, E.L., Perlstein, E.O., and Schreiber, S.L. (2004). Global nucleosome occupancy in yeast. *Genome Biol* 5, R62.

- Billon, P., and Cote, J. (2012). Precise deposition of histone H2A.Z in chromatin for genome expression and maintenance. *Biochim Biophys Acta* 1819, 290-302.
- Blosser, T.R., Yang, J.G., Stone, M.D., Narlikar, G.J., and Zhuang, X. (2009). Dynamics of nucleosome remodelling by individual ACF complexes. *Nature* 462, 1022-1027.
- Bohm, V., Hieb, A.R., Andrews, A.J., Gansen, A., Rocker, A., Toth, K., Luger, K., and Langowski, J. (2011). Nucleosome accessibility governed by the dimer/tetramer interface. *Nucleic Acids Res* 39, 3093-3102.
- Bortvin, A., and Winston, F. (1996). Evidence that Spt6p controls chromatin structure by a direct interaction with histones. *Science* 272, 1473-1476.
- Branzei, D., and Foiani, M. (2008). Regulation of DNA repair throughout the cell cycle. *Nat Rev Mol Cell Biol* 9, 297-308.
- Burma, S., Chen, B.P., Murphy, M., Kurimasa, A., and Chen, D.J. (2001). ATM phosphorylates histone H2AX in response to DNA double-strand breaks. *J Biol Chem* 276, 42462-42467.
- Bushnell, D.A., Westover, K.D., Davis, R.E., and Kornberg, R.D. (2004). Structural basis of transcription: an RNA polymerase II-TFIIB cocrystal at 4.5 Angstroms. *Science* 303, 983-988.
- Cai, Y., Jin, J., Yao, T., Gottschalk, A.J., Swanson, S.K., Wu, S., Shi, Y., Washburn, M.P., Florens, L., Conaway, R.C., *et al.* (2007). YY1 functions with INO80 to activate transcription. *Nat Struct Mol Biol* 14, 872-874.
- Chaban, Y., Ezeokonkwo, C., Chung, W.H., Zhang, F., Kornberg, R.D., Maier-Davis, B., Lorch, Y., and Asturias, F.J. (2008). Structure of a RSC-nucleosome complex and insights into chromatin remodeling. *Nat Struct Mol Biol* 15, 1272-1277.
- Chambers, A.L., Ormerod, G., Durley, S.C., Sing, T.L., Brown, G.W., Kent, N.A., and Downs, J.A. (2012). The INO80 chromatin remodeling complex prevents polyploidy and maintains normal chromatin structure at centromeres. *Genes Dev* 26, 2590-2603.
- Chen, L., Cai, Y., Jin, J., Florens, L., Swanson, S.K., Washburn, M.P., Conaway, J.W., and Conaway, R.C. (2011). Subunit organization of the human INO80 chromatin remodeling complex: an evolutionarily conserved core complex catalyzes ATP-dependent nucleosome remodeling. *J Biol Chem* 286, 11283-11289.
- Chen, Z.A., Jawhari, A., Fischer, L., Buchen, C., Tahir, S., Kamenski, T., Rasmussen, M., Lariviere, L., Bukowski-Wills, J.C., Nilges, M., *et al.* (2010). Architecture of the RNA polymerase II-TFIIF complex revealed by cross-linking and mass spectrometry. *EMBO J* 29, 717-726.
- Cheung, K.L., Huen, J., Kakiyama, Y., Houry, W.A., and Ortega, J. (2010). Alternative oligomeric states of the yeast Rvb1/Rvb2 complex induced by histidine tags. *J Mol Biol* 404, 478-492.
- Ciferri, C., Lander, G.C., Maiolica, A., Herzog, F., Aebersold, R., and Nogales, E. (2012). Molecular architecture of human polycomb repressive complex 2. *Elife* 1, e00005.
- Ciferri, C., Musacchio, A., and Petrovic, A. (2007). The Ndc80 complex: hub of kinetochore activity. *FEBS Lett* 581, 2862-2869.
- Ciferri, C., Pasqualato, S., Screpanti, E., Varetto, G., Santaguida, S., Dos Reis, G., Maiolica, A., Polka, J., De Luca, J.G., De Wulf, P., *et al.* (2008). Implications for kinetochore-microtubule attachment from the structure of an engineered Ndc80 complex. *Cell* 133, 427-439.
- Cimprich, K.A., and Cortez, D. (2008). ATR: an essential regulator of genome integrity. *Nat Rev Mol Cell Biol* 9, 616-627.
- Clapier, C.R., and Cairns, B.R. (2009). The biology of chromatin remodeling complexes. *Annu Rev Biochem* 78, 273-304.
- Clapier, C.R., and Cairns, B.R. (2012). Regulation of ISWI involves inhibitory modules antagonized by nucleosomal epitopes. *Nature* 492, 280-284.
- Clapier, C.R., Chakravarthy, S., Petosa, C., Fernandez-Tornero, C., Luger, K., and Muller, C.W. (2008). Structure of the *Drosophila* nucleosome core particle highlights evolutionary constraints on the H2A-H2B histone dimer. *Proteins* 71, 1-7.

- Cote, J., Quinn, J., Workman, J.L., and Peterson, C.L. (1994). Stimulation of GAL4 derivative binding to nucleosomal DNA by the yeast SWI/SNF complex. *Science* 265, 53-60.
- Dang, W., and Bartholomew, B. (2007). Domain architecture of the catalytic subunit in the ISW2-nucleosome complex. *Mol Cell Biol* 27, 8306-8317.
- de Jager, M., van Noort, J., van Gent, D.C., Dekker, C., Kanaar, R., and Wyman, C. (2001). Human Rad50/Mre11 is a flexible complex that can tether DNA ends. *Mol Cell* 8, 1129-1135.
- Dechassa, M.L., Zhang, B., Horowitz-Scherer, R., Persinger, J., Woodcock, C.L., Peterson, C.L., and Bartholomew, B. (2008). Architecture of the SWI/SNF-nucleosome complex. *Mol Cell Biol* 28, 6010-6021.
- Delacroix, S., Wagner, J.M., Kobayashi, M., Yamamoto, K., and Karnitz, L.M. (2007). The Rad9-Hus1-Rad1 (9-1-1) clamp activates checkpoint signaling via TopBP1. *Genes Dev* 21, 1472-1477.
- Diop, S.B., Bertaux, K., Vasanthi, D., Sarkeshik, A., Goirand, B., Aragnol, D., Tolwinski, N.S., Cole, M.D., Pradel, J., Yates, J.R., 3rd, *et al.* (2008). Reptin and Pontin function antagonistically with PcG and TrxG complexes to mediate Hox gene control. *EMBO Rep* 9, 260-266.
- Downs, J.A., Allard, S., Jobin-Robitaille, O., Javaheri, A., Auger, A., Bouchard, N., Kron, S.J., Jackson, S.P., and Cote, J. (2004). Binding of chromatin-modifying activities to phosphorylated histone H2A at DNA damage sites. *Mol Cell* 16, 979-990.
- Doyon, Y., Selleck, W., Lane, W.S., Tan, S., and Cote, J. (2004). Structural and functional conservation of the NuA4 histone acetyltransferase complex from yeast to humans. *Mol Cell Biol* 24, 1884-1896.
- Durr, H., Flaus, A., Owen-Hughes, T., and Hopfner, K.P. (2006). Snf2 family ATPases and DExx box helicases: differences and unifying concepts from high-resolution crystal structures. *Nucleic Acids Res* 34, 4160-4167.
- Durr, H., Korner, C., Muller, M., Hickmann, V., and Hopfner, K.P. (2005). X-ray structures of the *Sulfolobus solfataricus* SWI2/SNF2 ATPase core and its complex with DNA. *Cell* 121, 363-373.
- Dyer, P.N., Edayathumangalam, R.S., White, C.L., Bao, Y., Chakravarthy, S., Muthurajan, U.M., and Luger, K. (2004). Reconstitution of nucleosome core particles from recombinant histones and DNA. *Methods Enzymol* 375, 23-44.
- Ebbert, R., Birkmann, A., and Schuller, H.J. (1999). The product of the SNF2/SWI2 paralogue INO80 of *Saccharomyces cerevisiae* required for efficient expression of various yeast structural genes is part of a high-molecular-weight protein complex. *Mol Microbiol* 32, 741-751.
- Eisen, J.A., Sweder, K.S., and Hanawalt, P.C. (1995). Evolution of the SNF2 family of proteins: subfamilies with distinct sequences and functions. *Nucleic Acids Res* 23, 2715-2723.
- Engelholm, M., de Jager, M., Flaus, A., Brenk, R., van Noort, J., and Owen-Hughes, T. (2009). Nucleosomes can invade DNA territories occupied by their neighbors. *Nat Struct Mol Biol* 16, 151-158.
- Fairman-Williams, M.E., Guenther, U.P., and Jankowsky, E. (2010). SF1 and SF2 helicases: family matters. *Curr Opin Struct Biol* 20, 313-324.
- Fan, J.Y., Gordon, F., Luger, K., Hansen, J.C., and Tremethick, D.J. (2002). The essential histone variant H2A.Z regulates the equilibrium between different chromatin conformational states. *Nat Struct Biol* 9, 172-176.
- Felsenfeld, G., and Groudine, M. (2003). Controlling the double helix. *Nature* 421, 448-453.
- Fenn, S., Breitsprecher, D., Gerhold, C.B., Witte, G., Faix, J., and Hopfner, K.P. (2011). Structural biochemistry of nuclear actin-related proteins 4 and 8 reveals their interaction with actin. *EMBO J* 30, 2153-2166.
- Fernandez-Capetillo, O., Lee, A., Nussenzweig, M., and Nussenzweig, A. (2004). H2AX: the histone guardian of the genome. *DNA Repair (Amst)* 3, 959-967.
- Fitzgerald, D.J., Berger, P., Schaffitzel, C., Yamada, K., Richmond, T.J., and Berger, I. (2006). Protein complex expression by using multigene baculoviral vectors. *Nat Methods* 3, 1021-1032.

- Flanagan, J.F., Mi, L.Z., Chruszcz, M., Cymborowski, M., Clines, K.L., Kim, Y., Minor, W., Rastinejad, F., and Khorasanizadeh, S. (2005). Double chromodomains cooperate to recognize the methylated histone H3 tail. *Nature* 438, 1181-1185.
- Flemming, D., Thierbach, K., Stelter, P., Bottcher, B., and Hurt, E. (2010). Precise mapping of subunits in multiprotein complexes by a versatile electron microscopy label. *Nat Struct Mol Biol* 17, 775-778.
- Ford, J., Odeyale, O., Eskandar, A., Kouba, N., and Shen, C.H. (2007). A SWI/SNF- and INO80-dependent nucleosome movement at the INO1 promoter. *Biochem Biophys Res Commun* 361, 974-979.
- Fritsch, O., Benvenuto, G., Bowler, C., Molinier, J., and Hohn, B. (2004). The INO80 protein controls homologous recombination in *Arabidopsis thaliana*. *Mol Cell* 16, 479-485.
- Gangaraju, V.K., and Bartholomew, B. (2007). Dependency of ISW1a chromatin remodeling on extranucleosomal DNA. *Mol Cell Biol* 27, 3217-3225.
- Gerhold, C.B., Winkler, D.D., Lakomek, K., Seifert, F.U., Fenn, S., Kessler, B., Witte, G., Luger, K., and Hopfner, K.P. (2012). Structure of Actin-related protein 8 and its contribution to nucleosome binding. *Nucleic Acids Res* 40, 11036-11046.
- Ghaemmaghami, S., Huh, W.K., Bower, K., Howson, R.W., Belle, A., Dephoure, N., O'Shea, E.K., and Weissman, J.S. (2003). Global analysis of protein expression in yeast. *Nature* 425, 737-741.
- Gietz, R.D., and Woods, R.A. (2002). Transformation of yeast by lithium acetate/single-stranded carrier DNA/polyethylene glycol method. *Methods Enzymol* 350, 87-96.
- Goodsell, D.S., and Dickerson, R.E. (1994). Bending and curvature calculations in B-DNA. *Nucleic Acids Res* 22, 5497-5503.
- Gorbalenya, A.E., and Koonin, E.V. (1993). Helicases - Amino-Acid-Sequence Comparisons and Structure-Function-Relationships. *Curr Opin Struc Biol* 3, 419-429.
- Gorynia, S., Bandejas, T.M., Pinho, F.G., McVey, C.E., Vonrhein, C., Round, A., Svergun, D.I., Donner, P., Matias, P.M., and Carrondo, M.A. (2011). Structural and functional insights into a dodecameric molecular machine - the RuvBL1/RuvBL2 complex. *J Struct Biol* 176, 279-291.
- Gribun, A., Cheung, K.L., Huen, J., Ortega, J., and Houry, W.A. (2008). Yeast Rvb1 and Rvb2 are ATP-dependent DNA helicases that form a heterohexameric complex. *Journal of molecular biology* 376, 1320-1333.
- Grove, A., Galeone, A., Mayol, L., and Geiduschek, E.P. (1996). Localized DNA flexibility contributes to target site selection by DNA-bending proteins. *J Mol Biol* 260, 120-125.
- Grune, T., Brzeski, J., Eberharder, A., Clapier, C.R., Corona, D.F., Becker, P.B., and Muller, C.W. (2003). Crystal structure and functional analysis of a nucleosome recognition module of the remodeling factor ISWI. *Mol Cell* 12, 449-460.
- Guillemette, B., Bataille, A.R., Gevry, N., Adam, M., Blanchette, M., Robert, F., and Gaudreau, L. (2005). Variant histone H2A.Z is globally localized to the promoters of inactive yeast genes and regulates nucleosome positioning. *PLoS Biol* 3, e384.
- Guy, C.P., and Bolt, E.L. (2005). Archaeal Hel308 helicase targets replication forks in vivo and in vitro and unwinds lagging strands. *Nucleic Acids Res* 33, 3678-3690.
- Hamers-Casterman, C., Atarhouch, T., Muyldermans, S., Robinson, G., Hamers, C., Songa, E.B., Bendahman, N., and Hamers, R. (1993). Naturally occurring antibodies devoid of light chains. *Nature* 363, 446-448.
- Harata, M., Oma, Y., Mizuno, S., Jiang, Y.W., Stillman, D.J., and Wintersberger, U. (1999). The nuclear actin-related protein of *Saccharomyces cerevisiae*, Act3p/Arp4, interacts with core histones. *Mol Biol Cell* 10, 2595-2605.
- Harper, J.W., and Elledge, S.J. (2007). The DNA damage response: ten years after. *Mol Cell* 28, 739-745.
- Hartley, P.D., and Madhani, H.D. (2009). Mechanisms that specify promoter nucleosome location and identity. *Cell* 137, 445-458.

- Hassan, A.H., Prochasson, P., Neely, K.E., Galasinski, S.C., Chandy, M., Carrozza, M.J., and Workman, J.L. (2002). Function and selectivity of bromodomains in anchoring chromatin-modifying complexes to promoter nucleosomes. *Cell* 111, 369-379.
- Hauk, G., McKnight, J.N., Nodelman, I.M., and Bowman, G.D. (2010). The chromodomains of the Chd1 chromatin remodeler regulate DNA access to the ATPase motor. *Mol Cell* 39, 711-723.
- Hausner, W., Wettach, J., Hethke, C., and Thomm, M. (1996). Two transcription factors related with the eucaryal transcription factors TATA-binding protein and transcription factor IIB direct promoter recognition by an archaeal RNA polymerase. *J Biol Chem* 271, 30144-30148.
- Herzog, F., Kahraman, A., Boehringer, D., Mak, R., Bracher, A., Walzthoeni, T., Leitner, A., Beck, M., Hartl, F.U., Ban, N., *et al.* (2012). Structural probing of a protein phosphatase 2A network by chemical cross-linking and mass spectrometry. *Science* 337, 1348-1352.
- Hogan, C.J., Aligianni, S., Durand-Dubief, M., Persson, J., Will, W.R., Webster, J., Wheeler, L., Mathews, C.K., Elderkin, S., Oxley, D., *et al.* (2010). Fission yeast *lec1-ino80*-mediated nucleosome eviction regulates nucleotide and phosphate metabolism. *Mol Cell Biol* 30, 657-674.
- Hopfner, K.P., Craig, L., Moncalian, G., Zinkel, R.A., Usui, T., Owen, B.A., Karcher, A., Henderson, B., Bodmer, J.L., McMurray, C.T., *et al.* (2002). The Rad50 zinc-hook is a structure joining Mre11 complexes in DNA recombination and repair. *Nature* 418, 562-566.
- Huynh, V.A., Robinson, P.J., and Rhodes, D. (2005). A method for the in vitro reconstitution of a defined "30 nm" chromatin fibre containing stoichiometric amounts of the linker histone. *J Mol Biol* 345, 957-968.
- Jackson, J.D., Falciano, V.T., and Gorovsky, M.A. (1996). A likely histone H2A.F/Z variant in *Saccharomyces cerevisiae*. *Trends Biochem Sci* 21, 466-467.
- Jacobson, R.H., Ladurner, A.G., King, D.S., and Tjian, R. (2000). Structure and function of a human TAFII250 double bromodomain module. *Science* 288, 1422-1425.
- Jankowsky, A., Guenther, U.P., and Jankowsky, E. (2011). The RNA helicase database. *Nucleic Acids Res* 39, D338-341.
- Jennebach, S., Herzog, F., Aebersold, R., and Cramer, P. (2012). Crosslinking-MS analysis reveals RNA polymerase I domain architecture and basis of rRNA cleavage. *Nucleic Acids Res* 40, 5591-5601.
- Jha, S., and Dutta, A. (2009). RVB1/RVB2: running rings around molecular biology. *Mol Cell* 34, 521-533.
- Jiang, C., and Pugh, B.F. (2009). Nucleosome positioning and gene regulation: advances through genomics. *Nat Rev Genet* 10, 161-172.
- Jin, C., and Felsenfeld, G. (2007). Nucleosome stability mediated by histone variants H3.3 and H2A.Z. *Genes Dev* 21, 1519-1529.
- Jin, J., Cai, Y., Yao, T., Gottschalk, A.J., Florens, L., Swanson, S.K., Gutierrez, J.L., Coleman, M.K., Workman, J.L., Mushegian, A., *et al.* (2005). A mammalian chromatin remodeling complex with similarities to the yeast INO80 complex. *J Biol Chem* 280, 41207-41212.
- Jonsson, Z.O., Jha, S., Wohlschlegel, J.A., and Dutta, A. (2004). Rvb1p/Rvb2p recruit Arp5p and assemble a functional Ino80 chromatin remodeling complex. *Mol Cell* 16, 465-477.
- Kagalwala, M.N., Glaus, B.J., Dang, W., Zofall, M., and Bartholomew, B. (2004). Topography of the ISW2-nucleosome complex: insights into nucleosome spacing and chromatin remodeling. *EMBO J* 23, 2092-2104.
- Kandasamy, M.K., McKinney, E.C., Deal, R.B., Smith, A.P., and Meagher, R.B. (2009). Arabidopsis actin-related protein ARP5 in multicellular development and DNA repair. *Dev Biol* 335, 22-32.
- Kapoor, P., Chen, M., Winkler, D.D., Luger, K., and Shen, X. (2013). Evidence for monomeric actin function in INO80 chromatin remodeling. *Nat Struct Mol Biol* 20, 426-432.
- Kiefer, F., Arnold, K., Kunzli, M., Bordoli, L., and Schwede, T. (2009). The SWISS-MODEL Repository and associated resources. *Nucleic acids research* 37, D387-392.

- Kim, J.H., Kim, B., Cai, L., Choi, H.J., Ohgi, K.A., Tran, C., Chen, C., Chung, C.H., Huber, O., Rose, D.W., *et al.* (2005). Transcriptional regulation of a metastasis suppressor gene by Tip60 and beta-catenin complexes. *Nature* 434, 921-926.
- Kitayama, K., Kamo, M., Oma, Y., Matsuda, R., Uchida, T., Ikura, T., Tashiro, S., Ohyama, T., Winsor, B., and Harata, M. (2009). The human actin-related protein hArap5: nucleo-cytoplasmic shuttling and involvement in DNA repair. *Exp Cell Res* 315, 206-217.
- Klass, J., Murphy, F.V.t., Fouts, S., Serenil, M., Changela, A., Siple, J., and Churchill, M.E. (2003). The role of intercalating residues in chromosomal high-mobility-group protein DNA binding, bending and specificity. *Nucleic Acids Res* 31, 2852-2864.
- Klymenko, T., Papp, B., Fischle, W., Kocher, T., Schelder, M., Fritsch, C., Wild, B., Wilm, M., and Muller, J. (2006). A Polycomb group protein complex with sequence-specific DNA-binding and selective methyl-lysine-binding activities. *Genes Dev* 20, 1110-1122.
- Kobor, M.S., Venkatasubrahmanyam, S., Meneghini, M.D., Gin, J.W., Jennings, J.L., Link, A.J., Madhani, H.D., and Rine, J. (2004). A protein complex containing the conserved Swi2/Snf2-related ATPase Swr1p deposits histone variant H2A.Z into euchromatin. *PLoS Biol* 2, E131.
- Konev, A.Y., Tribus, M., Park, S.Y., Podhraski, V., Lim, C.Y., Emelyanov, A.V., Vershilova, E., Pirrotta, V., Kadonaga, J.T., Lusser, A., *et al.* (2007). CHD1 motor protein is required for deposition of histone variant H3.3 into chromatin in vivo. *Science* 317, 1087-1090.
- Krogan, N.J., Keogh, M.C., Datta, N., Sawa, C., Ryan, O.W., Ding, H., Haw, R.A., Pootoolal, J., Tong, A., Canadien, V., *et al.* (2003). A Snf2 family ATPase complex required for recruitment of the histone H2A variant Htz1. *Mol Cell* 12, 1565-1576.
- Kumagai, A., Lee, J., Yoo, H.Y., and Dunphy, W.G. (2006). TopBP1 activates the ATR-ATRIP complex. *Cell* 124, 943-955.
- Kuroda, T.S., Maita, H., Tabata, T., Taira, T., Kitaura, H., Ariga, H., and Iguchi-Ariga, S.M. (2004). A novel nucleolar protein, PAPA-1, induces growth arrest as a result of cell cycle arrest at the G1 phase. *Gene* 340, 83-98.
- Kusch, T., Florens, L., Macdonald, W.H., Swanson, S.K., Glaser, R.L., Yates, J.R., 3rd, Abmayr, S.M., Washburn, M.P., and Workman, J.L. (2004). Acetylation by Tip60 is required for selective histone variant exchange at DNA lesions. *Science* 306, 2084-2087.
- Ladurner, A.G., Inouye, C., Jain, R., and Tjian, R. (2003). Bromodomains mediate an acetyl-histone encoded antisilencing function at heterochromatin boundaries. *Mol Cell* 11, 365-376.
- Lander, G.C., Saibil, H.R., and Nogales, E. (2012). Go hybrid: EM, crystallography, and beyond. *Curr Opin Struct Biol* 22, 627-635.
- Larkin, M.A., Blackshields, G., Brown, N.P., Chenna, R., McGettigan, P.A., McWilliam, H., Valentin, F., Wallace, I.M., Wilm, A., Lopez, R., *et al.* (2007). Clustal W and Clustal X version 2.0. *Bioinformatics* 23, 2947-2948.
- Leitner, A., Joachimiak, L.A., Bracher, A., Monkemeyer, L., Walzthoeni, T., Chen, B., Pechmann, S., Holmes, S., Cong, Y., Ma, B., *et al.* (2012a). The molecular architecture of the eukaryotic chaperonin TRiC/CCT. *Structure* 20, 814-825.
- Leitner, A., Reischl, R., Walzthoeni, T., Herzog, F., Bohn, S., Forster, F., and Aebersold, R. (2012b). Expanding the chemical cross-linking toolbox by the use of multiple proteases and enrichment by size exclusion chromatography. *Mol Cell Proteomics* 11, M111 014126.
- Leitner, A., Walzthoeni, T., Kahraman, A., Herzog, F., Rinner, O., Beck, M., and Aebersold, R. (2010). Probing native protein structures by chemical cross-linking, mass spectrometry, and bioinformatics. *Mol Cell Proteomics* 9, 1634-1649.
- Leschziner, A.E. (2011). Electron microscopy studies of nucleosome remodelers. *Curr Opin Struct Biol* 21, 709-718.

- Leschziner, A.E., Lemon, B., Tjian, R., and Nogales, E. (2005). Structural studies of the human PBAF chromatin-remodeling complex. *Structure* **13**, 267-275.
- Leschziner, A.E., Saha, A., Wittmeyer, J., Zhang, Y., Bustamante, C., Cairns, B.R., and Nogales, E. (2007). Conformational flexibility in the chromatin remodeler RSC observed by electron microscopy and the orthogonal tilt reconstruction method. *Proc Natl Acad Sci U S A* **104**, 4913-4918.
- Li, B., Pattenden, S.G., Lee, D., Gutierrez, J., Chen, J., Seidel, C., Gerton, J., and Workman, J.L. (2005). Preferential occupancy of histone variant H2AZ at inactive promoters influences local histone modifications and chromatin remodeling. *Proc Natl Acad Sci U S A* **102**, 18385-18390.
- Liu, Q., Guntuku, S., Cui, X.S., Matsuoka, S., Cortez, D., Tamai, K., Luo, G., Carattini-Rivera, S., DeMayo, F., Bradley, A., *et al.* (2000). Chk1 is an essential kinase that is regulated by Atr and required for the G(2)/M DNA damage checkpoint. *Genes Dev* **14**, 1448-1459.
- Lopez-Perrote, A., Munoz-Hernandez, H., Gil, D., and Llorca, O. (2012). Conformational transitions regulate the exposure of a DNA-binding domain in the RuvBL1-RuvBL2 complex. *Nucleic Acids Res* **40**, 11086-11099.
- Love, J.J., Li, X., Case, D.A., Giese, K., Grosschedl, R., and Wright, P.E. (1995). Structural basis for DNA bending by the architectural transcription factor LEF-1. *Nature* **376**, 791-795.
- Lowary, P.T., and Widom, J. (1998). New DNA sequence rules for high affinity binding to histone octamer and sequence-directed nucleosome positioning. *J Mol Biol* **276**, 19-42.
- Luger, K., Dechassa, M.L., and Tremethick, D.J. (2012). New insights into nucleosome and chromatin structure: an ordered state or a disordered affair? *Nat Rev Mol Cell Biol* **13**, 436-447.
- Luger, K., Mader, A.W., Richmond, R.K., Sargent, D.F., and Richmond, T.J. (1997). Crystal structure of the nucleosome core particle at 2.8 Å resolution. *Nature* **389**, 251-260.
- Luk, E., Ranjan, A., Fitzgerald, P.C., Mizuguchi, G., Huang, Y., Wei, D., and Wu, C. (2010). Stepwise histone replacement by SWR1 requires dual activation with histone H2A.Z and canonical nucleosome. *Cell* **143**, 725-736.
- Lusser, A., Urwin, D.L., and Kadonaga, J.T. (2005). Distinct activities of CHD1 and ACF in ATP-dependent chromatin assembly. *Nat Struct Mol Biol* **12**, 160-166.
- Masse, J.E., Wong, B., Yen, Y.M., Allain, F.H., Johnson, R.C., and Feigon, J. (2002). The *S. cerevisiae* architectural HMGB protein NHP6A complexed with DNA: DNA and protein conformational changes upon binding. *J Mol Biol* **323**, 263-284.
- Matias, P.M., Gorynia, S., Donner, P., and Carrondo, M.A. (2006). Crystal structure of the human AAA+ protein RuvBL1. *J Biol Chem* **281**, 38918-38929.
- Mavrich, T.N., Ioshikhes, I.P., Venters, B.J., Jiang, C., Tomsho, L.P., Qi, J., Schuster, S.C., Albert, I., and Pugh, B.F. (2008). A barrier nucleosome model for statistical positioning of nucleosomes throughout the yeast genome. *Genome Res* **18**, 1073-1083.
- Meneghini, M.D., Wu, M., and Madhani, H.D. (2003). Conserved histone variant H2A.Z protects euchromatin from the ectopic spread of silent heterochromatin. *Cell* **112**, 725-736.
- Migneault, I., Dartiguenave, C., Bertrand, M.J., and Waldron, K.C. (2004). Glutaraldehyde: behavior in aqueous solution, reaction with proteins, and application to enzyme crosslinking. *Biotechniques* **37**, 790-796, 798-802.
- Mimitou, E.P., and Symington, L.S. (2008). Sae2, Exo1 and Sgs1 collaborate in DNA double-strand break processing. *Nature* **455**, 770-774.
- Mizuguchi, G., Shen, X., Landry, J., Wu, W.H., Sen, S., and Wu, C. (2004). ATP-driven exchange of histone H2AZ variant catalyzed by SWR1 chromatin remodeling complex. *Science* **303**, 343-348.
- Morrison, A.J., Highland, J., Krogan, N.J., Arbel-Eden, A., Greenblatt, J.F., Haber, J.E., and Shen, X. (2004). INO80 and gamma-H2AX interaction links ATP-dependent chromatin remodeling to DNA damage repair. *Cell* **119**, 767-775.

- Morrison, A.J., Kim, J.A., Person, M.D., Highland, J., Xiao, J., Wehr, T.S., Hensley, S., Bao, Y., Shen, J., Collins, S.R., *et al.* (2007). Mec1/Tel1 phosphorylation of the INO80 chromatin remodeling complex influences DNA damage checkpoint responses. *Cell* **130**, 499-511.
- Morrison, A.J., and Shen, X. (2009). Chromatin remodelling beyond transcription: the INO80 and SWR1 complexes. *Nat Rev Mol Cell Biol* **10**, 373-384.
- Muller, J., Oma, Y., Vallar, L., Friederich, E., Poch, O., and Winsor, B. (2005). Sequence and comparative genomic analysis of actin-related proteins. *Mol Biol Cell* **16**, 5736-5748.
- Muyldermans, S., Cambillau, C., and Wyns, L. (2001). Recognition of antigens by single-domain antibody fragments: the superfluous luxury of paired domains. *Trends Biochem Sci* **26**, 230-235.
- Narlikar, G.J., Sundaramoorthy, R., and Owen-Hughes, T. (2013). Mechanisms and Functions of ATP-Dependent Chromatin-Remodeling Enzymes. *Cell* **154**, 490-503.
- Neumann, F.R., Dion, V., Gehlen, L.R., Tsai-Pflugfelder, M., Schmid, R., Taddei, A., and Gasser, S.M. (2012). Targeted INO80 enhances subnuclear chromatin movement and ectopic homologous recombination. *Genes Dev* **26**, 369-383.
- Nguyen, V.Q., Ranjan, A., Stengel, F., Wei, D., Aebersold, R., Wu, C., and Leschziner, A.E. (2013). Molecular Architecture of the ATP-Dependent Chromatin-Remodeling Complex SWR1. *Cell* **154**, 1220-1231.
- Niewiarowski, A., Bradley, A.S., Gor, J., McKay, A.R., Perkins, S.J., and Tsaneva, I.R. (2010). Oligomeric assembly and interactions within the human RuvB-like RuvBL1 and RuvBL2 complexes. *The Biochemical journal* **429**, 113-125.
- Nikolov, D.B., Chen, H., Halay, E.D., Usheva, A.A., Hisatake, K., Lee, D.K., Roeder, R.G., and Burley, S.K. (1995). Crystal structure of a TFIIB-TBP-TATA-element ternary complex. *Nature* **377**, 119-128.
- Ohndorf, U.M., Rould, M.A., He, Q., Pabo, C.O., and Lippard, S.J. (1999). Basis for recognition of cisplatin-modified DNA by high-mobility-group proteins. *Nature* **399**, 708-712.
- Orphanides, G., Wu, W.H., Lane, W.S., Hampsey, M., and Reinberg, D. (1999). The chromatin-specific transcription elongation factor FACT comprises human SPT16 and SSRP1 proteins. *Nature* **400**, 284-288.
- Papamichos-Chronakis, M., and Peterson, C.L. (2008). The Ino80 chromatin-remodeling enzyme regulates replisome function and stability. *Nat Struct Mol Biol* **15**, 338-345.
- Papamichos-Chronakis, M., Watanabe, S., Rando, O.J., and Peterson, C.L. (2011). Global Regulation of H2A.Z Localization by the INO80 Chromatin-Remodeling Enzyme Is Essential for Genome Integrity. *Cell* **144**, 200-213.
- Petoukhov, M.V., and Svergun, D.I. (2013). Applications of small-angle X-ray scattering to biomacromolecular solutions. *Int J Biochem Cell Biol* **45**, 429-437.
- Pettersen, E.F., Goddard, T.D., Huang, C.C., Couch, G.S., Greenblatt, D.M., Meng, E.C., and Ferrin, T.E. (2004). UCSF Chimera--a visualization system for exploratory research and analysis. *J Comput Chem* **25**, 1605-1612.
- Petukhov, M., Dagkessamanskaja, A., Bommer, M., Barrett, T., Tsaneva, I., Yakimov, A., Queval, R., Shvetsov, A., Khodorkovskiy, M., Kas, E., *et al.* (2012). Large-scale conformational flexibility determines the properties of AAA+ TIP49 ATPases. *Structure* **20**, 1321-1331.
- Placek, B.J., Harrison, L.N., Villers, B.M., and Gloss, L.M. (2005). The H2A.Z/H2B dimer is unstable compared to the dimer containing the major H2A isoform. *Protein Sci* **14**, 514-522.
- Polach, K.J., and Widom, J. (1995). Mechanism of protein access to specific DNA sequences in chromatin: a dynamic equilibrium model for gene regulation. *J Mol Biol* **254**, 130-149.
- Pugh, B.F. (2013). Molecular biology: The ends justify the means. *Nature* **497**, 48-49.
- Puri, T., Wendler, P., Sigala, B., Saibil, H., and Tsaneva, I.R. (2007). Dodecameric structure and ATPase activity of the human TIP48/TIP49 complex. *Journal of molecular biology* **366**, 179-192.

- Putnam, C.D., Clancy, S.B., Tsuruta, H., Gonzalez, S., Wetmur, J.G., and Tainer, J.A. (2001). Structure and mechanism of the RuvB Holliday junction branch migration motor. *J Mol Biol* **311**, 297-310.
- Racki, L.R., Yang, J.G., Naber, N., Partensky, P.D., Acevedo, A., Purcell, T.J., Cooke, R., Cheng, Y., and Narlikar, G.J. (2009). The chromatin remodeller ACF acts as a dimeric motor to space nucleosomes. *Nature* **462**, 1016-1021.
- Ranjan, A., Mizuguchi, G., Fitzgerald, P.C., Wei, D., Wang, F., Huang, Y., Luk, E., Woodcock, C.L., and Wu, C. (2013). Nucleosome-free Region Dominates Histone Acetylation in Targeting SWR1 to Promoters for H2A.Z Replacement. *Cell* **154**, 1232-1245.
- Rasmussen, S.G., DeVree, B.T., Zou, Y., Kruse, A.C., Chung, K.Y., Kobilka, T.S., Thian, F.S., Chae, P.S., Pardon, E., Calinski, D., *et al.* (2011). Crystal structure of the beta2 adrenergic receptor-Gs protein complex. *Nature* **477**, 549-555.
- Ray, S., and Grove, A. (2009). The yeast high mobility group protein HMO2, a subunit of the chromatin-remodeling complex INO80, binds DNA ends. *Nucleic Acids Res* **37**, 6389-6399.
- Ray, S., and Grove, A. (2012). Interaction of *Saccharomyces cerevisiae* HMO2 domains with distorted DNA. *Biochemistry* **51**, 1825-1835.
- Redon, C., Pilch, D., Rogakou, E., Sedelnikova, O., Newrock, K., and Bonner, W. (2002). Histone H2A variants H2AX and H2AZ. *Curr Opin Genet Dev* **12**, 162-169.
- Reid, R.J., Lisby, M., and Rothstein, R. (2002). Cloning-free genome alterations in *Saccharomyces cerevisiae* using adaptamer-mediated PCR. *Methods Enzymol* **350**, 258-277.
- Rinner, O., Seebacher, J., Walzthoeni, T., Mueller, L.N., Beck, M., Schmidt, A., Mueller, M., and Aebersold, R. (2008). Identification of cross-linked peptides from large sequence databases. *Nat Methods* **5**, 315-318.
- Robinson, P.J., Fairall, L., Huynh, V.A., and Rhodes, D. (2006). EM measurements define the dimensions of the "30-nm" chromatin fiber: evidence for a compact, interdigitated structure. *Proc Natl Acad Sci U S A* **103**, 6506-6511.
- Rossmann, M.G., Morais, M.C., Leiman, P.G., and Zhang, W. (2005). Combining X-ray crystallography and electron microscopy. *Structure* **13**, 355-362.
- Rothbauer, U., Zolghadr, K., Tillib, S., Nowak, D., Schermelleh, L., Gahl, A., Backmann, N., Conrath, K., Muyldermans, S., Cardoso, M.C., *et al.* (2006). Targeting and tracing antigens in live cells with fluorescent nanobodies. *Nat Methods* **3**, 887-889.
- Ruhl, D.D., Jin, J., Cai, Y., Swanson, S., Florens, L., Washburn, M.P., Conaway, R.C., Conaway, J.W., and Chrivia, J.C. (2006). Purification of a human SRCAP complex that remodels chromatin by incorporating the histone variant H2A.Z into nucleosomes. *Biochemistry* **45**, 5671-5677.
- Saravanan, M., Wuerges, J., Bose, D., McCormack, E.A., Cook, N.J., Zhang, X., and Wigley, D.B. (2012). Interactions between the nucleosome histone core and Arp8 in the INO80 chromatin remodeling complex. *Proc Natl Acad Sci U S A* **109**, 20883-20888.
- Sasse, J., and Gallagher, S.R. (2009). Staining proteins in gels. *Curr Protoc Mol Biol* *Chapter 10*, Unit 10 16.
- Schubert, H.L., Wittmeyer, J., Kasten, M.M., Hinata, K., Rawling, D.C., Heroux, A., Cairns, B.R., and Hill, C.P. (2013). Structure of an actin-related subcomplex of the SWI/SNF chromatin remodeler. *Proc Natl Acad Sci U S A*.
- Schulze, J.M., Kane, C.M., and Ruiz-Manzano, A. (2010). The YEATS domain of Taf14 in *Saccharomyces cerevisiae* has a negative impact on cell growth. *Mol Genet Genomics* **283**, 365-380.
- Seeber, A., Dion, V., and Gasser, S.M. (2013a). Checkpoint kinases and the INO80 nucleosome remodeling complex enhance global chromatin mobility in response to DNA damage. *Genes Dev* **27**, 1999-2008.
- Seeber, A., Hauer, M., and Gasser, S.M. (2013b). Nucleosome remodelers in double-strand break repair. *Curr Opin Genet Dev*.

- Sermwittayawong, D., and Tan, S. (2006). SAGA binds TBP via its Spt8 subunit in competition with DNA: implications for TBP recruitment. *EMBO J* 25, 3791-3800.
- Shen, X. (2004). Preparation and analysis of the INO80 complex. *Methods Enzymol* 377, 401-412.
- Shen, X., Mizuguchi, G., Hamiche, A., and Wu, C. (2000). A chromatin remodelling complex involved in transcription and DNA processing. *Nature* 406, 541-544.
- Shen, X., Ranallo, R., Choi, E., and Wu, C. (2003). Involvement of actin-related proteins in ATP-dependent chromatin remodeling. *Mol Cell* 12, 147-155.
- Shimada, K., Oma, Y., Schleker, T., Kugou, K., Ohta, K., Harata, M., and Gasser, S.M. (2008). Ino80 chromatin remodeling complex promotes recovery of stalled replication forks. *Curr Biol* 18, 566-575.
- Shukla, M.S., Syed, S.H., Goutte-Gattat, D., Richard, J.L., Montel, F., Hamiche, A., Travers, A., Faivre-Moskalenko, C., Bednar, J., Hayes, J.J., *et al.* (2011). The docking domain of histone H2A is required for H1 binding and RSC-mediated nucleosome remodeling. *Nucleic Acids Res* 39, 2559-2570.
- Skiniotis, G., Moazed, D., and Walz, T. (2007). Acetylated histone tail peptides induce structural rearrangements in the RSC chromatin remodeling complex. *J Biol Chem* 282, 20804-20808.
- Smith, C.L., Horowitz-Scherer, R., Flanagan, J.F., Woodcock, C.L., and Peterson, C.L. (2003). Structural analysis of the yeast SWI/SNF chromatin remodeling complex. *Nat Struct Biol* 10, 141-145.
- Stargell, L.A., Bowen, J., Dadd, C.A., Dedon, P.C., Davis, M., Cook, R.G., Allis, C.D., and Gorovsky, M.A. (1993). Temporal and spatial association of histone H2A variant hv1 with transcriptionally competent chromatin during nuclear development in *Tetrahymena thermophila*. *Genes Dev* 7, 2641-2651.
- Stockdale, C., Flaus, A., Ferreira, H., and Owen-Hughes, T. (2006). Analysis of nucleosome repositioning by yeast ISWI and Chd1 chromatin remodeling complexes. *J Biol Chem* 281, 16279-16288.
- Stott, K., Tang, G.S., Lee, K.B., and Thomas, J.O. (2006). Structure of a complex of tandem HMG boxes and DNA. *J Mol Biol* 360, 90-104.
- Stros, M. (2010). HMGB proteins: interactions with DNA and chromatin. *Biochim Biophys Acta* 1799, 101-113.
- Sudarsanam, P., and Winston, F. (2000). The Swi/Snf family nucleosome-remodeling complexes and transcriptional control. *Trends Genet* 16, 345-351.
- Suto, R.K., Clarkson, M.J., Tremethick, D.J., and Luger, K. (2000). Crystal structure of a nucleosome core particle containing the variant histone H2A.Z. *Nat Struct Biol* 7, 1121-1124.
- Szerlong, H., Hinata, K., Viswanathan, R., Erdjument-Bromage, H., Tempst, P., and Cairns, B.R. (2008). The HSA domain binds nuclear actin-related proteins to regulate chromatin-remodeling ATPases. *Nat Struct Mol Biol* 15, 469-476.
- Tang, G., Peng, L., Baldwin, P.R., Mann, D.S., Jiang, W., Rees, I., and Ludtke, S.J. (2007). EMAN2: an extensible image processing suite for electron microscopy. *J Struct Biol* 157, 38-46.
- Thambirajah, A.A., Dryhurst, D., Ishibashi, T., Li, A., Maffey, A.H., and Ausio, J. (2006). H2A.Z stabilizes chromatin in a way that is dependent on core histone acetylation. *J Biol Chem* 281, 20036-20044.
- Thoma, N.H., Czyzewski, B.K., Alexeev, A.A., Mazin, A.V., Kowalczykowski, S.C., and Pavletich, N.P. (2005). Structure of the SWI2/SNF2 chromatin-remodeling domain of eukaryotic Rad54. *Nat Struct Mol Biol* 12, 350-356.
- Torreira, E., Jha, S., Lopez-Blanco, J.R., Arias-Palomo, E., Chacon, P., Canas, C., Ayora, S., Dutta, A., and Llorca, O. (2008). Architecture of the pontin/reptin complex, essential in the assembly of several macromolecular complexes. *Structure* 16, 1511-1520.
- Tosi, A., Haas, C., Herzog, F., Gilmozzi, A., Berninghausen, O., Ungewickell, C., Gerhold, C.B., Lakomek, K., Aebersold, R., Beckmann, R., *et al.* (2013). Structure and Subunit Topology of the INO80 Chromatin Remodeler and Its Nucleosome Complex. *Cell* 154, 1207-1219.
- Tsukuda, T., Fleming, A.B., Nickoloff, J.A., and Osley, M.A. (2005). Chromatin remodelling at a DNA double-strand break site in *Saccharomyces cerevisiae*. *Nature* 438, 379-383.

- Udugama, M., Sabri, A., and Bartholomew, B. (2011). The INO80 ATP-dependent chromatin remodeling complex is a nucleosome spacing factor. *Molecular and cellular biology* 31, 662-673.
- Ugrinova, I., Pashev, I.G., and Pasheva, E.A. (2009). Nucleosome binding properties and Co-remodeling activities of native and in vivo acetylated HMGB-1 and HMGB-2 proteins. *Biochemistry* 48, 6502-6507.
- Ulyanova, N.P., and Schnitzler, G.R. (2005). Human SWI/SNF generates abundant, structurally altered dinucleosomes on polynucleosomal templates. *Mol Cell Biol* 25, 11156-11170.
- Unsal-Kacmaz, K., and Sancar, A. (2004). Quaternary structure of ATR and effects of ATRIP and replication protein A on its DNA binding and kinase activities. *Mol Cell Biol* 24, 1292-1300.
- van Attikum, H., Fritsch, O., and Gasser, S.M. (2007). Distinct roles for SWR1 and INO80 chromatin remodeling complexes at chromosomal double-strand breaks. *EMBO J* 26, 4113-4125.
- van Attikum, H., Fritsch, O., Hohn, B., and Gasser, S.M. (2004). Recruitment of the INO80 complex by H2A phosphorylation links ATP-dependent chromatin remodeling with DNA double-strand break repair. *Cell* 119, 777-788.
- van Daal, A., and Elgin, S.C. (1992). A histone variant, H2AvD, is essential in *Drosophila melanogaster*. *Mol Biol Cell* 3, 593-602.
- Vary, J.C., Jr., Gangaraju, V.K., Qin, J., Landel, C.C., Kooperberg, C., Bartholomew, B., and Tsukiyama, T. (2003). Yeast Isw1p forms two separable complexes in vivo. *Mol Cell Biol* 23, 80-91.
- Venters, B.J., and Pugh, B.F. (2013). Genomic organization of human transcription initiation complexes. *Nature*.
- Vincent, J.A., Kwong, T.J., and Tsukiyama, T. (2008). ATP-dependent chromatin remodeling shapes the DNA replication landscape. *Nat Struct Mol Biol* 15, 477-484.
- Vorobiev, S., Strokopytov, B., Drubin, D.G., Frieden, C., Ono, S., Condeelis, J., Rubenstein, P.A., and Almo, S.C. (2003). The structure of nonvertebrate actin: implications for the ATP hydrolytic mechanism. *Proc Natl Acad Sci U S A* 100, 5760-5765.
- Walzthoeni, T., Claassen, M., Leitner, A., Herzog, F., Bohn, S., Forster, F., Beck, M., and Aebersold, R. (2012). False discovery rate estimation for cross-linked peptides identified by mass spectrometry. *Nat Methods* 9, 901-903.
- Wang, A.Y., Schulze, J.M., Skordalakes, E., Gin, J.W., Berger, J.M., Rine, J., and Kobor, M.S. (2009). Asf1-like structure of the conserved Yaf9 YEATS domain and role in H2A.Z deposition and acetylation. *Proc Natl Acad Sci U S A* 106, 21573-21578.
- Wanzel, M., Kleine-Kohlbrecher, D., Herold, S., Hock, A., Berns, K., Park, J., Hemmings, B., and Eilers, M. (2005). Akt and 14-3-3eta regulate Miz1 to control cell-cycle arrest after DNA damage. *Nat Cell Biol* 7, 30-41.
- Ward, I.M., and Chen, J. (2001). Histone H2AX is phosphorylated in an ATR-dependent manner in response to replicational stress. *J Biol Chem* 276, 47759-47762.
- Watanabe, S., Radman-Livaja, M., Rando, O.J., and Peterson, C.L. (2013). A histone acetylation switch regulates H2A.Z deposition by the SWR-C remodeling enzyme. *Science* 340, 195-199.
- Weber, C.M., Henikoff, J.G., and Henikoff, S. (2010). H2A.Z nucleosomes enriched over active genes are homotypic. *Nat Struct Mol Biol* 17, 1500-1507.
- Welch, M.D., and Drubin, D.G. (1994). A nuclear protein with sequence similarity to proteins implicated in human acute leukemias is important for cellular morphogenesis and actin cytoskeletal function in *Saccharomyces cerevisiae*. *Mol Biol Cell* 5, 617-632.
- Wong, B., Masse, J.E., Yen, Y.M., Giannikopoulos, P., Feigon, J., and Johnson, R.C. (2002). Binding to cisplatin-modified DNA by the *Saccharomyces cerevisiae* HMGB protein Nhp6A. *Biochemistry* 41, 5404-5414.

- Wu, S., Shi, Y., Mulligan, P., Gay, F., Landry, J., Liu, H., Lu, J., Qi, H.H., Wang, W., Nickoloff, J.A., *et al.* (2007). A YY1-INO80 complex regulates genomic stability through homologous recombination-based repair. *Nat Struct Mol Biol* 14, 1165-1172.
- Wu, W.H., Alami, S., Luk, E., Wu, C.H., Sen, S., Mizuguchi, G., Wei, D., and Wu, C. (2005). Swc2 is a widely conserved H2AZ-binding module essential for ATP-dependent histone exchange. *Nat Struct Mol Biol* 12, 1064-1071.
- Wu, W.H., Wu, C.H., Ladurner, A., Mizuguchi, G., Wei, D., Xiao, H., Luk, E., Ranjan, A., and Wu, C. (2009). N terminus of Swr1 binds to histone H2AZ and provides a platform for subunit assembly in the chromatin remodeling complex. *J Biol Chem* 284, 6200-6207.
- Yamada, K., Frouws, T.D., Angst, B., Fitzgerald, D.J., DeLuca, C., Schimmele, K., Sargent, D.F., and Richmond, T.J. (2011). Structure and mechanism of the chromatin remodelling factor ISW1a. *Nature* 472, 448-453.
- Yamada, K., Kunishima, N., Mayanagi, K., Ohnishi, T., Nishino, T., Iwasaki, H., Shinagawa, H., and Morikawa, K. (2001). Crystal structure of the Holliday junction migration motor protein RuvB from *Thermus thermophilus* HB8. *Proc Natl Acad Sci U S A* 98, 1442-1447.
- Yang, Z., Fang, J., Chittuluru, J., Asturias, F.J., and Penczek, P.A. (2012). Iterative stable alignment and clustering of 2D transmission electron microscope images. *Structure* 20, 237-247.
- Yao, T., Song, L., Jin, J., Cai, Y., Takahashi, H., Swanson, S.K., Washburn, M.P., Florens, L., Conaway, R.C., Cohen, R.E., *et al.* (2008). Distinct modes of regulation of the Uch37 deubiquitinating enzyme in the proteasome and in the Ino80 chromatin-remodeling complex. *Mol Cell* 31, 909-917.
- Yen, K., Vinayachandran, V., Batta, K., Koerber, R.T., and Pugh, B.F. (2012). Genome-wide nucleosome specificity and directionality of chromatin remodelers. *Cell* 149, 1461-1473.
- Yen, K., Vinayachandran, V., and Pugh, B.F. (2013). SWR-C and INO80 Chromatin Remodelers Recognize Nucleosome-free Regions Near +1 Nucleosomes. *Cell* 154, 1246-1256.
- Yen, Y.M., Wong, B., and Johnson, R.C. (1998). Determinants of DNA binding and bending by the *Saccharomyces cerevisiae* high mobility group protein NHP6A that are important for its biological activities. Role of the unique N terminus and putative intercalating methionine. *J Biol Chem* 273, 4424-4435.
- Young, M.M., Tang, N., Hempel, J.C., Oshiro, C.M., Taylor, E.W., Kuntz, I.D., Gibson, B.W., and Dollinger, G. (2000). High throughput protein fold identification by using experimental constraints derived from intramolecular cross-links and mass spectrometry. *Proc Natl Acad Sci U S A* 97, 5802-5806.
- Yuan, G.C., Liu, Y.J., Dion, M.F., Slack, M.D., Wu, L.F., Altschuler, S.J., and Rando, O.J. (2005). Genome-scale identification of nucleosome positions in *S. cerevisiae*. *Science* 309, 626-630.
- Zhang, H., Roberts, D.N., and Cairns, B.R. (2005). Genome-wide dynamics of Htz1, a histone H2A variant that poises repressed/basal promoters for activation through histone loss. *Cell* 123, 219-231.
- Zlatanova, J., and Thakar, A. (2008). H2A.Z: view from the top. *Structure* 16, 166-179.

8 Curriculum Vitae

Curriculum Vitae of Alessandro Tosi

Education

PhD thesis in Karl-Peter Hopfner's group, Gene Center, Ludwig-Maximilians-University Munich (LMU), Germany	Since 03/2010
In collaboration with Roland Beckmann's group, Gene Center and Ruedi Aebersold's group, ETH Zurich	
Master in Biochemistry at the Ludwig-Maximilians-University Munich	03/2008 - 01/2010
ø 1.1, Master Thesis 1.0	
Bachelor in Chemistry and Biochemistry at the Ludwig-Maximilians-University and Technical University, Munich	10/2004 - 02/2008
Abitur at St.-Anna Gymnasium, Munich	09/1994 - 05/2003

Experience

PhD thesis in Karl-Peter Hopfner's group, Gene Center Munich	Since 03/2010
<i>"Structure and subunit topology of the chromatin remodeler INO80 and its interaction with the nucleosome"</i>	
Master thesis in Arne Klungland's group, Center for Molecular Biology and Neuroscience, Oslo, Norway	06/2009 - 01/2010
<i>"A modified chromatin immunoprecipitation (ChIP) protocol allows streamlined epigenetic analysis of spermatogenesis to implicate a role for the testis specific histone variant TH2B"</i>	
Internship in Heinrich Leonhardt's group, LMU Biocenter, Munich	08/2008 - 10/2008
<i>"Analysis of the Dnmt1 activity and DNA specificity using an <i>in vitro</i> fluorescent binding and trapping assay"</i>	
Internship in Erich Nigg's group, Max-Planck-Institute, Munich	03/2008 - 05/2008
<i>"Functional analysis of BubR1 by time-lapse fluorescence video microscopy"</i>	
Bachelor Thesis in Karl-Peter Hopfner's group, Gene Center, Munich	10/2007 - 02/2008
<i>"Cloning, purification and structural characterization of <i>S.pombe</i> Nse2 protein"</i>	
Student assistant in Karl-Peter Hopfner's group, Gene Center, Munich	12/2006 - 09/2007
Internship in an environmental trace analysis lab, Obermeyer, Munich	08/2005

Publication

Tosi A, Haas C, Herzog F, Gilmozzi A, Berninghausen O, Ungewickell O, Gerhold CB, Lakomek K, Aebersold R, Beckmann R and Hopfner KP: Structure and subunit topology of the INO80 chromatin remodeler and its nucleosome complex. *Cell in press*

Research Skills

Structural Biology

Cross-linking and mass spectrometry, bioinformatics (homology modelling and molecular docking), and protein crystallization screening using robotic systems

Protein purification

Establishment of purification protocol for a large multi-subunit complex using chromatography techniques (Ni- and FLAG-affinity, ion exchange, size exclusion) and handling of standard and analytical Äkta systems

Protein characterisation

SDS and native gel electrophoresis, Western blotting, EMSA, radioactive ATPase assays, immunofluorescence microscopy, ChIP assays

Protein Expression

Recombinant expression of proteins in *E.coli* and insect cells (baculovirus system), endogenous expression in *S.cerevisiae* and large scale yeast fermentation

Molecular Biology

Molecular cloning in bacteria and yeast, working with human cell cultures

Scholarship and Presentations

Oral presentation and poster presentation at the "Helicases and nucleic acid translocases", EMBO, Harden conference, Cambridge, United Kingdom, 04-08. August 2013

Poster presentation at the "Epigenetics & Chromatin: Interactions and processes", conference, Boston,

USA, 11-13. March 2013

Poster presentation at the "Protein-protein and protein-nucleic acid cross-linking and mass spectrometry",

EMBO practical course, Göttingen, Germany, 23-29. October 2011

Scholarship for Master Thesis in Oslo, Norway given by "Deutscher Akademischer

Austauschdienst" (DAAD),

June 2009 – October 2009

Social Commitment

Gap year ("Freiwillig Soziales Jahr") at the "Malteser Hilfsdienst" in emergency medical service and patient transport with education as emergency medical technician. This replaced the compulsory community service ("Zivildienst").	09/2003 - 08/2004
--	----------------------

Miscellaneous

- Course in business studies at the LMU ("Student und Arbeitsmarkt")
- Personality training with video feedback (LMU Center for Leadership and Peoplemanagement)
- Communication training (LMU Center for Leadership and Peoplemanagement)

Languages

- German – native language
- English – speak fluently, write and read with proficiency
- French – basic competence

Software Skills

MS Office, Adobe Creative Suite (Photoshop and Illustrator), LINUX (basic competence)

9 Acknowledgments

First of all I would like to thank my supervisor Prof. Dr. Karl-Peter Hopfner for giving me the opportunity to work on this fantastic project in his group. I always admired Karl-Peter ingenious ideas. I am also very grateful for his constant advice and leaving me the freedom to design my own experiments und projects. Thank you for the great and really fruitful time.

One of the highlights during my PhD was certainly that Karl-Peter gave me the opportunity to collaborate with Dr. Franz Herzog from the Ruedi Aebersold lab. It was not only a productive collaboration, but Franz was also a great mentor.

I also would like to thank Prof. Dr. Roland Beckmann not only for his razor sharp advice in biochemical and visual related questions, but also for giving us “private” lessons in scientific writing.

I am also thankful to all the members of the “Happy Hopfner” laboratory for always being supportive not only lab and data wise, but also just for having a nice chat on the floor and helping me through my PhD. Further acknowledgments go especially to the INO80-gang (Christian B. Gerhold, Kristina Lakomek, Sebastian Fenn, Marianne Schwarz, Sebastian Eustermann, Sandra Schneller, Brigitte Keßler and Manuela Moldt) for the great teamwork. I am also thankful for the helping hands of my students Maurine Rothe and Isabel Blunck.

I am also very grateful to the members of the Cramer and Halic groups for helping me with fermentation, cell lysis methods, sharing equipment and advice.

In addition, I would like to thank Karl-Peter and Roland for paving the way for the fruitful collaboration with Caroline Haas from the Roland Beckmann lab. This also showed us that we not only work as a private team, but can also apply this successfully to work.

Zuletzt möchte ich mich noch bei meinen Eltern bedanken, ohne die ich es bestimmt nicht soweit geschafft hätte.